Charles University in Prague
Faculty of Mathematics and Physics

MASTER'S THESIS
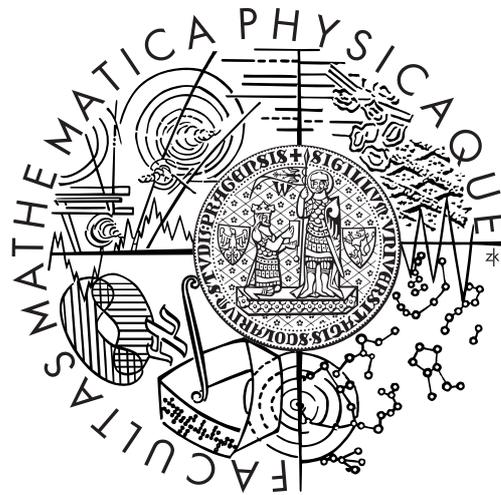
Štěpán Uxa

Magnetooptical Properties of Semiconductor Quantum Structures

Institute of Physics of Charles University

Supervisor: Assoc. Prof. Roman Grill, PhD

Study program: Physics, Optics and Optoelectronics

Acknowledgement

I would like to express my gratitude to my supervisor Assoc. Prof. Roman Grill, PhD for his invaluable help and challenging consultations, and to Assoc. Prof. Jiří Bok, PhD for programming advices and printing of this work. I would also like to thank to my parents for their support during my studies, to my brother, who let me finish the electronic version of my master's thesis although working on the bachelor's thesis of his own, and last but not least to my girlfriend, who was daily forced to listen to my talks about the work but still stood by me to encourage me the most.

I confess that I have written my master's thesis on my own and using only the quoted sources. I agree to lend it.

Prague, July 13, 2009

Štěpán Uxa

Contents

Název práce: Magnetooptické vlastnosti polovodičových kvantových struktur

Autor: Štěpán Uxa

Katedra: Fyzikální ústav Univerzity Karlovy

Vedoucí diplomové práce: doc. RNDr. Roman Grill, CSc.

E-mail vedoucího: grill@karlov.mff.cuni.cz

Abstrakt: V této teoretické práci je představena podrobná studie optických vlastností excitonů v dvojitých kvantových jamách umístěných v magnetickém a electrickém poli. Vycházejíce ze známých Luttingerových vztahů popisujících reálnou strukturu valečního pásu polovodičových sloučenin typu III-V, rozvinuli jsme efektivní způsob řešení Schrödingerovy rovnice pro coulombicky vázaný pár elektron-díra tvořící exciton. Odvozené vztahy byly ilustrovány na odpovídajících obrázcích, dávajíce nám možnost lépe porozumět efektům vnějších polí na studovaný systém. Byly spočteny disperzní relace, posun energetických hladin v elektrickém poli, absorpční a luminiscenční spektra i rozložení nábojové hustoty, a dosažené výsledky byly podrobně diskutovány.

Klíčová slova: exciton, dvojitá kvantová jáma, vázané kvantové jámy, Luttingerův (-Kohnův) hamiltonián, míchání stavů ve valenčním pásu

Title: Magnetooptical Properties of Semiconductor Quantum Structures

Author: Štěpán Uxa

Department: Institute of Physics of Charles University

Supervisor: Assoc. Prof. Roman Grill, PhD

Supervisor's e-mail address: grill@karlov.mff.cuni.cz

Abstract: In this theoretical work, a detailed study of optical properties of excitons in double quantum wells subject to magnetic and electric fields is presented. Starting from the well-known Luttinger formulae describing the real valence-band structure of III-V semiconductor compounds, we developed an efficient way to solve the Schrödinger equation of a coulombically-bound pair electron-hole forming an exciton. Derived formulae were illustrated on relevant figures, giving us an opportunity to better understand the effects of external fields on the studied system. Dispersion relations, the shift of energy levels in an electric field, absorption and photoluminescence spectra, and charge density distribution were calculated and achieved results were discussed in detail.

Keywords: exciton, double quantum well, coupled quantum wells, Luttinger (-Kohn) hamiltonian, valence-subband mixing

Chapter 1

Introduction

In 1972, Charles H. Henry realized that there is a complete analogy between the confinement of light by a slab waveguide and the confinement of electron by the potential well formed in the conduction band of a double heterostructure, created from two semiconductors with different bandgaps. He calculated that the quantization of energy states in a quantum well (QW) alters the density of states (and thus optical absorption as well) that instead of increasing smoothly as in bulk materials, would have a step-like character. His predictions were experimentally verified in 1973 by R. Dingle on a thin heterostructure, which was made by W. Wiegmann using molecular beam epitaxy (MBE) [1]. Henry and his colleagues as well as other physicist all over the world have been further developing the idea, resulting in a construction of the first quantum-well laser in 1977.

In following years, advanced epitaxial techniques such as MBE or metal-organic chemical vapour deposition (MOCVD) have made it possible to grow interfaces between two semiconductors flat up to one atomic monolayer. The possibility of fabricating a heterostructure of strictly-defined parameters, a quasi-two-dimensional nature and sharp density of states, has stimulated both theoretical and experimental research and shortly found various applications: LEDs, diode lasers (including blue laser), high electron mobility transistors (HEMTs), infrared photodetectors, etc. The most popular materials for heterostructure growth are ternary (pseudo-binary) compounds of GaAs and AlAs, since they are perfectly lattice-matched. By changing the amount x of Al in $Al_xGa_{1-x}As$, the bandgap width can be changed linearly for $x < 0.45$ [2] to set the proper value for optical or optoelectronic applications.

The most simple heterostructure is a single QW. If there are two QWs close to each other to make mutual interaction possible, we talk about coupled quantum wells or, in other words, a double quantum well (DQW). It will be of main interest in this thesis. The reason for why DQWs have been intensively studied is the strong dependence of optical and electrical properties of heterostructures, including DQWs, on applied external fields. The existence of excitons, bound states of electrons and holes, in DQWs is also important since their binding energy in low-dimensional structures is much larger than in the bulk.

There is a large number of published results related to electrical and optical properties of excitons in DQWs. Well-known works of Baldereschi and Lipari [3] and Altarelli and

4

Lipari [4] from early 1970s are available as well as the latter work of Gorbatsevich and Tokatly [5]. Excitonic properties in the electric field have been studied by Sanders and Bajaj in [6], Dignam and Sipe [7] and Soubusta *et al.* [8]. The effect of the perpendicular magnetic field has been investigated e. g. by Lyo [9], that of the in-plane magnetic field has been published by Orlita *et al.* in [10, 11]. A lot of other works exist.

Apart from many research facilities all over the world, Institute of Physics of Charles University in Prague in cooperation with Institute of Physics of the Academy of Sciences of the Czech Republic and Institute of Technical Physics I of Friedrich-Alexander University in Erlangen, Germany, participates in a long-standing fundamental research of DQW systems. The aim of this work is to develop an efficient way of solving the Schrödinger equation of an exciton in a DQW and then calculate theoretical absorption and photoluminescence spectra. Starting from Grochol [12], who followed the procedure proposed in [5], this approach is generalized to include the real valence-band structure. The results are presented in such a way to make it possible to compare them with available experimental data.

Chapter 2

General properties of III-V compounds

In this chapter, some remarks concerning crystalline and electrical properties, dispersion relations and band structure of electrons and holes, as well as a general overview of well-known models and common techniques of solving related problems in both bulk materials and heterostructures, will be given. Though it is thoroughly studied in [13], the most important results are reviewed in the first four sections of this chapter.

2.1   Crystalline and electronic properties

The III-V compounds crystallize in the zinc-blende (sphalerite) structure consisting of two interpenetrating face-centred cubic lattices, displaced from one another by a fourth of the one of the cube main diagonals. The elementary cell contains two atoms. The reciprocal lattice of the Bravais lattice corresponding to a zinc-blende structure is a body centred cubic lattice, the first Brillouin zone of which is a truncated octahedron, see Fig. 2.1. Several high symmetry points of the first Brillouin zone have received specific notations, e. g. the Γ, X or L points, however, the most important of them for us will be the Γ point, representing the centre of the reciprocal (momentum) space.

In III-V binary compounds like GaAs, there are eight outer electrons per unit cell, which contribute to the chemical bonds and are responsible for electrical and optical properties. They hybridize to form tetrahedral bonds between one kind of atom and its four nearest neighbours. Since there is a large number of unit cells, bonding and antibonding levels, originating from the interaction between s-like or p-like orbitals of each two neighbouring atoms, broaden into bands. The bonding s-levels are deeply bound and always occupied by two electrons per unit cell, the remaining six electrons per unit cell completely fill the three bonding p-orbitals. The antibonding orbitals are all empty, the lowest-lying one, always s-like, forms the conduction band of the material.

The top of the valence band in all III-V materials is at the centre of the Brillouin zone (Γ point). The three valence p-like bands are affected by the spin-orbit coupling, giving rise
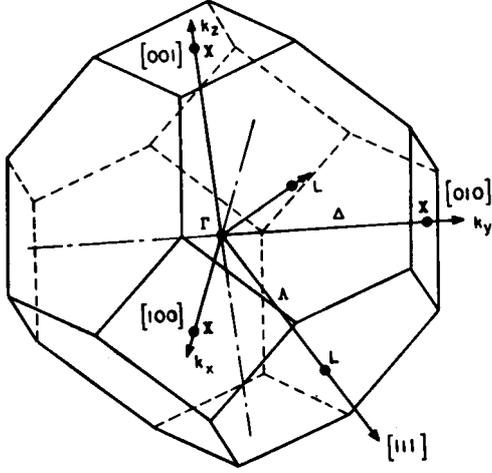
Figure 2.1: The first Brillouin zone of the reciprocal lattice of a semiconductor with the zinc-blende structure, [13].
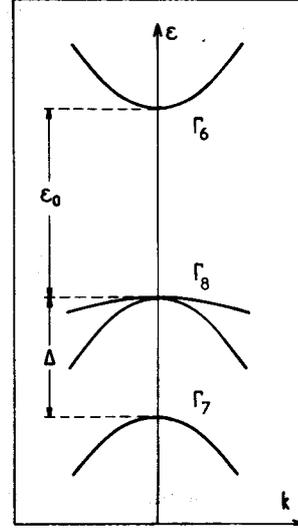
Figure 2.2: Band structure of a direct-bandgap semiconductor in the vicinity of the centre of the first Brillouin zone, [13].

to a quadruplet (symmetry Γ_8) corresponding to the total angular momentum of $J = \frac{3}{2}$, and to a doublet (symmetry Γ_7) associated with $J = \frac{1}{2}$.

The conduction band edge of III-V compounds (symmetry Γ_6) is found either at the Γ point or near the L or the X point. In GaAs, it is located at the Γ point and since the top of the valence band is at the centre of the Brillouin zone as well (see Fig. 2.2), this compound has the "direct-bandgap" structure, making it a good material for optoelectronic applications. In AlAs, the conduction band edge occurs near the X point, resulting in the "indirect-bandgap" structure. Several parameters of these two binary compounds are summarized in Tab. 2.1.

However, not only binary compounds of various III-V elements could be created, it is also possible to form ternary (pseudo-binary) solid solutions of III-V (or II-VI) binaries. Although they are actually not crystalline from the electronic structure point of view (since there is no translantional symmetry due to the random distribution of atoms at the sites of the zinc-blende lattice), one may use so called virtual crystal approximation to describe electronic states of such an alloy. For example: in $AB_{1-x}C_x$ alloy, the actual potential V is replaced by an average potential $\langle V \rangle$ of the form $\langle V \rangle = V_A + (1 - x)V_B + xV_C$, where $V_{A(B,C)}$ are potentials created by A (B, C) atoms separately. Since it is periodic, the translational invariance is restored, enabling us to introduce Bloch functions, the Brillouin zone, etc. $Al_xGa_{1-x}As$ is a nice example of such a compound. The bandgap width E_g^{AlGaAs} at $T = 300$ K is given by [2]

$$E_g^{\text{AlGaAs}} = \begin{cases} 1.424 + 1.247x & x < 0.45 \\ 1.900 + 0.125x + 0.143x^2 & x > 0.45 \end{cases} \text{ eV,} \qquad (2.1)$$

Table 2.1: Low temperature parameters of GaAs and AlAs according to [13, 14, 15].

parameter	GaAs	AlAs
ϵ (eV)	1.5192	3.13
Δ (eV)	0.341	0.275
a (nm)†	5.6533	5.6610
m_{Γ_6}/m_0	0.0665	0.15
m_{hh}/m_0	0.34*	0.76
m_{lh}/m_0	0.094	0.137
m_{SO}/m_0	0.15	0.24
bandgap	direct	indirect

†Values for the room temperature $T = 300$ K.
*Mean value as the heavy-hole subband in not rotationally parabolic.

while for the electron effective mass m_e^{AlGaAs} at the room temperature, we have [2]

$$m_e^{\text{AlGaAs}} = (0.063 + 0.083x)m_0 \qquad x < 0.45. \tag{2.2}$$

We see that for $x < 0.45$, the bandgap width, as well as the electron effective mass, increases linearly, proving that the virtual crystal approximation is well applicable. To proceed further, let us take a look at the electronic band structure.

2.2 Electronic dispersion relations in the vicinity of the zone centre

In a bulk crystal, the one-electron Schrödinger equation is [13]:

$$\left[\frac{\hat{\mathbf{p}}^2}{2m_0} + V(\mathbf{r}) + \frac{\hbar}{4m_0^2 c^2}(\boldsymbol{\sigma} \times \nabla V) \cdot \hat{\mathbf{p}} + \mathcal{H}_r \right] \psi(\mathbf{r}) = \mathcal{E}\psi(\mathbf{r}), \tag{2.3}$$

where m_0 is the free-electron mass, $\boldsymbol{\sigma}$ is the vector of Pauli spin matrices, and $V(\mathbf{r})$ is the periodic crystalline potential. The third and fourth terms in the latter equation are relativistic corrections: the spin-orbit coupling, and so called mass-velocity and Darwin corrections included in the last term, $\mathcal{H}_r$.

The solution of Eq. (2.3) can be written in the Bloch form [13, 16]

$$\psi_{n\mathbf{k}}(\mathbf{r}) = N u_{n\mathbf{k}}(\mathbf{r}) \exp(\mathrm{i}\,\mathbf{k} \cdot \mathbf{r}), \tag{2.4}$$

if N is a normalization constant and $u_{n\mathbf{k}}(\mathbf{r})$ is a function with the periodicity of the lattice. Eq. (2.4) is usually normalized over the volume of the crystal.

Neglecting the relativistic terms other than the spin-orbit coupling, the periodic parts $u_{n\mathbf{k}}(\mathbf{r})$ of the Bloch functions are the solutions of

$$\left[\frac{\hat{\mathbf{p}}^2}{2m_0} + V(\mathbf{r}) + \frac{\hbar}{4m_0^2 c^2}(\boldsymbol{\sigma} \times \nabla V) \cdot \hat{\mathbf{p}} + \frac{\hbar^2 k^2}{2m_0} \right.$$
$$\left. + \frac{\hbar \mathbf{k}}{m_0} \cdot \left(\mathbf{p} + \frac{\hbar}{4m_0 c^2} \boldsymbol{\sigma} \times \nabla V \right) \right] u_{n\mathbf{k}}(\mathbf{r}) = \mathcal{E}_{n\mathbf{k}} u_{n\mathbf{k}}(\mathbf{r}). \quad (2.5)$$

Since the $\mathbf{k}$-dependent terms in Eq. (2.5) commute with translation operator and vanish for $\mathbf{k} = \mathbf{0}$, we can expand the solution of Eq. (2.5) in the following form:

$$u_{n\mathbf{k}}(\mathbf{r}) = \sum_m c_m(\mathbf{k}) u_{m\mathbf{0}}(\mathbf{r}). \quad (2.6)$$

After the insertion of the latter expansion into Eq. (2.5), multiplication by $u_{l\mathbf{0}}^*(\mathbf{r})$ and integration over a unit cell, one obtains

$$\sum_m \left[\left(\mathcal{E}_{n\mathbf{0}} - \mathcal{E}_{n\mathbf{k}} + \frac{\hbar^2 k^2}{2m_0} \right) \delta_{nm} + \frac{\hbar \mathbf{k}}{m_0} \cdot \langle n\mathbf{0}|\mathbf{p} + \frac{\hbar}{4m_0 c^2}(\boldsymbol{\sigma} \times \nabla V)|m\mathbf{0}\rangle \right] c_m(\mathbf{k}) = 0, \quad (2.7)$$

where as usual

$$\langle n\mathbf{0}|\mathbf{p} + \frac{\hbar}{4m_0 c^2}(\boldsymbol{\sigma} \times \nabla V)|m\mathbf{0}\rangle = \int_{\text{unit cell}} u_{n\mathbf{0}}^* \left(\mathbf{p} + \frac{\hbar}{4m_0 c^2}(\boldsymbol{\sigma} \times \nabla V) \right) u_{m\mathbf{0}} \, \mathrm{d}^3 \mathbf{r}. \quad (2.8)$$

Eq. (2.7) is well suited for a perturbative approach. Supposing that the nth band edge is non-degenerate (apart from spin), we can assume that $c_m(\mathbf{k})$'s are small in comparison to $c_n(\mathbf{k})$ and that they are proportional to $\mathbf{k}$ (and thus vanish for $\mathbf{k} = \mathbf{0}$), since $c_m(\mathbf{0}) = \delta_{nm}$. Therefore, we have

$$c_m(\mathbf{k}) = \frac{\hbar \mathbf{k}}{m_0} \cdot \boldsymbol{\pi}_{nm} \frac{1}{\mathcal{E}_{n\mathbf{0}} - \mathcal{E}_{m\mathbf{0}}} \quad (2.9)$$

in the first order of the perturbation theory, while

$$\mathcal{E}_{n\mathbf{k}} = \mathcal{E}_{n\mathbf{0}} + \frac{\hbar^2 k^2}{2m_0} + \frac{\hbar^2}{m_0^2} \sum_{m \neq n} \frac{|\boldsymbol{\pi}_{nm} \cdot \mathbf{k}|^2}{\mathcal{E}_{n\mathbf{0}} - \mathcal{E}_{m\mathbf{0}}} \quad (2.10)$$

gives the second order correction to energy, if the vector $\boldsymbol{\pi}$ is defined as

$$\boldsymbol{\pi} = \mathbf{p} + \frac{\hbar}{4m_0 c^2}(\boldsymbol{\sigma} \times \nabla V). \quad (2.11)$$

Because we have restricted our considerations to small $\mathbf{k}$'s, under the assumption that the band edge gaps $\mathcal{E}_{n\mathbf{0}} - \mathcal{E}_{m\mathbf{0}}$ are much larger than $\mathcal{E}_{n\mathbf{k}} - \mathcal{E}_{n\mathbf{0}}$, one can rewrite Eq. (2.10) in the following form:

$$\mathcal{E}_{n\mathbf{k}} = \mathcal{E}_{n\mathbf{0}} + \frac{\hbar^2}{2} \sum_{\alpha,\beta} k_\alpha \frac{1}{\mu_n^{\alpha\beta}} k_\beta, \qquad \alpha, \beta = x, y, z, \quad (2.12)$$

where

$$\frac{1}{\mu_n^{\alpha\beta}} = \frac{1}{m_0}\delta_{\alpha\beta} + \frac{2}{m_0^2}\sum_{n\neq m}\frac{\pi_{mn}^{\alpha}\pi_{nm}^{\beta}}{\mathcal{E}_{n\mathbf{0}} - \mathcal{E}_{m\mathbf{0}}} \tag{2.13}$$

is the effective mass tensor of the nth band edge in the vicinity of the zone centre.

2.3   Kane model

To better describe the band structure of III-V semiconductors, another way of solving Eq. (2.5) is known. Since in III-V compounds the bandgap width is relatively small and the lowest-lying conduction band and the three topmost valence bands are far enough from the other bands, according to Eq. (2.10), the influence of further bands is only of a small effect. Thus, Kane [17] came up with an idea to diagonalize $\mathbf{k} \neq \mathbf{0}$ terms of Eq. (2.5) in a basis formed from linear combinations of $\mathbf{k} = \mathbf{0}$ eigenfunctions associated with these four bands ($|S\uparrow\rangle$, $|S\downarrow\rangle$, $|X\uparrow\rangle$, $|X\downarrow\rangle$, $|Y\uparrow\rangle$, $|Y\downarrow\rangle$, and $|Z\uparrow\rangle$, $|Z\downarrow\rangle$). These functions are such that the total angular momentum $\mathbf{J} = \mathbf{L} + \boldsymbol{\sigma}$ and its projection J_z along the z axis are diagonal in the new basis. For the S edge, the addition of $L = 0$ and $\sigma = \frac{1}{2}$ only gives $J = \frac{1}{2}$ (Γ_6 symmetry), however, for the P edges, adding $L = 1$ to $\sigma = \frac{1}{2}$ gives either $J = \frac{3}{2}$ (Γ_8 symmetry) or $J = \frac{1}{2}$ (Γ_7 symmetry). In III-V compounds, the quadruplet $J = \frac{3}{2}$ ($m_J = \pm\frac{3}{2}, \pm\frac{1}{2}$) is always higher in energy than the doublet $J = \frac{1}{2}$ ($m_J = \pm\frac{1}{2}$). The energy separation of Γ_6 and Γ_8 bands at the zone centre is noted $\mathcal{E}_0$, that of Γ_8 and Γ_7 bands is Δ:

$$\mathcal{E}_0 = \mathcal{E}_{\Gamma_6} - \mathcal{E}_{\Gamma_8}, \tag{2.14}$$
$$\Delta = \mathcal{E}_{\Gamma_8} - \mathcal{E}_{\Gamma_7}, \tag{2.15}$$

compare with Fig. 2.2. With the help of one additional parameter P, which is defined by equation

$$P = -\frac{\mathrm{i}}{m_0}\langle S|\hat{p}_x|X\rangle = -\frac{\mathrm{i}}{m_0}\langle S|\hat{p}_y|Y\rangle = -\frac{\mathrm{i}}{m_0}\langle S|\hat{p}_z|Z\rangle, \tag{2.16}$$

dispersion relations $\mathcal{E}(\mathbf{k})$ of the bands under consideration can be found, for more details please refer to [13]. For illustration, the effective masses of particular band edges obtained in the Kane model are

$$\frac{1}{m_{\Gamma_6}} = \frac{1}{m_0} + \frac{4P^2}{3\mathcal{E}_0} + \frac{2P^2}{3(\mathcal{E}_0 + \Delta)}, \tag{2.17}$$

$$\frac{1}{m_{\Gamma_7}} = \frac{1}{m_0} - \frac{2P^2}{3(\mathcal{E}_0 + \Delta)}, \tag{2.18}$$

$$\frac{1}{m_{\Gamma_8}^l} = \frac{1}{m_0} - \frac{4P^2}{3\mathcal{E}_0}. \tag{2.19}$$

Note that $m_{\Gamma_6} > 0$ and m_{Γ_7}, $m_{\Gamma_8}^l < 0$. The effective heavy-hole mass is the same as the free-electron mass, $m_{\Gamma_8}^h = m_0$. To achieve better results, it is necessary to include higher bands [17].

2.4 Envelope function approximation

As we have been so far interested in bulk materials only, we will turn our attention to heterostructures from now on. Modern epitaxial techniques (MBE, MOCVD) have made it possible to grow interfaces between two semiconductors flat up to one atomic monolayer. It is common to represent such an ideal interface in terms of a continuously varying position-dependent band edge that varies slowly in comparison to the lattice constant, assuming a perfectly bi-dimensional growth. Hence, an electron moving from one material (A) to the other material (B) across the interface experiences one-electron potential of a perfect bulk material A, whereas on the other side on the interface, its motion is determined by one-electron potential of a perfect bulk material B.

We suppose that both materials forming the heterostructure are perfectly lattice-matched and of the same crystallographic structure, which is true for GaAs/AlGaAs based heterostructures. There are two key assumptions made for the envelope function approximation [13]:

- Inside each layer, the wavefunction is expanded to the periodic parts of the Bloch functions of the edges under consideration:

$$\psi(\mathbf{r}) = \sum_l f_l^{A(B)}(\mathbf{r}) u_{l\mathbf{k}_0}^{A(B)}(\mathbf{r}), \qquad (2.20)$$

  where $\mathbf{k}_0$ is the point in the Brillouin zone, around which the heterostructure states are built, and the summation over l runs over all states included in calculations.

- The periodic parts of the Bloch functions are assumed to be the same in each layer that constitutes the heterostructure:

$$u_{l\mathbf{k}_0}^A(\mathbf{r}) \equiv u_{l\mathbf{k}_0}^B(\mathbf{r}) \equiv u_{l\mathbf{k}_0}(\mathbf{r}). \qquad (2.21)$$

Our objective will be to find $f_l^{A(B)}(\mathbf{r})$. According to [13], the truncation of summation in Eq. (2.20) to a finite number of band edges means that the heterostructure states are built with the host wavevectors $\mathbf{k}_A$, $\mathbf{k}_B$, which are close to $\mathbf{k}_0$. It was proven that in both GaAs and AlAs, the conduction- and valence-band states are fairly well reproduced by the Kane model. As the lattice constant is assumed to be the same in both layers, the heterostructure is translationally invariant, which results in the factorization of $f_l^{A(B)}(\mathbf{r})$ into:

$$f_l^{A(B)}(\mathbf{r}_\parallel, z) = \frac{1}{\sqrt{S}} \exp(i\,\mathbf{k}_\parallel \cdot \mathbf{r}_\parallel) \chi_l^{A(B)}(z), \qquad (2.22)$$

where S is the sample area and $\mathbf{k}_\parallel = (k_x, k_y)$ is a bi-dimensional wavevector, which is the same in A and B layers. Therefore, the wavefunction (2.20) is a sum of rapid-varying functions $u_{l\mathbf{k}_0}(\mathbf{r})$ and slowly-varying envelope functions $f_l^{A(B)}(\mathbf{r})$.

The heterostructure hamiltonian $\hat{H}$ takes the form of [13]

$$\hat{H} = \frac{\hat{\mathbf{p}}^2}{2m_0} + V_A(\mathbf{r})\theta_A(\mathbf{r}) + V_B(\mathbf{r})\theta_B(\mathbf{r}), \qquad (2.23)$$

where $V_{A(B)}(\mathbf{r})$ is one-electron potential of layer A (B) and $\theta_{A(B)}(\mathbf{r})$ is a step function, which is unity in layer A (B) and zero otherwhere. If we let this hamiltonian act upon $\psi(\mathbf{r})$, multiply it by the complex conjugate and integrate over space, we will obtain the set of eigenvalue equations:

$$\mathbf{D}^{(0)}\left(z, -\mathrm{i}\hbar\frac{\partial}{\partial z}\right)\boldsymbol{\chi} = \mathcal{E}\boldsymbol{\chi}, \tag{2.24}$$

where $\mathbf{D}^{(0)}$ is an $N \times N$ matrix and $\boldsymbol{\chi}$ is an N–dimensional column vector, if N denotes the number of band edges retained in Eq. (2.20). The $\mathbf{D}^{(0)}$ matrix elements $D_{lm}^{(0)}$ are functions of z and $\frac{\partial}{\partial z}$ so that

$$D_{lm}^{(0)}\left(z, \frac{\partial}{\partial z}\right) = \left(\mathcal{E}_{l\mathbf{0}}^{A}\,\theta_A(\mathbf{r}) + \mathcal{E}_{l\mathbf{0}}^{B}\,\theta_B(\mathbf{r}) + \frac{\hbar^2 k_\parallel^2}{2m_0} - \frac{\hbar^2}{2m_0}\frac{\partial^2}{\partial z^2}\right)\delta_{lm}$$
$$+ \frac{\hbar\mathbf{k}}{m_0}\cdot\langle l|\hat{\mathbf{p}}_\parallel|m\rangle - \frac{\mathrm{i}\hbar}{m_0}\langle l|\hat{p}_z|m\rangle\frac{\partial}{\partial z}, \tag{2.25}$$

since

$$\hat{H}u_{l\mathbf{0}}(\mathbf{r}) = \left(\mathcal{E}_{l\mathbf{0}}^{A}\,\theta_A(\mathbf{r}) + \mathcal{E}_{l\mathbf{0}}^{B}\,\theta_B(\mathbf{r})\right)u_{l\mathbf{0}}(\mathbf{r}). \tag{2.26}$$

The matrix element of $\hat{\mathbf{p}}_\parallel$ in Eq. (2.25) is treated in a usual way. The larger N, the more accurate the results will be. In practice, N is restricted to eight since studying the heterostructure states attached to Γ_6, Γ_7, and Γ_8 bands of the host materials. Inclusion of higher bands is treated as the second order correction in $\hat{\mathbf{p}}$ applied on $\mathbf{D}^{(0)}$, hence, instead of $\mathbf{D}^{(0)}$, we have

$$\mathbf{D} = \mathbf{D}^{(0)} - \frac{\hbar^2}{2}\sum_{\alpha,\beta}\frac{\partial}{\partial r_\alpha}\frac{1}{M^{\alpha\beta}}\frac{\partial}{\partial r_\beta}, \tag{2.27}$$

where $\alpha, \beta = x, y, z$ and $M^{\alpha\beta}$, an 8×8 matrix, is given by

$$\frac{1}{M_{lm}^{\alpha\beta}} = \frac{2}{m_0^2}\sum_\nu\langle l|\hat{p}_\alpha|\nu\rangle\frac{1}{\bar{\mathcal{E}} - \mathcal{E}_{\nu\mathbf{0}}^{A} - V_\nu(z)}\langle l|\hat{p}_\beta|\nu\rangle, \tag{2.28}$$

while $\bar{\mathcal{E}}$ is an average energy of the Γ_6, Γ_7, Γ_8 set in the heterostructure and $V_\nu(z)$ defines the energy shift of the νth band edge when going from the A to the B material [13]:

$$V_\nu(z) = \begin{cases} 0 & \text{if } z \text{ corresponds to the A layer,} \\ \mathcal{E}_\nu^B - \mathcal{E}_\nu^A & \text{if } z \text{ corresponds to the B layer.} \end{cases} \tag{2.29}$$

The problem of the heterostructure energy levels has been reduced to the solution of a set of second-order partial differential equations for the slowly-varying envelope functions. The microscopic details of the heterostructure have disappeared being substituted by effective parameters: the interband matrix elements $\langle l|\hat{\mathbf{p}}|m\rangle$, the effective mass tensor $M_{lm}^{\alpha\beta}$ and the band offsets V_ν.

The presented procedure can further be developed assuming different effective masses in layers A and B of the heterostructure, while restricted to the parabolic bands. It is

called the Ben Daniel-Duke model and is well applicable to electronic states in quantum wells (QWs). One of the results provided by the model is the different effective mass in the QW plane and in the direction perpendicular to it (i. e. in the growth direction). However, its applicability to holes is limited. For more details, please see [13]. How to describe the real structure of the valence band, including so called valence-subband mixing of light- and heavy-hole states, will be demonstrated in the next section.

2.5 Luttinger hamiltonian

It was shown by Luttinger in his works [18, 19] that the hamiltonian of a hole in the valence band of a semiconductor with $\mathcal{T}_d$ symmetry, written in the basis composed of the eigenfunctions of the total angular momentum, takes the form of a 4×4 matrix

$$
\hat{\mathbb{H}}_h = \begin{pmatrix} \hat{H}_{hh} & \hat{b} & \hat{c} & 0 \\ \hat{b}^* & \hat{H}_{lh} & 0 & \hat{c} \\ \hat{c}^* & 0 & \hat{H}_{lh} & -\hat{b} \\ 0 & \hat{c}^* & -\hat{b}^* & \hat{H}_{hh} \end{pmatrix} \begin{array}{|l} |\frac{3}{2},+\frac{3}{2}\rangle \\ |\frac{3}{2},+\frac{1}{2}\rangle \\ |\frac{3}{2},-\frac{1}{2}\rangle \\ |\frac{3}{2},-\frac{3}{2}\rangle \end{array} . \tag{2.30}
$$

The ket-vectors on the right side of Eq. (2.30) show the chosen order of the eigenfunctions which will be kept throughout the work. The terms $\hat{H}_{hh}$ $\hat{H}_{lh}$, $\hat{b}$, and $\hat{c}$ are given as follows

$$
\hat{H}_{hh} = \frac{\gamma_1 - 2\gamma_2}{2m_0}\hat{p}_z^2 + \frac{\gamma_1 + \gamma_2}{2m_0}\left(\hat{p}_x^2 + \hat{p}_y^2\right), \tag{2.31}
$$

$$
\hat{H}_{lh} = \frac{\gamma_1 + 2\gamma_2}{2m_0}\hat{p}_z^2 + \frac{\gamma_1 - \gamma_2}{2m_0}\left(\hat{p}_x^2 + \hat{p}_y^2\right), \tag{2.32}
$$

$$
\hat{b} = -\frac{\sqrt{3}\gamma_3}{2m_0}\left[(\hat{p}_y\hat{p}_z + \hat{p}_z\hat{p}_y) + \mathrm{i}(\hat{p}_x\hat{p}_z + \hat{p}_z\hat{p}_x)\right], \tag{2.33}
$$

$$
\hat{c} = \frac{\sqrt{3}}{2m_0}\left[\gamma_2(\hat{p}_x^2 - \hat{p}_y^2) - \mathrm{i}\gamma_3(\hat{p}_x\hat{p}_y + \hat{p}_y\hat{p}_x)\right], \tag{2.34}
$$

where γ_i are so called Luttinger parameters describing the coupling between Γ_8 and all the hosts' edges (including Γ_6) and which are considered to be position-independent, $\hat{p}_j = -\mathrm{i}\hbar\frac{\partial}{\partial r_j}$, $j = x, y, z$ denotes the corresponding component of the momentum operator $\hat{\mathbf{p}}$. To simplify our model, we neglect single-particle g-factors of both electrons and holes. Consequently, the terms (2.33) and (2.34) are both symmetrized, which means we write $\frac{1}{2}(\hat{p}_x\hat{p}_y + \hat{p}_y\hat{p}_x)$ instead of writing $\hat{p}_x\hat{p}_y$, and analogically for $\hat{p}_x\hat{p}_z$ and $\hat{p}_y\hat{p}_z$.

In the presence of external fields, it is necessary to make the substitution

$$
\hat{\mathbf{p}} \leftrightarrow \hat{\mathbf{p}} - e\mathbf{A} \tag{2.35}
$$

to involve the magnetic field. The electric field is included by the addition of $e\tilde{\varphi}$, where e denotes the electronic charge ($e = 1.602 \times 10^{-16}$ C), while $\mathbf{A}$ marks the magnetic vector
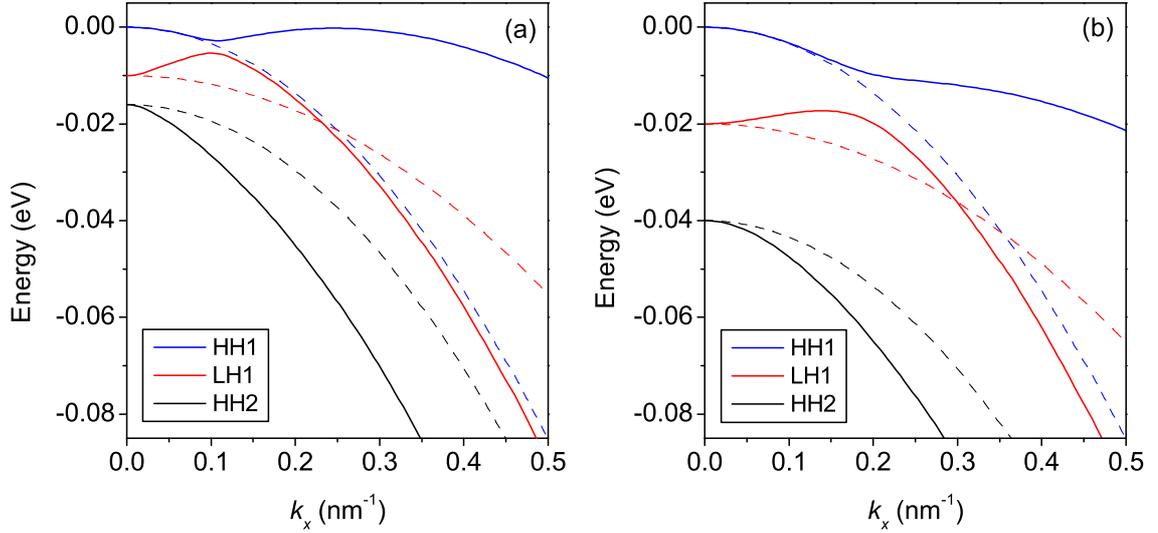
Figure 2.3: In-plane dispersion relations of a hole in a single QW computed for $\gamma_1 = 6.85$, $\gamma_2 = 2.10$, and $\gamma_3 = 2.90$. The well width is $L = 10$ nm and the QW bound energies are chosen to be $E_{\mathrm{HH1}}^{(0)} = 0$, $E_{\mathrm{LH1}}^{(0)} = -0.01$ eV, $E_{\mathrm{HH2}}^{(0)} = -0.016$ eV (a), and $E_{\mathrm{HH1}}^{(0)} = 0$, $E_{\mathrm{LH1}}^{(0)} = -0.02$ eV, $E_{\mathrm{HH2}}^{(0)} = -0.04$ eV (b).

potential and $\tilde{\varphi}$ is the electric potential. The specific choice of these quantities will be discussed later. For electrons, the sign of e is opposite.

To demonstrate the valence-subband mixing, energy levels in a single rectangular quantum well have been calculated using the Luttinger hamiltonian (2.30) for the following set of parameters: $\gamma_1 = 6.85$, $\gamma_2 = 2.10$, and $\gamma_3 = 2.90$. To preserve the standard valence-band scheme, the energies shown in Fig. 2.3 are taken negative. Solid line depicts the eigenvalues of Eq. (2.30), whereas dashed line is used for parabolic dispersion relations, which are the eigenvalues of the diagonal part of Eq. (2.30). Strong valence-subband mixing is responsible for an upward-bending of the light-hole dispersion line, resulting in the negative effective mass of a light-hole in the vicinity of the origin. Valence-subband coupling also prevents the dispersion lines from crossing one another, giving rise to the anti-crossing effect.

Chapter 3

Excitons in III-V compounds

Electrons in the conduction band are electrically charged particles. The same holds for holes in the valence band. When a semiconductor with direct bandgap is shone by light with a wavelength near the bandgap width, these oppositely charged particles are generated. Because of the Coulomb interaction, electron-hole bound states can be created. Such states are called *excitons*.

3.1   Excitons in idealized bulk materials

To show how the Coulomb interaction affects crystalline states, analogously to [13], we consider a bulk semiconductor, the band structure of which can be approximated by a single spherical conduction band with dispersion relation

$$\epsilon_c(\mathbf{k}) = E_g + \frac{\hbar^2 k^2}{2m_c},$$
(3.1)

separated by the bandgap E_g from a single spherical valence band with dispersion relation

$$\epsilon_v(\mathbf{k}) = -\frac{\hbar^2 k^2}{2m_v},$$
(3.2)

where m_c and m_v are corresponding effective masses. The ground state of the semiconductor is a state with completely filled valence band and empty conduction band. If an electron with a wavevector $\mathbf{k}_v$ is promoted to the conduction band, one place in the valence band is left unoccupied. The whole situation can equally be viewed as a fully filled valence band plus *a hole* with a wavevector $\mathbf{k}_h = -\mathbf{k}_v$, characterized by a positive mass $m_h = -m_v$ and a positive charge $+e$ [13]. Without the Coulomb interaction, the energy of the first excited crystalline state would be E_g. But as the coulombic interaction modifies the energy spectrum, the energy of the first excited state is determined by the solution of the equation

$$\left[\frac{\hat{\mathbf{p}}_e^2}{2m_e} + \frac{\hat{\mathbf{p}}_h^2}{2m_h} - \frac{e^2}{4\pi\epsilon|\mathbf{r}_e - \mathbf{r}_h|} \right] \psi(\mathbf{r}_e, \mathbf{r}_h) = (E - E_g)\psi(\mathbf{r}_e, \mathbf{r}_h),$$
(3.3)

where we have denoted $m_e \equiv m_c$, while ϵ is the static dielectric constant of the semiconductor. The structure of Eq. (3.3) is the same as of the Schrödinger equation describing the hydrogen atom and is treated in the same way. New coordinate system is defined:

$$\mathbf{r} = \mathbf{r}_e - \mathbf{r}_h, \tag{3.4}$$

$$\mathbf{R} = \frac{m_e\mathbf{r}_e + m_h\mathbf{r}_h}{m_e + m_h}, \tag{3.5}$$

$\mathbf{r}$ is then the relative distance between particles and $\mathbf{R}$ is the centre-of-mass position vector. The corresponding quantum-mechanical operators are given by the equations

$$\hat{\mathbf{p}} = -i\hbar\frac{\partial}{\partial\mathbf{r}}, \tag{3.6}$$

$$\hat{\mathbf{P}} = -i\hbar\frac{\partial}{\partial\mathbf{R}}. \tag{3.7}$$

After the introduction of the reduced mass μ of the electron-hole pair

$$\mu = \frac{m_e m_h}{m_e + m_h}, \tag{3.8}$$

it is straightforward to rewrite Eq. (3.3) in the following form:

$$\left[\frac{\hat{\mathbf{P}}^2}{2M} + \frac{\hat{\mathbf{p}}^2}{2\mu} - \frac{e^2}{4\pi\epsilon r}\right]\psi(\mathbf{r}, \mathbf{R}) = (E - E_g)\psi(\mathbf{r}, \mathbf{R}), \tag{3.9}$$

if $M = m_e + m_h$ marks the total mass of the exciton. The structure of the latter equation gives us a clue, in which form one should be looking for the solution of Eq. (3.9). Since $\mathbf{P} = \hbar\mathbf{K}$ is a good quantum number, we have

$$\psi(\mathbf{r}, \mathbf{R}) = \frac{1}{\sqrt{W}}\exp(i\mathbf{K}\cdot\mathbf{R})\varphi(\mathbf{r}), \tag{3.10}$$

where W is the volume of the crystal. After the substitution to Eq. (3.9), we are finally given

$$\left[\frac{\hat{\mathbf{p}}^2}{2\mu} - \frac{e^2}{4\pi\epsilon r}\right]\varphi(\mathbf{r}) = \mathcal{E}\varphi(\mathbf{r}), \tag{3.11}$$

a simple equation which has to be solved to obtain the excitonic energy spectrum, while

$$E = E_g + \frac{\hbar^2 K^2}{2M} + \mathcal{E}. \tag{3.12}$$

From the similarity to the quantum-mechanical description of the hydrogen atom, solutions of Eq. (3.11) are hydrogen-like wavefunctions. For the ground state, we have [13]

$$\varphi(\mathbf{r}) = \frac{1}{\sqrt{\pi a_B^3}}\exp(-r/a_B), \tag{3.13}$$

$$\mathcal{E} = -\frac{\mu e^4}{32\pi^2\epsilon^2\hbar^2}, \tag{3.14}$$
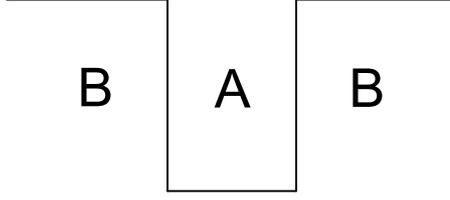
Figure 3.1: Idealized quantum well structure.

where $a_B = 4\pi\epsilon\hbar^2/\mu e^2$ is the excitonic effective Bohr radius. Eqs. (3.13)–(3.14) then determine the first excited crystalline state, the energy of which is smaller than the bandgap width E_g, $E < E_g$.

Therefore, the exciton can be viewed as a fictitious particle with mass $M = m_e + m_h$ composed of an electron and a hole orbiting around each other and whose centre-of-mass moves with kinetic energy $\hbar^2 K^2/2M$.

3.2 Excitons in idealized heterostructures

We have demonstrated how the Coulomb interaction modifies the energy spectrum of bulk materials. As it is of our interest in this thesis, let us show how the situation changes when proceeding from bulk crystals to quantum well structures.

Consider a slab of material A inserted between two layers of material B, see Fig. 3.1. Let us further assume that both materials have the same dielectric constant ϵ, effective masses m_e and m_h are equal in A and B and that dispersion relations in the valence and conduction bands are spherical and thus given by Eqs. (3.1)–(3.2). Under these assumptions, the Schrödinger equation of the system is [13]

$$\left[\frac{\hat{\mathbf{p}}_e^2}{2m_e} + \frac{\hat{\mathbf{p}}_h^2}{2m_h} - \frac{e^2}{4\pi\epsilon|\mathbf{r}_e - \mathbf{r}_h|} + U_e + U_h \right]\psi(\mathbf{r}_e, \mathbf{r}_h) = (E - E_g)\psi(\mathbf{r}_e, \mathbf{r}_h), \qquad (3.15)$$

where U_e and U_h are step-like quantum-well confining potentials for electrons and holes along the z axis.[1] The whole procedure performed in the previous section can be repeated once again, but with one difference now: it cannot be used in the z direction since the structure of Eq. (3.15), modified by the presence of U_e, U_h, is different from that of Eq. (3.3). Nevertheless, in the x, y directions, we can do so. We introduce the in-plane relative distance $\mathbf{r}_\parallel$ and the in-plane centre-of-mass position vector $\mathbf{R}_\parallel$ by formulae

$$\mathbf{r}_\parallel = \mathbf{r}_{e\parallel} - \mathbf{r}_{h\parallel}, \qquad (3.16)$$

$$\mathbf{R}_\parallel = \frac{m_e\mathbf{r}_{e\parallel} + m_h\mathbf{r}_{h\parallel}}{m_e + m_h}, \qquad (3.17)$$

---

[1]In a rectangular QW of infinite depth, these are constant inside the well, but zero otherwhere.

where $\mathbf{r}_{e\parallel} = (x_e, y_e)$ and $\mathbf{r}_{h\parallel} = (x_h, y_h)$ are the in-plane position vectors of an electron and a hole. It is easy to rewrite Eq. (3.15) into a new coordinate system, giving

$$\left[\frac{\hat{\mathbf{P}}_{\parallel}^2}{2M} + \frac{\hat{\mathbf{p}}_{\parallel}^2}{2\mu} - \frac{e^2}{4\pi\epsilon\sqrt{\rho^2 + (z_e - z_h)^2}} + U_e + U_h \right] \psi(\mathbf{r}_{\parallel}, \mathbf{R}_{\parallel}, z_e, z_h) = (E - E_g)\psi(\mathbf{r}_{\parallel}, \mathbf{R}_{\parallel}, z_e, z_h),$$
(3.18)

which implies that the factorization of $\psi(\mathbf{r}_{\parallel}, \mathbf{R}_{\parallel}, z_e, z_h)$ reads [13]

$$\psi(\mathbf{r}_{\parallel}, \mathbf{R}_{\parallel}, z_e, z_h) = \frac{1}{\sqrt{S}} \exp(i\mathbf{K}_{\parallel} \cdot \mathbf{R}_{\parallel}) \, \varphi(\mathbf{r}_{\parallel}, z_e, z_h),$$
(3.19)

if S is the sample area, $\rho = |\mathbf{r}_{\parallel}|$, and $\hat{\mathbf{p}}_{\parallel}$, $\hat{\mathbf{P}}_{\parallel}$ are the quantum-mechanical operators associated with $\mathbf{r}_{\parallel}$, $\mathbf{R}_{\parallel}$. Two methods have been attempted to solve Eq. (3.18) [13]: either by using Gaussian basis sets or non-linear variational parameters. In the second case, $\varphi(\mathbf{r}_{\parallel}, z_e, z_h)$ is written in the form [20]

$$\varphi(\mathbf{r}_{\parallel}, z_e, z_h) = N\chi_e(z_e)\chi_h(z_h) \exp\left(-\sqrt{\rho^2 + (z_e - z_h)^2}/\varsigma \right),$$
(3.20)

where N is a normalization constant, ς is the variational parameter, and $\chi_e(z_e)$ and $\chi_h(z_h)$ are the eigenfunctions of the conduction- and valence-band QWs, respectively.

The presented procedure is simple and easy to follow, however, it does not reflect the real valence-band structure, since the actual situation is a little more complicated. We will be concerned in this problem below.

3.3 Excitons in actual double quantum wells

In the following sections, we will derive important equations with the main goal to describe optical properties of excitons in DQWs, schematically depicted in Fig. 3.2. Let us start fair from the beginning.

3.3.1 Excitonic hamiltonian

To construct the hamiltonian of an exciton in a DQW that reflects the real structure of the valence band, we need nothing more than it has been written so far. Such a hamiltonian $\hat{\mathbb{H}}$ consists of five parts: the hole $\hat{\mathbb{H}}_h$ and the electronic $\hat{H}_e$ non-interacting hamiltonians, step-like DQW potentials U_e, U_h for electrons and holes, and the Coulomb interaction V. Therefore, after substituting from Eq. (2.30)

$$\hat{\mathbb{H}} = \hat{\mathbb{H}}_h + (\hat{H}_e + U_e + U_h + V)\mathbb{1} = \begin{pmatrix} \hat{H}_{hh} + \hat{\mathcal{H}} & \hat{b} & \hat{c} & 0 \\ \hat{b}^* & \hat{H}_{lh} + \hat{\mathcal{H}} & 0 & \hat{c} \\ \hat{c}^* & 0 & \hat{H}_{lh} + \hat{\mathcal{H}} & -\hat{b} \\ 0 & \hat{c}^* & -\hat{b}^* & \hat{H}_{hh} + \hat{\mathcal{H}} \end{pmatrix}, \quad (3.21)$$
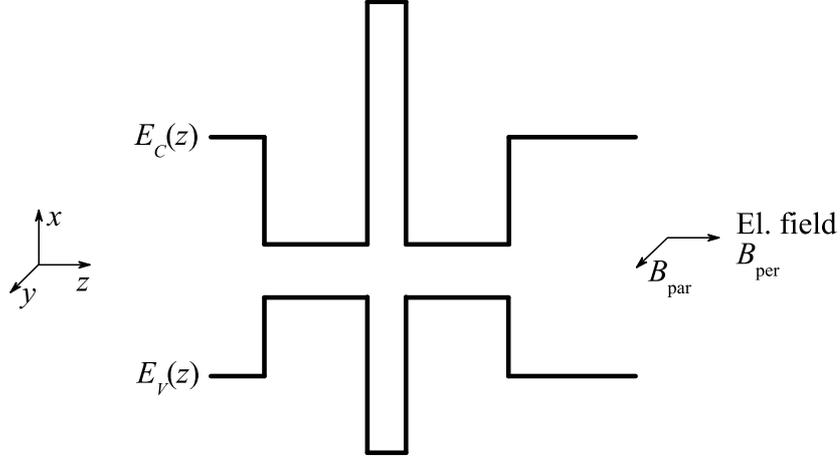
Figure 3.2: Simple scheme of a DQW structure and orientations of the coordinate system and external electric and magnetic fields.

where the symbol $\mathbb{1}$ stands for the 4×4 identity matrix and $\hat{\mathcal{H}} = \hat{H}_e + U_e + U_h + V$. The electronic hamiltonian $\hat{H}_e$ is as usual given by

$$\hat{H}_e = \frac{\hat{\mathbf{p}}_e^2}{2m_e} = \frac{\hat{p}_{z_e}^2}{2m_e} + \frac{\hat{p}_{x_e}^2 + \hat{p}_{y_e}^2}{2m_e}, \tag{3.22}$$

with the same "perpendicular" and "in-plane" effective mass.

The hamiltonian (3.21) acts on the four-component wavefunction

$$\Psi(\mathbf{r}_e, \mathbf{r}_h) = c_{|\frac{3}{2}, +\frac{3}{2}\rangle}(\mathbf{r}_e, \mathbf{r}_h) u_{|\frac{3}{2}, +\frac{3}{2}\rangle}(\mathbf{r}_h) u_e(\mathbf{r}_e) + c_{|\frac{3}{2}, +\frac{1}{2}\rangle}(\mathbf{r}_e, \mathbf{r}_h) u_{|\frac{3}{2}, +\frac{1}{2}\rangle}(\mathbf{r}_h) u_e(\mathbf{r}_e)$$
$$+ c_{|\frac{3}{2}, -\frac{1}{2}\rangle}(\mathbf{r}_e, \mathbf{r}_h) u_{|\frac{3}{2}, -\frac{1}{2}\rangle}(\mathbf{r}_h) u_e(\mathbf{r}_e) + c_{|\frac{3}{2}, -\frac{3}{2}\rangle}(\mathbf{r}_e, \mathbf{r}_h) u_{|\frac{3}{2}, -\frac{3}{2}\rangle}(\mathbf{r}_h) u_e(\mathbf{r}_e), \tag{3.23}$$

which is the solution of the time-independent Schrödinger equation

$$\hat{\mathbb{H}} \Psi(\mathbf{r}_e, \mathbf{r}_h) = E \Psi(\mathbf{r}_e, \mathbf{r}_h). \tag{3.24}$$

Functions $u_{|\frac{3}{2}, \pm\frac{1}{2}(\frac{3}{2})\rangle}(\mathbf{r}_h)$ are the periodic parts of the Bloch functions at the centre of the Brillouin zone (Γ point) describing valence-band light (heavy) hole states with Γ_8 symmetry,[2] function $u_e(\mathbf{r}_e)$ describes the electronic Γ_6 states in the conduction band. It can be found in [13] that

$$u_{|\frac{3}{2}, +\frac{3}{2}\rangle} = \frac{1}{\sqrt{2}} |(X + iY)\uparrow\rangle, \tag{3.25}$$

$$u_{|\frac{3}{2}, +\frac{1}{2}\rangle} = -\sqrt{\frac{2}{3}} |Z\uparrow\rangle + \frac{1}{\sqrt{6}} |(X + iY)\downarrow\rangle, \tag{3.26}$$

---

[2]These are the eigenfunctions of the total angular momentum, which is, as well as its projection along the z axis, diagonal in this basis.

$$u_{|\frac{3}{2},-\frac{1}{2}\rangle} = -\sqrt{\frac{2}{3}}|Z\downarrow\rangle - \frac{1}{\sqrt{6}}|(X-iY)\uparrow\rangle, \tag{3.27}$$

$$u_{|\frac{3}{2},-\frac{3}{2}\rangle} = \frac{1}{\sqrt{2}}|(X-iY)\downarrow\rangle, \tag{3.28}$$

where $|X\rangle$, $|Y\rangle$, and $|Z\rangle$ functions describe the crystal states for energies which correspond to the top of the occupied valence band. They are associated with wavefunctions which transform in the same way as the atomic x, y, and z functions under the symmetry operations that map the local tetrahedron ($\mathcal{T}_d$ symmetry group) onto itself. Arrows $\uparrow$ and $\downarrow$ show the spin orientation. For the electronic part, we have

$$u_e = i|S\uparrow\rangle \quad \text{or} \quad i|S\downarrow\rangle, \tag{3.29}$$

but from now on, we neglect the electron spin in our calculations. Function $|S\rangle$ describes the crystal state for energies which correspond to the bottom of the lowest-lying empty conduction band and transforms just like the previous functions do.

It was mentioned before that an external magnetic field is involved by performing the substitution (2.35) in hamiltonian (3.21). Our choice of the vector potential $\mathbf{A}$, analogous to that proposed in [5], is

$$\mathbf{A} = yB_\parallel\mathbf{e}_z + \frac{1}{2}\mathbf{e}_z \times \mathbf{r}B_\perp, \tag{3.30}$$

describing the general orientation of the magnetic field with magnitude $B_\perp$ in the growth direction and $B_\parallel$ in the DQW plane. The reason for such a choice will be clarified later.

Denoting the electric potential by symbol $\tilde{\varphi}$, an electric field acting on an electron (a hole) is described by term $\pm e\tilde{\varphi}$ added to the hamiltonian, if the lower sign holds for electrons and the upper one for holes. The homogenous electric field $\boldsymbol{\mathcal{E}}$ in the z direction, $\boldsymbol{\mathcal{E}} = \mathcal{E}\mathbf{e}_z$, is then characterized by the potential $\tilde{\varphi} = -\mathcal{E}z$. Therefore, for electrons we have $ez_e\mathcal{E}$, while $-ez_e\mathcal{E}$ is the corresponding term for holes.

We can now straightforwards rewrite the formulae (3.22) and (2.31)–(2.34), giving

$$\hat{H}_e = \frac{1}{2m_e}\left[\left(\hat{p}_{x_e} - \frac{1}{2}eB_\perp y_e\right)^2 + \left(\hat{p}_{y_e} + \frac{1}{2}eB_\perp x_e\right)^2 + \left(\hat{p}_{z_e} + eB_\parallel y_e\right)^2\right]$$
$$+ ez_e\mathcal{E} + U_e(z_e) \tag{3.31}$$

for the electronic part and

$$\hat{H}_{hh} = \frac{\gamma_1 + \gamma_2}{2m_0}\left[\left(\hat{p}_{x_h} + \frac{1}{2}eB_\perp y_h\right)^2 + \left(\hat{p}_{y_h} - \frac{1}{2}eB_\perp x_h\right)^2\right]$$
$$+ \frac{\gamma_1 - 2\gamma_2}{2m_0}(\hat{p}_{z_h} - eB_\parallel y_h)^2 - ez_h\mathcal{E} + U_h(z_h), \tag{3.32}$$

$$\hat{H}_{lh} = \frac{\gamma_1 - \gamma_2}{2m_0}\left[\left(\hat{p}_{x_h} + \frac{1}{2}eB_\perp y_h\right)^2 + \left(\hat{p}_{y_h} - \frac{1}{2}eB_\perp x_h\right)^2\right]$$
$$+ \frac{\gamma_1 + 2\gamma_2}{2m_0}(\hat{p}_{z_h} - eB_\parallel y_h)^2 - ez_h\mathcal{E} + U_h(z_h), \tag{3.33}$$

$$\hat{b} = -\frac{\sqrt{3}\gamma_3}{2m_0}\left\{\left[\left(\hat{p}_{y_h} - \frac{1}{2}eB_\perp x_h\right)(\hat{p}_{z_h} - eB_\| y_h) + (\hat{p}_{z_h} - eB_\| y_h)\left(\hat{p}_{y_h} - \frac{1}{2}eB_\perp x_h\right)\right]\right.$$

$$\left. + \mathrm{i}\left[\left(\hat{p}_{x_h} + \frac{1}{2}eB_\perp y_h\right)(\hat{p}_{z_h} - eB_\| y_h) + (\hat{p}_{z_h} - eB_\| y_h)\left(\hat{p}_{x_h} + \frac{1}{2}eB_\perp y_h\right)\right]\right\}, \quad (3.34)$$

$$\hat{c} = \frac{\sqrt{3}}{2m_0}\left\{\gamma_2\left[\left(\hat{p}_{x_h} + \frac{1}{2}eB_\perp y_h\right)^2 - \left(\hat{p}_{y_h} - \frac{1}{2}eB_\perp x_h\right)^2\right] - \mathrm{i}\gamma_3\left[\left(\hat{p}_{x_h} + \frac{1}{2}eB_\perp y_h\right)\right.\right.$$

$$\left.\left. \cdot \left(\hat{p}_{y_h} - \frac{1}{2}eB_\perp x_h\right) + \left(\hat{p}_{y_h} - \frac{1}{2}eB_\perp x_h\right)\left(\hat{p}_{x_h} + \frac{1}{2}eB_\perp y_h\right)\right]\right\} \quad (3.35)$$

for the hole part of the excitonic hamiltonian. We have involved DQW potentials U_e and U_h into Eqs. (3.31)–(3.33). Formulae (3.34) and (3.35) can be further modified to despatch the compound derivatives. It is also often way to substitute γ_2 and γ_3 in Eq. (3.35) by their arithmetic mean to simplify this term, setting $\gamma_5 = \frac{1}{2}(\gamma_2 + \gamma_3)$ we finally obtain

$$\hat{b} = -\frac{\sqrt{3}\gamma_3}{2m_0}\left\{2\mathrm{i}\left(\hat{p}_{x_h} + \frac{1}{2}eB_\perp y_h\right)(\hat{p}_{z_h} - eB_\| y_h) + \left[2(\hat{p}_{z_h} - eB_\| y_h)\hat{p}_{y_h}\right.\right.$$

$$\left.\left. - eB_\perp x_h\hat{p}_{z_h} + e^2 B_\perp B_\| x_h y_h + \mathrm{i}e\hbar B_\|\right]\right\}, \quad (3.36)$$

$$\hat{c} = \frac{\gamma_5\sqrt{3}}{2m_0}\left[\left(\hat{p}_{x_h} + \frac{1}{2}eB_\perp y_h\right)^2 - \mathrm{i}\left(\hat{p}_{y_h} - \frac{1}{2}eB_\perp x_h\right)^2\right] = \frac{\gamma_5\sqrt{3}}{2m_0}\left\{\left(\hat{p}_{x_h} + \frac{1}{2}eB_\perp y_h\right)^2\right.$$

$$\left. - \left(\hat{p}_{y_h} - \frac{1}{2}eB_\perp x_h\right)^2 - \mathrm{i}\left[2\hat{p}_{x_h}\hat{p}_{y_h} - eB_\perp(x_h\hat{p}_{x_h} - y_h\hat{p}_{y_h}) - \frac{1}{2}e^2 B_\perp^2 x_h y_h\right]\right\}. \quad (3.37)$$

3.3.2   Tight-binding basis

Before we proceed further, similarly to [5], we introduce the magnetic field dependent "single-particle" tight-binding basis functions $|e(\eta), j\rangle$, where $j = 1, 2$ is the QW number and $\eta \in \{h0, h1, l\}$ marks the hole state in an isolated QW:[3]

$$|e, j\rangle = \varphi_e^j(z_e)\exp\left(-\mathrm{i}\frac{z_e - z_j}{\hbar}eB_\| y_e\right), \quad (3.38)$$

$$|h0, j\rangle = \varphi_{h0}^j(z_h)\exp\left(\mathrm{i}\frac{z_h - z_j}{\hbar}eB_\| y_h\right), \quad (3.39)$$

$$|h1, j\rangle = \varphi_{h1}^j(z_h)\exp\left(\mathrm{i}\frac{z_h - z_j}{\hbar}eB_\| y_h\right), \quad (3.40)$$

$$|l, j\rangle = \varphi_l^j(z_h)\exp\left(\mathrm{i}\frac{z_h - z_j}{\hbar}eB_\| y_h\right), \quad (3.41)$$

---

[3]It is obvious that we have restricted our considerations to the three topmost hole energy levels, which are assumed to be the ground and the first excited heavy-hole states and the ground light-hole state.

where $\varphi_{e(\eta)}^j(z_{e(h)})$ is the tight-binding basis function describing an electron (a hole) in the jth well located at z_j in the absence of external fields. To describe excitonic effects, we introduce the "two-particle" tight-binding basis constructed from the functions given above (Eqs. (3.38)–(3.41)), containing twelve basis functions

$$
\begin{array}{cccc}
|e,1\rangle\,|l,1\rangle & |e,1\rangle\,|l,2\rangle & |e,2\rangle\,|l,1\rangle & |e,2\rangle\,|l,2\rangle \\
|e,1\rangle\,|h0,1\rangle & |e,1\rangle\,|h0,2\rangle & |e,2\rangle\,|h0,1\rangle & |e,2\rangle\,|h0,2\rangle \\
|e,1\rangle\,|h1,1\rangle & |e,1\rangle\,|h1,2\rangle & |e,2\rangle\,|h1,1\rangle & |e,2\rangle\,|h1,2\rangle
\end{array}
. \tag{3.42}
$$

It will be demonstrated later that such a choice of the basis enables us to separate parallel and transverse motion and to derive the matrix Schrödinger equation for wavefunctions depending only on the in-plane coordinates $x_{e(h)}$, $y_{e(h)}$.

At this point, it is necessary to set up a new notation to make following formulae well-arranged and simpler. Thus instead of (3.42), we write

$$
\begin{array}{cccc}
|1\alpha 1\rangle & |1\alpha 2\rangle & |2\alpha 1\rangle & |2\alpha 2\rangle \\
|1\beta 1\rangle & |1\beta 2\rangle & |2\beta 1\rangle & |2\beta 2\rangle \\
|1\gamma 1\rangle & |1\gamma 2\rangle & |2\gamma 1\rangle & |2\gamma 2\rangle
\end{array}
. \tag{3.43}
$$

Here, α substitutes l, β marks $h0$, and finally γ stands for $h1$.

We know from previous text that the wavefunction (3.23), which the excitonic hamiltonian (3.21) acts on, is four-component. Each component depends on six coordinates: three electronic (x_e, y_e, z_e) and three hole (x_h, y_h, z_h). To reduce the number of independent variables, we further expand these components in the following manner:

$$
c_{|\frac{3}{2},+\frac{3}{2}\rangle}(\mathbf{r}_e,\mathbf{r}_h) = \sum_{i,j=1,2} \left[a_{i\beta j}^+(\mathbf{r}_{e\parallel},\mathbf{r}_{h\parallel})|i\beta j\rangle + a_{i\gamma j}^+(\mathbf{r}_{e\parallel},\mathbf{r}_{h\parallel})|i\gamma j\rangle \right], \tag{3.44}
$$

$$
c_{|\frac{3}{2},+\frac{1}{2}\rangle}(\mathbf{r}_e,\mathbf{r}_h) = \sum_{i,j=1,2} d_{i\alpha j}^+(\mathbf{r}_{e\parallel},\mathbf{r}_{h\parallel})|i\alpha j\rangle, \tag{3.45}
$$

$$
c_{|\frac{3}{2},-\frac{1}{2}\rangle}(\mathbf{r}_e,\mathbf{r}_h) = \sum_{i,j=1,2} d_{i\alpha j}^-(\mathbf{r}_{e\parallel},\mathbf{r}_{h\parallel})|i\alpha j\rangle, \tag{3.46}
$$

$$
c_{|\frac{3}{2},-\frac{3}{2}\rangle}(\mathbf{r}_e,\mathbf{r}_h) = \sum_{i,j=1,2} \left[a_{i\beta j}^-(\mathbf{r}_{e\parallel},\mathbf{r}_{h\parallel})|i\beta j\rangle + a_{i\gamma j}^-(\mathbf{r}_{e\parallel},\mathbf{r}_{h\parallel})|i\gamma j\rangle \right], \tag{3.47}
$$

where $\mathbf{r}_{e(h)\parallel} = (x_{e(h)}, y_{e(h)})$ is the in-plane position vector. In Eqs. (3.44)–(3.47), only the basis functions (3.43) depend on $z_{e(h)}$ coordinate. Thus, the number of independent variables has been reduced to four (in-plane) coordinates. If we let the hamiltonian (3.21) act on such an expansion, we can derive equations for the set of 24 unknown functions $a_{i\beta(\gamma)j}^\pm(\mathbf{r}_{e\parallel},\mathbf{r}_{h\parallel})$, $d_{i\alpha j}^\pm(\mathbf{r}_{e\parallel},\mathbf{r}_{h\parallel})$ — just like promised — depending on the in-plane coordinates $x_{e(h)}$, $y_{e(h)}$ only. This is the goal of the next advance. But before we do this, it is necessary to choose the tight-binding basis functions $\varphi_{e(\eta)}^j(z_{e(h)})$. Our choice consists of

$$
\varphi_{e(h0,l)}^j(z_{e(h)}) = \sqrt{\frac{2}{L}} \cos \frac{\pi}{L}(z_{e(h)} - z_j), \tag{3.48}
$$

$$
\varphi_{h1}^j(z_h) = \sqrt{\frac{2}{L}} \sin \frac{2\pi}{L}(z_h - z_j), \tag{3.49}
$$

where, once again, z_j is the coordinate of the jth QW centre and L is the well width. Although functions (3.48)–(3.49) describe a particle in the rectangular QW of infinite depth, which means that the probability of finding such a particle outside the well equals zero, it still remains a good approximation to our system.

The non-zero terms of the 24×24 matrix hamiltonian are summarized as follows, function χ in these formulae stands for the coefficients $a^{+}_{i\beta(\gamma)j}(\mathbf{r}_{e\parallel}, \mathbf{r}_{h\parallel})$, $d^{+}_{i\alpha j}(\mathbf{r}_{e\parallel}, \mathbf{r}_{h\parallel})$ in expansions (3.44)–(3.47). We introduce the notation

$$E_e(B_\parallel) = \langle\varphi_e^{1(2)}|\frac{\hat{p}_{z_e}^2}{2m_e} + U_e(z_e) + \frac{e^2 B_\parallel^2}{2m_e}(z_e - z_{1(2)})^2|\varphi_e^{1(2)}\rangle, \tag{3.50}$$

$$t_e(B_\parallel) = -\langle\varphi_e^{1(2)}|\frac{\hat{p}_{z_e}^2}{2m_e} + U_e(z_e) + \frac{e^2 B_\parallel^2}{2m_e}(z_e - z_{2(1)})^2|\varphi_e^{2(1)}\rangle, \tag{3.51}$$

$$E_{h0(1)}(B_\parallel) = \langle\varphi_{h0(1)}^{1(2)}|\frac{\gamma_1 - 2\gamma_2}{2m_0}\hat{p}_{z_h}^2 + U_h(z_h) + \frac{\gamma_1 + \gamma_2}{2m_0}e^2 B_\parallel^2(z_h - z_{1(2)})^2|\varphi_{h0(1)}^{1(2)}\rangle, \tag{3.52}$$

$$t_{h0(1)}(B_\parallel) = -\langle\varphi_{h0(1)}^{1(2)}|\frac{\gamma_1 - 2\gamma_2}{2m_0}\hat{p}_{z_h}^2 + U_h(z_h) + \frac{\gamma_1 + \gamma_2}{2m_0}e^2 B_\parallel^2(z_h - z_{2(1)})^2|\varphi_{h0(1)}^{2(1)}\rangle, \tag{3.53}$$

$$E_l(B_\parallel) = \langle\varphi_l^{1(2)}|\frac{\gamma_1 + 2\gamma_2}{2m_0}\hat{p}_{z_h}^2 + U_h(z_h) + \frac{\gamma_1 - \gamma_2}{2m_0}e^2 B_\parallel^2(z_h - z_{1(2)})^2|\varphi_l^{1(2)}\rangle, \tag{3.54}$$

$$t_l(B_\parallel) = -\langle\varphi_l^{1(2)}|\frac{\gamma_1 + 2\gamma_2}{2m_0}\hat{p}_{z_h}^2 + U_h(z_h) + \frac{\gamma_1 - \gamma_2}{2m_0}e^2 B_\parallel^2(z_h - z_{2(1)})^2|\varphi_l^{2(1)}\rangle \tag{3.55}$$

for the energy levels in the z direction and the tunneling matrix elements and

$$w = \frac{\gamma_1 + \gamma_2}{m_0}eB_\parallel\langle\varphi_{h0}^{1(2)}|z_h - z_{1(2)}|\varphi_{h1}^{1(2)}\rangle, \tag{3.56}$$

$$g = -\frac{\gamma_3\sqrt{3}}{m_0}\langle\varphi_{h1}^{1(2)}|\hat{p}_{z_h}|\varphi_l^{1(2)}\rangle, \tag{3.57}$$

$$f = -\frac{\gamma_3\sqrt{3}}{m_0}eB_\parallel\langle\varphi_{h1}^{1(2)}|z_h - z_{1(2)}|\varphi_l^{1(2)}\rangle, \tag{3.58}$$

$$F = -\frac{\gamma_3\sqrt{3}}{2m_0}e^2 B_\parallel^2\langle\varphi_{h0}^{1(2)}|(z_h - z_{1(2)})^2|\varphi_l^{1(2)}\rangle. \tag{3.59}$$

for some auxiliary quantities. Since it does not change the qualitative results, we neglect the intrawell Stark effect. The tunneling matrix elements are considered to be field-independent, $t_{e(h0,h1,l)}(B_\parallel) \equiv t_{e(h0,h1,l)}$. Such simplifications enable us to write three terms coming from the electronic hamiltonian $\hat{H}_e$ (Eq. (3.31)):

$$\hat{H}_e^1\chi \equiv \langle e,1|\,\hat{H}_e\chi\,|e,1\rangle = \left\{\frac{1}{2m_e}\left[\left(\hat{p}_{x_e} - \frac{1}{2}eB_\perp y_e\right)^2 + \left(\hat{p}_{y_e} + \frac{1}{2}eB_\perp x_e\right)^2\right]\right.$$
$$\left. + E_e(B_\parallel) + ez_1\mathcal{E}\right\}\chi, \tag{3.60}$$

$$\hat{H}_e^2\chi \equiv \langle e,2|\,\hat{H}_e\chi\,|e,2\rangle = \left\{\frac{1}{2m_e}\left[\left(\hat{p}_{x_e} - \frac{1}{2}eB_\perp y_e\right)^2 + \left(\hat{p}_{y_e} + \frac{1}{2}eB_\perp x_e\right)^2\right]\right.$$
$$\left. + E_e(B_\parallel) + ez_2\mathcal{E}\right\}\chi, \quad (3.61)$$

$$\hat{H}_e^3\chi \equiv \langle e,1|\,\hat{H}_e\chi\,|e,2\rangle = \langle e,2|\,\hat{H}_e\chi\,|e,1\rangle^* = -t_e\exp\left(\mathrm{i}\frac{deB_\parallel}{\hbar}y_e\right)\chi, \quad (3.62)$$

another seven terms originating from $\hat{H}_{hh}$ (Eq. (3.32)):

$$\hat{H}_{hh}^1\chi \equiv \langle h0,1|\,\hat{H}_{hh}\chi\,|h0,1\rangle = \left\{\frac{\gamma_1+\gamma_2}{2m_0}\left[\left(\hat{p}_{x_h} + \frac{1}{2}eB_\perp y_h\right)^2 + \left(\hat{p}_{y_h} - \frac{1}{2}eB_\perp x_h\right)^2\right]\right.$$
$$\left. + E_{h0}(B_\parallel) - ez_1\mathcal{E}\right\}\chi, \quad (3.63)$$

$$\hat{H}_{hh}^2\chi \equiv \langle h0,1|\,\hat{H}_{hh}\chi\,|h1,1\rangle = \left[w\left(\hat{p}_{y_h} - \frac{1}{2}eB_\perp x_h\right) - e\mathcal{Z}\mathcal{E}\right]\chi, \quad (3.64)$$

$$\hat{H}_{hh}^3\chi \equiv \langle h0,1|\,\hat{H}_{hh}\chi\,|h0,2\rangle = \langle h0,2|\,\hat{H}_{hh}\chi\,|h0,1\rangle^* = -t_{h0}\exp\left(-\mathrm{i}\frac{deB_\parallel}{\hbar}y_h\right)\chi, \quad (3.65)$$

$$\hat{H}_{hh}^4\chi \equiv \langle h1,1|\,\hat{H}_{hh}\chi\,|h1,1\rangle = \left\{\frac{\gamma_1+\gamma_2}{2m_0}\left[\left(\hat{p}_{x_h} + \frac{1}{2}eB_\perp y_h\right)^2 + \left(\hat{p}_{y_h} - \frac{1}{2}eB_\perp x_h\right)^2\right]\right.$$
$$\left. + E_{h1}(B_\parallel) - ez_1\mathcal{E}\right\}\chi, \quad (3.66)$$

$$\hat{H}_{hh}^5\chi \equiv \langle h1,1|\,\hat{H}_{hh}\chi\,|h1,2\rangle = \langle h1,2|\,\hat{H}_{hh}\chi\,|h1,1\rangle^* = -t_{h1}\exp\left(-\mathrm{i}\frac{deB_\parallel}{\hbar}y_h\right)\chi, \quad (3.67)$$

$$\hat{H}_{hh}^6\chi \equiv \langle h0,2|\,\hat{H}_{hh}\chi\,|h0,2\rangle = \left\{\frac{\gamma_1+\gamma_2}{2m_0}\left[\left(\hat{p}_{x_h} + \frac{1}{2}eB_\perp y_h\right)^2 + \left(\hat{p}_{y_h} - \frac{1}{2}eB_\perp x_h\right)^2\right]\right.$$
$$\left. + E_{h0}(B_\parallel) - ez_2\mathcal{E}\right\}\chi, \quad (3.68)$$

$$\hat{H}_{hh}^7\chi \equiv \langle h1,2|\,\hat{H}_{hh}\chi\,|h1,2\rangle = \left\{\frac{\gamma_1+\gamma_2}{2m_0}\left[\left(\hat{p}_{x_h} + \frac{1}{2}eB_\perp y_h\right)^2 + \left(\hat{p}_{y_h} - \frac{1}{2}eB_\perp x_h\right)^2\right]\right.$$
$$\left. + E_{h1}(B_\parallel) - ez_2\mathcal{E}\right\}\chi, \quad (3.69)$$

24

and finally three terms corresponding to $\hat{H}_{lh}$ (Eq. (3.33)):

$$
\hat{H}_{lh}^1 \chi \equiv \langle l, 1 | \hat{H}_{lh} \chi | l, 1 \rangle = \left\{ \frac{\gamma_1 - \gamma_2}{2m_0} \left[\left(\hat{p}_{x_h} + \frac{1}{2} e B_\perp y_h \right)^2 + \left(\hat{p}_{y_h} - \frac{1}{2} e B_\perp x_h \right)^2 \right] \right.
$$
$$
\left. + E_l(B_\parallel) - e z_1 \mathcal{E} \right\} \chi, \quad (3.70)
$$

$$
\hat{H}_{lh}^2 \chi \equiv \langle l, 2 | \hat{H}_{lh} \chi | l, 2 \rangle = \left\{ \frac{\gamma_1 - \gamma_2}{2m_0} \left[\left(\hat{p}_{x_h} + \frac{1}{2} e B_\perp y_h \right)^2 + \left(\hat{p}_{y_h} - \frac{1}{2} e B_\perp x_h \right)^2 \right] \right.
$$
$$
\left. + E_l(B_\parallel) - e z_2 \mathcal{E} \right\} \chi, \quad (3.71)
$$

$$
\hat{H}_{lh}^3 \chi \equiv \langle l, 1 | \hat{H}_{lh} \chi | l, 2 \rangle = \langle l, 2 | \hat{H}_{lh} \chi | l, 1 \rangle^* = -t_l \exp\left(-\mathrm{i} \frac{de B_\parallel}{\hbar} y_h \right) \chi, \quad (3.72)
$$

$d = z_2 - z_1$ is the interwell distance and $\mathcal{Z} = \langle \varphi_{h0}^{1(2)} | z_h | \varphi_{h1}^{1(2)} \rangle$. Only two different non-zero terms proceed both from $\hat{b}$ (Eq. (3.36)) and $\hat{c}$ (Eq. (3.37)):

$$
\hat{b}_1 \chi \equiv \langle h1, 1 | \hat{b} \chi | l, 1 \rangle = g \left[\mathrm{i} \left(\hat{p}_{x_h} + \frac{1}{2} e B_\perp y_h \right) + \left(\hat{p}_{y_h} - \frac{1}{2} e B_\perp x_h \right) \right] \chi, \quad (3.73)
$$

$$
\hat{b}_2 \chi \equiv \langle l, 1 | \hat{b} \chi | h1, 1 \rangle = g^* \left[\mathrm{i} \left(\hat{p}_{x_h} + \frac{1}{2} e B_\perp y_h \right) + \left(\hat{p}_{y_h} - \frac{1}{2} e B_\perp x_h \right) \right] \chi, \quad (3.74)
$$

while

$$
\hat{c}_1 \chi \equiv \langle h0, 1 | \hat{c} \chi | l, 1 \rangle = \frac{\gamma_5 \sqrt{3}}{2m_0} \left\{ \left(\hat{p}_{x_h} + \frac{1}{2} e B_\perp y_h \right)^2 - \left(\hat{p}_{y_h} - \frac{1}{2} e B_\perp x_h \right)^2 \right.
$$
$$
\left. - \mathrm{i} \left[2 \hat{p}_{x_h} \hat{p}_{y_h} - e B_\perp (x_h \hat{p}_{x_h} - y_h \hat{p}_{y_h}) - \frac{1}{2} e^2 B_\perp^2 x_h y_h \right] \right\} \chi + F \chi, \quad (3.75)
$$

$$
\hat{c}_2 \chi \equiv \langle h1, 1 | \hat{c} \chi | l, 1 \rangle = f \left[\mathrm{i} \left(\hat{p}_{x_h} + \frac{1}{2} e B_\perp y_h \right) + \left(\hat{p}_{y_h} - \frac{1}{2} e B_\perp x_h \right) \right] \chi. \quad (3.76)
$$

The problem we deal with has turned into a solving of the system of 24 coupled partial differential equations for coefficients of expansions (3.44)–(3.47). Such a system can be described by 24×24 matrix hamiltonian

$$\hat{\mathbb{H}} = \begin{pmatrix} \hat{\mathbb{H}}^{++} & \hat{\mathbb{H}}^{+-} \\ \hat{\mathbb{H}}^{-+} & \hat{\mathbb{H}}^{--} \end{pmatrix}, \tag{3.77}$$

whose diagonal parts are

$\hat{\mathbb{H}}^{++} =$

$$= \begin{pmatrix} \hat{H}_{1\beta1} & \hat{H}_{hh}^2 & \hat{H}_{hh}^3 & 0 & \hat{H}_e^3 & 0 & 0 & 0 & 0 & 0 & 0 & 0 \\ & \hat{H}_{1\gamma1} & 0 & \hat{H}_{hh}^5 & 0 & \hat{H}_e^3 & 0 & 0 & \hat{b}_1 & 0 & 0 & 0 \\ & & \hat{H}_{1\beta2} & \hat{H}_{hh}^2 + V_5 & 0 & 0 & \hat{H}_e^3 & 0 & 0 & 0 & 0 & 0 \\ & & & \hat{H}_{1\gamma2} & 0 & 0 & 0 & \hat{H}_e^3 & 0 & \hat{b}_1 & 0 & 0 \\ & & & & \hat{H}_{2\beta1} & \hat{H}_{hh}^2 + V_6 & \hat{H}_{hh}^3 & 0 & 0 & 0 & 0 & 0 \\ & & & & & \hat{H}_{2\gamma1} & 0 & \hat{H}_{hh}^5 & 0 & 0 & \hat{b}_1 & 0 \\ & & & & & & \hat{H}_{2\beta2} & \hat{H}_{hh}^2 & 0 & 0 & 0 & 0 \\ & & \text{h. c.} & & & & & \hat{H}_{2\gamma2} & 0 & 0 & 0 & \hat{b}_1 \\ & & & & & & & & \hat{H}_{1\alpha1} & \hat{H}_{lh}^3 & \hat{H}_e^3 & 0 \\ & & & & & & & & & \hat{H}_{1\alpha2} & 0 & \hat{H}_e^3 \\ & & & & & & & & & & \hat{H}_{2\alpha1} & \hat{H}_{lh}^3 \\ & & & & & & & & & & & \hat{H}_{2\alpha2} \end{pmatrix},$$

$$\tag{3.78}$$

and

$\hat{\mathbb{H}}^{--} =$

$$= \begin{pmatrix} \hat{H}_{1\alpha1} & \hat{H}_{lh}^3 & \hat{H}_e^3 & 0 & 0 & -\hat{b}_2 & 0 & 0 & 0 & 0 & 0 & 0 \\ & \hat{H}_{1\alpha2} & 0 & \hat{H}_e^3 & 0 & 0 & -\hat{b}_2 & 0 & 0 & 0 & 0 \\ & & \hat{H}_{2\alpha1} & \hat{H}_{lh}^3 & 0 & 0 & 0 & 0 & 0 & -\hat{b}_2 & 0 \\ & & & \hat{H}_{2\alpha2} & 0 & 0 & 0 & 0 & 0 & 0 & 0 & -\hat{b}_2 \\ & & & & \hat{H}_{1\beta1} & \hat{H}_{hh}^2 & \hat{H}_{hh}^3 & 0 & \hat{H}_e^3 & 0 & 0 & 0 \\ & & & & & \hat{H}_{1\gamma1} & 0 & \hat{H}_{hh}^5 & 0 & \hat{H}_e^3 & 0 & 0 \\ & & & & & & \hat{H}_{1\beta2} & \hat{H}_{hh}^2 + V_5 & 0 & 0 & \hat{H}_e^3 & 0 \\ & & \text{h. c.} & & & & & \hat{H}_{1\gamma2} & 0 & 0 & 0 & \hat{H}_e^3 \\ & & & & & & & & \hat{H}_{2\beta1} & \hat{H}_{hh}^2 + V_6 & \hat{H}_{hh}^3 & 0 \\ & & & & & & & & & \hat{H}_{2\gamma1} & 0 & \hat{H}_{hh}^5 \\ & & & & & & & & & & \hat{H}_{2\beta2} & \hat{H}_{hh}^2 \\ & & & & & & & & & & & \hat{H}_{2\gamma2} \end{pmatrix}.$$

$$\tag{3.79}$$

Since $\hat{\mathbb{H}}$ is hermitian, $\hat{\mathbb{H}} = \hat{\mathbb{H}}^\dagger$, the following relations hold:

$$\hat{\mathbb{H}}^{++} = \left(\hat{\mathbb{H}}^{++}\right)^\dagger, \qquad \hat{\mathbb{H}}^{--} = \left(\hat{\mathbb{H}}^{--}\right)^\dagger, \qquad \hat{\mathbb{H}}^{+-} = \left(\hat{\mathbb{H}}^{-+}\right)^\dagger. \qquad (3.80)$$

That is why we show only the upper diagonal parts of matrices (3.78) and (3.79), while the symbol "h. c." stands for the hermitian conjugation. Finally, $\hat{\mathbb{H}}^{+-}$ is given by

$$\hat{\mathbb{H}}^{+-} = \begin{pmatrix} \hat{c}_1 & 0 & . & . & . & . & . & . & . & . & . & . & . & . & . & . & . & 0 \\ \hat{c}_2 & 0 & . & . & . & . & . & . & . & . & . & . & . & . & . & . & . & 0 \\ 0 & \hat{c}_1 & 0 & . & . & . & . & . & . & . & . & . & . & . & . & . & . & 0 \\ \vdots & \hat{c}_2 & 0 & . & . & . & . & . & . & . & . & . & . & . & . & . & . & 0 \\ \vdots & & 0 & \hat{c}_1 & 0 & . & . & . & . & . & . & . & . & . & . & . & . & 0 \\ \vdots & & 0 & \hat{c}_2 & 0 & . & . & . & . & . & . & . & . & . & . & . & . & 0 \\ 0 & . & & 0 & \hat{c}_1 & 0 & . & . & . & . & . & . & . & . & . & . & . & 0 \\ 0 & . & & 0 & \hat{c}_2 & 0 & . & . & . & . & . & . & . & . & . & . & . & 0 \\ 0 & . & . & . & 0 & \hat{c}_1 & \hat{c}_2 & 0 & . & . & . & . & . & . & . & . & . & 0 \\ 0 & . & . & . & . & . & . & . & 0 & \hat{c}_1 & \hat{c}_2 & 0 & . & . & . & . & . & 0 \\ 0 & . & . & . & . & . & . & . & . & . & . & 0 & \hat{c}_1 & \hat{c}_2 & 0 & . & \vdots & \\ 0 & . & . & . & . & . & . & . & . & . & . & & 0 & \hat{c}_1 & \hat{c}_2 & \end{pmatrix}, \qquad (3.81)$$

from which $\hat{\mathbb{H}}^{-+}$ can be obtained using (3.80). The hamiltonian (3.77) acts on the wave-function Φ, whose 24 components are[4]

$$\Phi(\mathbf{r}_{e\parallel}, \mathbf{r}_{h\parallel}) = (a_{1\beta1}^+, a_{1\gamma1}^+, a_{1\beta2}^+, a_{1\gamma2}^+, a_{2\beta1}^+, a_{2\gamma1}^+, a_{2\beta2}^+, a_{2\gamma2}^+, d_{1\alpha1}^+, d_{1\alpha2}^+, d_{2\alpha1}^+, d_{2\alpha2}^+,$$
$$d_{1\alpha1}^-, d_{1\alpha2}^-, d_{2\alpha1}^-, d_{2\alpha2}^-, a_{1\beta1}^-, a_{1\gamma1}^-, a_{1\beta2}^-, a_{1\gamma2}^-, a_{2\beta1}^-, a_{2\gamma1}^-, a_{2\beta2}^-, a_{2\gamma2}^-), \quad (3.82)$$

each one depending on $\mathbf{r}_{e\parallel}, \mathbf{r}_{h\parallel}$.

The diagonal parts of Eqs. (3.78)–(3.79) are summarized as follows:

$$\begin{aligned}
\hat{H}_{1\beta1} &= \hat{H}_e^1 + \hat{H}_{hh}^1 + V_1, & \hat{H}_{1\beta2} &= \hat{H}_e^1 + \hat{H}_{hh}^6 + V_2, \\
\hat{H}_{2\beta1} &= \hat{H}_e^2 + \hat{H}_{hh}^1 + V_2, & \hat{H}_{2\beta2} &= \hat{H}_e^2 + \hat{H}_{hh}^6 + V_1, \\
\hat{H}_{1\gamma1} &= \hat{H}_e^1 + \hat{H}_{hh}^4 + V_3, & \hat{H}_{1\gamma2} &= \hat{H}_e^1 + \hat{H}_{hh}^7 + V_4, \\
\hat{H}_{2\gamma1} &= \hat{H}_e^2 + \hat{H}_{hh}^4 + V_4, & \hat{H}_{2\gamma2} &= \hat{H}_e^2 + \hat{H}_{hh}^7 + V_3, \\
\hat{H}_{1\alpha1} &= \hat{H}_e^1 + \hat{H}_{lh}^1 + V_1, & \hat{H}_{1\alpha2} &= \hat{H}_e^1 + \hat{H}_{lh}^2 + V_2, \\
\hat{H}_{2\alpha1} &= \hat{H}_e^2 + \hat{H}_{lh}^1 + V_2, & \hat{H}_{2\alpha2} &= \hat{H}_e^2 + \hat{H}_{lh}^2 + V_1.
\end{aligned} \qquad (3.83)$$

---

[4]From now on, it is necessary to preserve the chosen order of these components.

The coulombic terms are calculated using

$$V_1 = \int \left(\varphi_e^{1(2)}\right)^2 \left(\varphi_{h0(l)}^{1(2)}\right)^2 V(\mathbf{r}_e - \mathbf{r}_h) \, \mathrm{d}z_e \mathrm{d}z_h,$$

$$V_2 = \int \left(\varphi_e^{1(2)}\right)^2 \left(\varphi_{h0(l)}^{2(1)}\right)^2 V(\mathbf{r}_e - \mathbf{r}_h) \, \mathrm{d}z_e \mathrm{d}z_h,$$

$$V_3 = \int \left(\varphi_e^{1(2)}\right)^2 \left(\varphi_{h1}^{1(2)}\right)^2 V(\mathbf{r}_e - \mathbf{r}_h) \, \mathrm{d}z_e \mathrm{d}z_h,$$

$$V_4 = \int \left(\varphi_e^{1(2)}\right)^2 \left(\varphi_{h1}^{2(1)}\right)^2 V(\mathbf{r}_e - \mathbf{r}_h) \, \mathrm{d}z_e \mathrm{d}z_h, \qquad (3.84)$$

$$V_5 = \int \left(\varphi_e^{1}\right)^2 \varphi_{h0}^2 \varphi_{h1}^2 V(\mathbf{r}_e - \mathbf{r}_h) \, \mathrm{d}z_e \mathrm{d}z_h,$$

$$V_6 = \int \left(\varphi_e^{2}\right)^2 \varphi_{h0}^1 \varphi_{h1}^1 V(\mathbf{r}_e - \mathbf{r}_h) \, \mathrm{d}z_e \mathrm{d}z_h,$$

where the Coulomb interaction V takes the standard form of $V(\mathbf{r}) = -e^2/(4\pi\epsilon_0\epsilon_r|\mathbf{r}|)$. On calculation of Eq. (3.84), a little more attention will be paid later.

A common way how to further treat with the excitonic hamiltonian, written in in-plane coordinate system, is to perform the centre-of-mass transformation.

3.3.3 Centre-of-mass transformation

Since the Coulomb interaction V between an electron and a hole forming an exciton depends on the relative distance of these particles only, it is advantageous to proceed with new coordinates $\mathbf{r}$, $\mathbf{R}$, which describe the in-plane relative distance and the in-plane centre-of-mass coordinate of the electron-hole pair, instead of treating with $\mathbf{r}_{e\|}, \mathbf{r}_{h\|}$. The coordinates $\mathbf{r}$, $\mathbf{R}$ are defined by well-known formulae (3.16) and (3.17):

$$\mathbf{r} = \mathbf{r}_{e\|} - \mathbf{r}_{h\|} \qquad (3.85)$$

and

$$\mathbf{R} = \frac{m_e \mathbf{r}_{e\|} + m_h \mathbf{r}_{h\|}}{m_e + m_h}. \qquad (3.86)$$

However, a little problem arises. Whereas the first of these two formulae could be used in our case, we have to take care of the second since there is *only one* hole mass in it. To describe both light- and heavy-hole excitons, we cannot simply use Eq. (3.86) when substituting m_h with one of m_{lh} or m_{hh}. We can neither use Eq. (3.86) twice, with different masses, since it would not be a correct transformation, nor restrict our considerations just on one, light- or heavy-hole, exciton, since we would neglect some interesting effects arising from the valence-subband mixing. We handle this situation by introducing the *generalized* centre-of-mass transformation

$$\mathbf{R} = \mu \mathbf{r}_{e\|} + \lambda \mathbf{r}_{h\|}, \qquad \mu + \lambda = 1, \qquad (3.87)$$

keeping in mind that the coefficients μ, λ will be determined later, probably by our pursuit for the most possible simplification of obtained equations.

It could be derived from Eq. (3.85) and (3.87) that

$$\begin{aligned}
\mathbf{r}_{e\parallel} &= \mathbf{R} + \lambda\mathbf{r}, \\
\mathbf{r}_{h\parallel} &= \mathbf{R} - \mu\mathbf{r},
\end{aligned} \tag{3.88}$$

from which it follows

$$\begin{aligned}
\hat{\mathbf{p}}_{e\parallel} &= \hat{\mathbf{p}} + \mu\hat{\mathbf{P}}, \\
\hat{\mathbf{p}}_{h\parallel} &= -\hat{\mathbf{p}} + \lambda\hat{\mathbf{P}}.
\end{aligned} \tag{3.89}$$

In the last equations, $\hat{\mathbf{p}}$ is the momentum operator corresponding to $\mathbf{r}$, $\hat{\mathbf{P}}$ the momentum operator associated with $\mathbf{R}$.

Just like proposed in [21] and generalized in [5], we will look for the solution (3.82) of (3.77) in the following form:

$$\Phi(\mathbf{r}_{e\parallel}, \mathbf{r}_{h\parallel}) = (u^+_{1\beta 1}, u^+_{1\gamma 1}, u^+_{1\beta 2}\mathrm{e}^+_2, u^+_{1\gamma 2}\mathrm{e}^+_2, u^+_{2\beta 1}\mathrm{e}^-_2, u^+_{2\gamma 1}\mathrm{e}^-_2, u^+_{2\beta 2}, u^+_{2\gamma 2}, v^+_{1\alpha 1}, v^+_{1\alpha 2}\mathrm{e}^+_2, v^+_{2\alpha 1}\mathrm{e}^-_2, v^+_{2\alpha 2},$$

$$v^-_{1\alpha 1}, v^-_{1\alpha 2}\mathrm{e}^+_2, v^-_{2\alpha 1}\mathrm{e}^-_2, v^-_{2\alpha 2}, u^-_{1\beta 1}, u^-_{1\gamma 1}, u^-_{1\beta 2}\mathrm{e}^+_2, u^-_{1\gamma 2}\mathrm{e}^+_2, u^-_{2\beta 1}\mathrm{e}^-_2, u^-_{2\gamma 1}\mathrm{e}^-_2, u^-_{2\beta 2}, u^-_{2\gamma 2})$$

$$\cdot \exp\left[\mathrm{i}\left(K_x - \frac{eB_\perp}{2\hbar}y\right)X + \mathrm{i}\left(K_y + \frac{eB_\perp}{2\hbar}x\right)Y\right], \quad (3.90)$$

where the symbol $\mathrm{e}^\pm_2$ denotes the additional phase factor

$$\mathrm{e}^\pm_2 = \exp\left(\pm\mathrm{i}\frac{deB_\parallel}{\hbar}Y\right) \tag{3.91}$$

and the functions $u^\pm_{i\beta(\gamma)j}$, $v^\pm_{i\alpha j}$ depend on the relative coordinates x, y only. We have managed to reduce the number of independent variables from six at the beginning to two at this moment. We can also derive rules that the operators $\hat{\mathbf{p}}$ and $\hat{\mathbf{P}}$ must obey while acting on components of (3.90). If we denote by symbol e_1 the phase factor on the third line of Eq. (3.90), then for any function χ depending on relative and centre-of-mass coordinates x, y, X, Y in such a way that it could be factorized into $\chi(x, y, X, Y) = u(x, y)\mathrm{e}_1\mathrm{e}^\pm_2$, one can write

$$\begin{aligned}
\hat{p}_x\chi &= [(\hat{p}_xu) + \tfrac{1}{2}eB_\perp Yu]\mathrm{e}_1\mathrm{e}^\pm_2, \\
\hat{p}_y\chi &= [(\hat{p}_yu) - \tfrac{1}{2}eB_\perp Xu]\mathrm{e}_1\mathrm{e}^\pm_2, \\
\hat{p}_x^2\chi &= [(\hat{p}_x^2u) + eB_\perp Y(\hat{p}_xu) + \tfrac{1}{4}e^2B_\perp^2 Y^2u]\mathrm{e}_1\mathrm{e}^\pm_2, \\
\hat{p}_y^2\chi &= [(\hat{p}_y^2u) - eB_\perp X(\hat{p}_yu) + \tfrac{1}{4}e^2B_\perp^2 X^2u]\mathrm{e}_1\mathrm{e}^\pm_2
\end{aligned} \tag{3.92}$$

for the operator $\hat{\mathbf{p}}$ and

$$\begin{aligned}
\hat{P}_x\chi &= (\hbar K_x - \tfrac{1}{2}eB_\perp y)u\mathrm{e}_1\mathrm{e}^\pm_2, \\
\hat{P}_y\chi &= (\hbar K_y + \tfrac{1}{2}eB_\perp x \pm deB_\parallel)u\mathrm{e}_1\mathrm{e}^\pm_2, \\
\hat{P}_x^2\chi &= (\hbar K_x - \tfrac{1}{2}eB_\perp y)^2u\mathrm{e}_1\mathrm{e}^\pm_2, \\
\hat{P}_y^2\chi &= (\hbar K_y + \tfrac{1}{2}eB_\perp x \pm deB_\parallel)^2u\mathrm{e}_1\mathrm{e}^\pm_2
\end{aligned} \tag{3.93}$$

29

for the operator $\hat{\mathbf{P}}$. When a component of (3.90) does not have $\mathrm{e}_2^{\pm}$ phase factor, $\pm deB_{\parallel}$ in Eq. (3.93) should be neglected.

It is straightforward to rewrite the formulae (3.60)–(3.76) in terms of the new coordinate system, which gives

$$
\begin{aligned}
\hat{H}_e^1 u\mathrm{e}_1\mathrm{e}_2^{\pm} = \Bigg\{ &\frac{1}{2m_e}\bigg[\Big(\hat{p}_x - \frac{1}{2}eB_{\perp}y\Big)^2 + \Big(\hat{p}_y + \frac{1}{2}eB_{\perp}x\Big)^2 \\
&+ 2\mu\big[\hbar K_x\hat{p}_x + (\hbar K_y \pm deB_{\parallel})\hat{p}_y\big] + \mu eB_{\perp}\big[(\hbar K_y \pm deB_{\parallel})x - \hbar K_x y\big] \\
&+ \mu^2\big[\hbar^2 K_x^2 + (\hbar K_y \pm deB_{\parallel})^2\big]\bigg] + E_e(B_{\parallel}) + ez_1\mathcal{E} \Bigg\}u\mathrm{e}_1\mathrm{e}_2^{\pm}, \quad (3.94)
\end{aligned}
$$

$$
\begin{aligned}
\hat{H}_e^2 u\mathrm{e}_1\mathrm{e}_2^{\pm} = \Bigg\{ &\frac{1}{2m_e}\bigg[\Big(\hat{p}_x - \frac{1}{2}eB_{\perp}y\Big)^2 + \Big(\hat{p}_y + \frac{1}{2}eB_{\perp}x\Big)^2 \\
&+ 2\mu\big[\hbar K_x\hat{p}_x + (\hbar K_y \pm deB_{\parallel})\hat{p}_y\big] + \mu eB_{\perp}\big[(\hbar K_y \pm deB_{\parallel})x - \hbar K_x y\big] \\
&+ \mu^2\big[\hbar^2 K_x^2 + (\hbar K_y \pm deB_{\parallel})^2\big]\bigg] + E_e(B_{\parallel}) + ez_2\mathcal{E} \Bigg\}u\mathrm{e}_1\mathrm{e}_2^{\pm}, \quad (3.95)
\end{aligned}
$$

$$
\hat{H}_e^3 u\mathrm{e}_1\mathrm{e}_2^- = -t_e \exp\Big(\mathrm{i}\,\frac{deB_{\parallel}}{\hbar}\lambda y\Big)u\mathrm{e}_1 \tag{3.96}
$$

for the electronic part of the hamiltonian. For the heavy-hole part, we have

$$
\begin{aligned}
\hat{H}_{hh}^1 u\mathrm{e}_1\mathrm{e}_2^{\pm} = \Bigg\{ &\frac{\gamma_1 + \gamma_2}{2m_0}\bigg[\Big(\hat{p}_x + \frac{1}{2}eB_{\perp}y\Big)^2 + \Big(\hat{p}_y - \frac{1}{2}eB_{\perp}x\Big)^2 \\
&- 2\lambda\big[\hbar K_x\hat{p}_x + (\hbar K_y \pm deB_{\parallel})\hat{p}_y\big] + \lambda eB_{\perp}\big[(\hbar K_y \pm deB_{\parallel})x - \hbar K_x y\big] \\
&+ \lambda^2\big[\hbar^2 K_x^2 + (\hbar K_y \pm deB_{\parallel})^2\big]\bigg] + E_{h0}(B_{\parallel}) - ez_1\mathcal{E} \Bigg\}u\mathrm{e}_1\mathrm{e}_2^{\pm}, \quad (3.97)
\end{aligned}
$$

$$
\hat{H}_{hh}^2 u\mathrm{e}_1\mathrm{e}_2^{\pm} = \Bigg\{ w\bigg[-\Big(\hat{p}_y - \frac{1}{2}eB_{\perp}x\Big) + \lambda(\hbar K_y \pm deB_{\parallel})\bigg] - e\mathcal{Z}\mathcal{E} \Bigg\}u\mathrm{e}_1\mathrm{e}_2^{\pm}, \tag{3.98}
$$

$$
\hat{H}_{hh}^3 u\mathrm{e}_1\mathrm{e}_2^+ = -t_{h0} \exp\Big(\mathrm{i}\,\frac{deB_{\parallel}}{\hbar}\mu y\Big)u\mathrm{e}_1, \tag{3.99}
$$

$$
\begin{aligned}
\hat{H}_{hh}^4 u\mathrm{e}_1\mathrm{e}_2^{\pm} = \Bigg\{ &\frac{\gamma_1 + \gamma_2}{2m_0}\bigg[\Big(\hat{p}_x + \frac{1}{2}eB_{\perp}y\Big)^2 + \Big(\hat{p}_y - \frac{1}{2}eB_{\perp}x\Big)^2 \\
&- 2\lambda\big[\hbar K_x\hat{p}_x + (\hbar K_y \pm deB_{\parallel})\hat{p}_y\big] + \lambda eB_{\perp}\big[(\hbar K_y \pm deB_{\parallel})x - \hbar K_x y\big] \\
&+ \lambda^2\big[\hbar^2 K_x^2 + (\hbar K_y \pm deB_{\parallel})^2\big]\bigg] + E_{h1}(B_{\parallel}) - ez_1\mathcal{E} \Bigg\}u\mathrm{e}_1\mathrm{e}_2^{\pm}, \quad (3.100)
\end{aligned}
$$

$$\hat{H}_{hh}^{5} u e_1 e_2^{+} = -t_{h1} \exp\left(i \frac{de B_{\parallel}}{\hbar} \mu y\right) u e_1, \tag{3.101}$$

$$\hat{H}_{hh}^{6} u e_1 e_2^{\pm} = \left\{ \frac{\gamma_1 + \gamma_2}{2m_0} \left[\left(\hat{p}_x + \frac{1}{2} e B_{\perp} y\right)^2 + \left(\hat{p}_y - \frac{1}{2} e B_{\perp} x\right)^2 \right. \right.$$
$$- 2\lambda \left[\hbar K_x \hat{p}_x + (\hbar K_y \pm de B_{\parallel})\hat{p}_y\right] + \lambda e B_{\perp} \left[(\hbar K_y \pm de B_{\parallel})x - \hbar K_x y\right]$$
$$\left. \left. + \lambda^2 \left[\hbar^2 K_x^2 + (\hbar K_y \pm de B_{\parallel})^2\right] \right] + E_{h0}(B_{\parallel}) - e z_2 \mathcal{E} \right\} u e_1 e_2^{\pm}, \tag{3.102}$$

$$\hat{H}_{hh}^{7} u e_1 e_2^{\pm} = \left\{ \frac{\gamma_1 + \gamma_2}{2m_0} \left[\left(\hat{p}_x + \frac{1}{2} e B_{\perp} y\right)^2 + \left(\hat{p}_y - \frac{1}{2} e B_{\perp} x\right)^2 \right. \right.$$
$$- 2\lambda \left[\hbar K_x \hat{p}_x + (\hbar K_y \pm de B_{\parallel})\hat{p}_y\right] + \lambda e B_{\perp} \left[(\hbar K_y \pm de B_{\parallel})x - \hbar K_x y\right]$$
$$\left. \left. + \lambda^2 \left[\hbar^2 K_x^2 + (\hbar K_y \pm de B_{\parallel})^2\right] \right] + E_{h1}(B_{\parallel}) - e z_2 \mathcal{E} \right\} u e_1 e_2^{\pm}. \tag{3.103}$$

The terms arising from the light-hole part are

$$\hat{H}_{lh}^{1} u e_1 e_2^{\pm} = \left\{ \frac{\gamma_1 - \gamma_2}{2m_0} \left[\left(\hat{p}_x + \frac{1}{2} e B_{\perp} y\right)^2 + \left(\hat{p}_y - \frac{1}{2} e B_{\perp} x\right)^2 \right. \right.$$
$$- 2\lambda \left[\hbar K_x \hat{p}_x + (\hbar K_y \pm de B_{\parallel})\hat{p}_y\right] + \lambda e B_{\perp} \left[(\hbar K_y \pm de B_{\parallel})x - \hbar K_x y\right]$$
$$\left. \left. + \lambda^2 \left[\hbar^2 K_x^2 + (\hbar K_y \pm de B_{\parallel})^2\right] \right] + E_{l}(B_{\parallel}) - e z_1 \mathcal{E} \right\} u e_1 e_2^{\pm}, \tag{3.104}$$

$$\hat{H}_{lh}^{2} u e_1 e_2^{\pm} = \left\{ \frac{\gamma_1 - \gamma_2}{2m_0} \left[\left(\hat{p}_x + \frac{1}{2} e B_{\perp} y\right)^2 + \left(\hat{p}_y - \frac{1}{2} e B_{\perp} x\right)^2 \right. \right.$$
$$- 2\lambda \left[\hbar K_x \hat{p}_x + (\hbar K_y \pm de B_{\parallel})\hat{p}_y\right] + \lambda e B_{\perp} \left[(\hbar K_y \pm de B_{\parallel})x - \hbar K_x y\right]$$
$$\left. \left. + \lambda^2 \left[\hbar^2 K_x^2 + (\hbar K_y \pm de B_{\parallel})^2\right] \right] + E_{l}(B_{\parallel}) - e z_2 \mathcal{E} \right\} u e_1 e_2^{\pm}, \tag{3.105}$$

$$\hat{H}_{lh}^{3} u e_1 e_2^{+} = -t_{l} \exp\left(i \frac{de B_{\parallel}}{\hbar} \mu y\right) u e_1. \tag{3.106}$$

Remember, $u = u(x, y)$ in all foregoing formulae. Furthermore, $\hat{b}$ terms are given as follows

$$\hat{b}_1 u e_1 e_2^{\pm} = g \left\{ i \left[-\left(\hat{p}_x + \frac{1}{2} e B_{\perp} y\right) + \lambda \hbar K_x \right] \right.$$
$$\left. + \left[-\left(\hat{p}_y - \frac{1}{2} e B_{\perp} x\right) + \lambda \left(\hbar K_y \pm de B_{\parallel}\right) \right] \right\} u e_1 e_2^{\pm}, \tag{3.107}$$

$$\hat{b}_2 u\mathrm{e}_1\mathrm{e}_2^{\pm} = g^* \left\{ \mathrm{i} \left[-\left(\hat{p}_x + \frac{1}{2}eB_\perp y\right) + \lambda\hbar K_x \right] \right.$$
$$\left. + \left[-\left(\hat{p}_y - \frac{1}{2}eB_\perp x\right) + \lambda\left(\hbar K_y \pm deB_\parallel\right) \right] \right\} u\mathrm{e}_1\mathrm{e}_2^{\pm}, \quad (3.108)$$

and finally for $\hat{c}$ terms, we have

$$\hat{c}_1 u\mathrm{e}_1\mathrm{e}_2^{\pm} = \frac{\sqrt{3}\gamma_5}{2m_0} \left\{ \left[\left(\hat{p}_x + \frac{1}{2}eB_\perp y\right)^2 - \left(\hat{p}_y - \frac{1}{2}eB_\perp x\right)^2 \right. \right.$$
$$- 2\lambda\left[\hbar K_x\hat{p}_x - (\hbar K_y \pm deB_\parallel)\hat{p}_y\right] - \lambda eB_\perp\left[(\hbar K_y \pm deB_\parallel)x + \hbar K_x y\right]$$
$$+ \lambda^2\left[\hbar^2 K_x^2 - (\hbar K_y \pm deB_\parallel)^2\right] \right] - \mathrm{i}\left[2\left[\hat{p}_x\hat{p}_y - \left(\lambda\hbar K_x - \frac{1}{2}eB_\perp y\right)\hat{p}_y\right.\right.$$
$$- \left(\lambda(\hbar K_y \pm deB_\parallel) + \frac{1}{2}eB_\perp x\right)\hat{p}_x\right] - \lambda eB_\perp\left[(\hbar K_y \pm deB_\parallel)y - \hbar K_x x\right]$$
$$\left. \left. - \frac{1}{2}e^2 B_\perp^2 xy + 2\lambda^2\hbar K_x(\hbar K_y \pm deB_\parallel)\right]\right\} u\mathrm{e}_1\mathrm{e}_2^{\pm} + Fu\mathrm{e}_1\mathrm{e}_2^{\pm}, \quad (3.109)$$

$$\hat{c}_2 u\mathrm{e}_1\mathrm{e}_2^{\pm} = f \left\{ \mathrm{i} \left[-\left(\hat{p}_x + \frac{1}{2}eB_\perp y\right) + \lambda\hbar K_x \right] \right.$$
$$\left. + \left[-\left(\hat{p}_y - \frac{1}{2}eB_\perp x\right) + \lambda\left(\hbar K_y \pm deB_\parallel\right) \right] \right\} u\mathrm{e}_1\mathrm{e}_2^{\pm}. \quad (3.110)$$

Let us mention once again that if a component of (3.90) does not have $\mathrm{e}_2^{\pm}$ phase factor, $\pm deB_\parallel$ should be neglected in Eqs. (3.94)–(3.110).

Though we have reduced our system to the two-dimensional set of differential equations (in x, y variables), it still remains analytically unsolvable problem. To overcome this, we will expand u, v components of (3.90) (we will call them *in-plane* components since $u = u(x, y)$, $v = v(x, y)$ depend only on in-plane relative distance between an electron and a hole) to a proper basis to be given a numerically solvable set of algebraic equations. But before we do that, let us give a more detailed discussion of particular terms in Eq. (3.84).

3.3.4 Coulombic terms

It was shown in the previous text that six different coulombic terms in our choice of tight-binding basis exist. These are summarized in Eq. (3.84). Each of these terms is calculated by performing the indicated two-dimensional integration. Since $V(\mathbf{r}_e - \mathbf{r}_h) \propto 1/\sqrt{x^2 + y^2 + (z_e - z_h)^2}$ and the integration runs over z_e and z_h, the resulting function is even in x, y. Moreover, it is proportional to $x^2 + y^2 = r^2$ and thus even in r.

Though the forementioned two-dimensional integration cannot be done analytically and we will treat it numerically, a little simplification can be performed: using the substitution
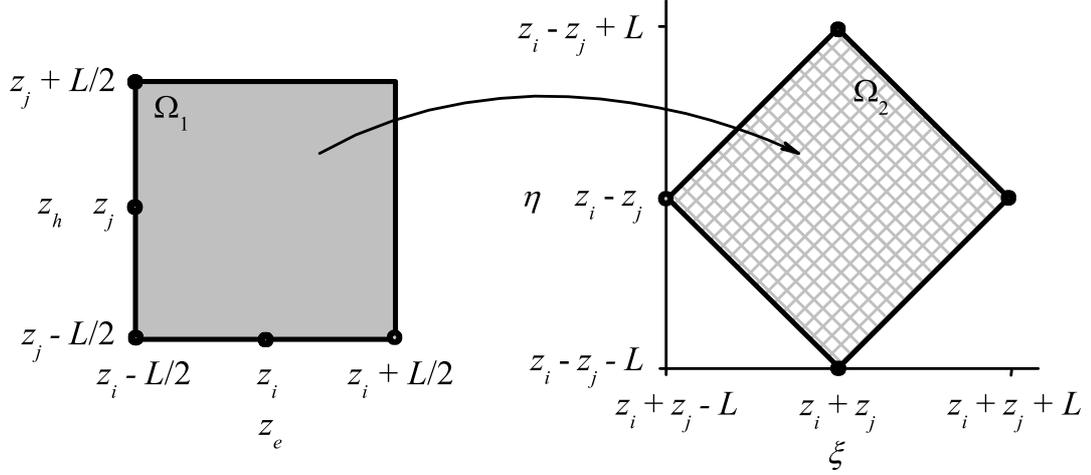
$$\eta = z_e - z_h,$$
$$\xi = z_e + z_h \quad (3.111)$$

Figure 3.3: The effect of transformation (3.111) on the integration area in z_e, z_h and η, ξ coordinate systems for the computation of coulombic terms.

one can reduce it to a one-dimensional problem. We are about to demonstrate the whole procedure on the first term of (3.84), V_1. After substitution from (3.48) and use of some well-known trigonometric formulae, we can write

$$
\begin{aligned}
V_1(r) &= \int_{\Omega_1} \left(\varphi_e^{1(2)}\right)^2 \left(\varphi_{h0(l)}^{1(2)}\right)^2 V(\mathbf{r}_e - \mathbf{r}_h)\, dz_e dz_h \\
&= -\frac{1}{L^2} \int_{\Omega_1} \cos^2 \frac{\pi}{L}(z_e - z_{1(2)}) \cos^2 \frac{\pi}{L}(z_h - z_{1(2)}) \frac{dz_e dz_h}{4\pi\epsilon_0\epsilon_r \sqrt{r^2 + (z_e - z_h)^2}} \\
&= -\frac{1}{L^2} \int_{\Omega_2} \frac{1}{2} \left[\cos^2 \frac{\pi}{L}(\xi \pm d) + 2\cos \frac{\pi}{L}(\xi \pm d)\cos \frac{\pi}{L}\eta + \cos^2 \frac{\pi}{L}\eta\right] \frac{d\xi d\eta}{4\pi\epsilon_0\epsilon_r \sqrt{r^2 + \eta^2}} \\
&= -\frac{1}{2L} \int_{-L}^{L} \left(1 + 2\cos^2 \frac{\pi}{L}\eta\right) \frac{d\eta}{4\pi\epsilon_0\epsilon_r \sqrt{r^2 + \eta^2}}.
\end{aligned}
$$
(3.112)

Few comments are necessary: the third line was achieved from the second one using the transformation (3.111), one half behind the integration mark comes from the jacobian of such a transformation. Remember, $z_{1(2)} = \mp\frac{d}{2}$. The integration area Ω_1 is a square, Ω_2 is more difficult, both are depicted for the general case in Fig. 3.3.[5] The last line of Eq. (3.112) is the resulting one-dimensional integral, which has to be calculated numerically. Another terms in Eq. (3.84) would be treated in the same way.

---

[5]In Fig. 3.3, z_i marks the QW-centre for electrons, z_j is the corresponding quantity for holes.

3.3.5 Expansion of in-plane components

It would bring some difficulties to find the exact solution of (3.77). It was shown in [12] that if we substitute the Coulomb potential with the parabolic one, the analytic solution is found easily. To be more specific, for the "in-plane" potential V of the form

$$V(x, y) = C(x^2 + y^2) - S, \qquad (3.113)$$

the eigenfunctions $\phi(x, y)$, which solve the equation $\left[\hat{H}_e^1 + \hat{H}_{hh}^1 + V(x, y)\right]\phi(x, y) = E\phi(x, y)$ if we substitute for $\hat{H}_e^1$ from (3.94) and for $\hat{H}_{hh}^1$ from (3.97), assuming $B_\perp = B_\parallel = 0$, are

$$\phi_{nm}(x, y) = N H_n\left(\sqrt{2A}x\right) H_m\left(\sqrt{2A}y\right) \exp\left[-A(x^2 + y^2)\right] \exp\left[i\,G(K_x x + K_y y)\right], \quad (3.114)$$

where N is a normalization constant, $H_{n(m)}$ is the Hermite polynomial of order $n(m)$, and

$$A = \frac{1}{4\hbar}\sqrt{\frac{8m_e m_h C}{m_e + m_h}}, \qquad G = \frac{\lambda m_e - \mu m_h}{m_e + m_h}, \qquad (3.115)$$

giving the eigenvalues

$$E = E_e(0) + E_{h0}(0) - S + \frac{\hbar^2}{2(m_e + m_h)}\left(K_x^2 + K_y^2\right) + \hbar\sqrt{\frac{2C(m_e + m_h)}{m_e m_h}}, \qquad (3.116)$$

analogous to the solution of the linear harmonical oscillator. Latter procedure can be repeated for another diagonal terms of the excitonic hamiltonian, giving similar results.

In the presence of an external magnetic field, there are no problems with the in-plane component, $B_\parallel$. The solution (3.114) holds true if we substitute K_y with $K_y \pm deB_\parallel/\hbar$. However, the presence of the perpendicular field, $B_\perp$, changes the form of corresponding equations and the solution (3.114) is no longer valid (within the meaning of the exact solution).

Nevertheless, we adopt the functions (3.114) as a good basis set since they are not the solution of (3.77) anyway: first of all, they are the eigenfunctions of its diagonal part only if $B_\perp = 0$ and the parabolic potential is present; secondly, the parabolic potential (3.113) is just a simplification of the "real" Coulomb potential given by terms analogous to (3.112), valid only under some other assumptions (detailed discussion could be found in [12]).

We expand the in-plane components $u_{i\beta(\gamma)j}^\pm$, $v_{i\alpha j}^\pm$ of the wavefunction (3.90) in the following manner:

$$u(v)_{i\beta(\gamma,\alpha)j}^\pm(x, y) = \sum_{n,m=0}^{n_{\max}, m_{\max}} c_{i\beta(\gamma,\alpha)j}^\pm(n, m) \phi_{nm}(x, y)$$

$$= \sum_{n,m=0}^{n_{\max}, m_{\max}} c_{i\beta(\gamma,\alpha)j}^\pm(n, m) H_n\left(\sqrt{2A}x\right) H_m\left(\sqrt{2A}y\right) \exp\left[-A(x^2 + y^2)\right]$$

$$\cdot \exp\left[i\,G(K_x x + K_y y)\right]. \quad (3.117)$$

In Eq. (3.115), hole mass m_h appears in both formulae for A, G coefficients. Furthermore, A is a function of C, which is, in our case, unknown parameter. Since we consider both light and heavy holes, we set m_h equal to the arithmetic mean of these values, $m_h = (m_{lh}+m_{hh})/2$. To improve the method while expanding the solution to a basis set composed of functions which are not the eingenfunctions of the diagonal part of (3.77), we choose parameter C as variational. Starting with some initial value, we find that value for which the energy of the excitonic ground level is the lowest.

Since the expansion (3.117) is independent in the x, y directions, we also tried two-dimensional variational method, which means that instead of having one parameter C (from which the corresponding value of A is calculated), we work with two separate parameters, C_x, C_y. From these quantities, two values A_x, A_y are obtained, while the expansion (3.117) takes form:

$$u(v)^{\pm}_{i\beta(\gamma,\alpha)j}(x,y) = \sum_{n,m=0}^{n_{\max},m_{\max}} c^{\pm}_{i\beta(\gamma,\alpha)j}(n,m)\phi^{2D}_{nm}(x,y)$$

$$= \sum_{n,m=0}^{n_{\max},m_{\max}} c^{\pm}_{i\beta(\gamma,\alpha)j}(n,m)H_n\left(\sqrt{2A_x}x\right)H_m\left(\sqrt{2A_y}y\right)\exp\left(-A_x x^2\right)\exp\left(-A_y y^2\right)$$

$$\cdot \exp\left[i\,G(K_x x + K_y y)\right]. \quad (3.118)$$

A comparison between these two approaches will be given later.

3.3.6 Wavefunction overview

The whole information about the quantum-mechanical system is contained in its wavefunction. The eigenvalues of the excitonic hamiltonian (3.77) (energy levels of the system) together with the corresponding eigenvectors give us all we have to know before calculating some experimentally-important results, such as optical spectra. Hence, before we proceed later, it is of major importance to realize how actually the total wavefunction Ψ_{ex} of the system we deal with looks like.

Several transformations and substitutions have been made. If we take a look back into the text and follow the procedure backwards, we hope one can easily find that

$$\Psi_{\text{ex}}(\mathbf{r}_e, \mathbf{r}_h) = N \exp\left[i\left(\mathbf{k}_{e\parallel} \cdot \mathbf{r}_{e\parallel} + \mathbf{k}_{h\parallel} \cdot \mathbf{r}_{h\parallel}\right)\right]\Psi(\mathbf{r}_e, \mathbf{r}_h), \quad (3.119)$$

where N is a normalization constant. It is necessary to substitute for Ψ from (3.23). After that, we have

$$\Psi_{\text{ex}}(\mathbf{r}_e, \mathbf{r}_h) = N \exp\left[i\left(\mathbf{k}_{e\parallel} \cdot \mathbf{r}_{e\parallel} + \mathbf{k}_{h\parallel} \cdot \mathbf{r}_{h\parallel}\right)\right]u_e(\mathbf{r}_e)\Big[c_{|\frac{3}{2},+\frac{3}{2}\rangle}(\mathbf{r}_e, \mathbf{r}_h)u_{|\frac{3}{2},+\frac{3}{2}\rangle}(\mathbf{r}_h)$$

$$+ c_{|\frac{3}{2},+\frac{1}{2}\rangle}(\mathbf{r}_e, \mathbf{r}_h)u_{|\frac{3}{2},+\frac{1}{2}\rangle}(\mathbf{r}_h) + c_{|\frac{3}{2},-\frac{1}{2}\rangle}(\mathbf{r}_e, \mathbf{r}_h)u_{|\frac{3}{2},-\frac{1}{2}\rangle}(\mathbf{r}_h) + c_{|\frac{3}{2},-\frac{3}{2}\rangle}(\mathbf{r}_e, \mathbf{r}_h)u_{|\frac{3}{2},-\frac{3}{2}\rangle}(\mathbf{r}_h)\Big].$$

$$(3.120)$$

Remember, the expansions for functions $c_{|\frac{3}{2},\pm\frac{1}{2}(\frac{3}{2})\rangle}$ are given by Eqs. (3.44)–(3.47). Moreover, each coefficient there was factorized from (3.82) into (3.90). Finally, the in-plane components $u^{\pm}_{i\beta(\gamma)j}$, $v^{\pm}_{i\alpha j}$ from (3.90) are expanded according to (3.117) for one-dimensional or in accordance with (3.118) for two-dimensional variational method, using the Hermite-Gauss basis set (3.114). We must give up our efforts to put all the expansions into one formula since it would be very long and not provide an easy survey.

3.3.7 Optical spectra

In this section, we will give short theory of absorption and photoluminescence and show how to apply it to our problem. At the end, the important formulae for calculation of optical spectra will be derived.

The Einstein coefficients link together spontaneous and stimulated emission and absorption. Therefore, let us calculate the probability $P_{v\to c}$ of transition from the initial state $|v\rangle$ in the valence band to the unoccupied conduction-band state $|c\rangle$, in other words, the probability of electron-hole recombination accompanied by emission of a photon with energy E. Similarly to [22], by the Fermi golden rule, we have

$$P_{v\to c} \propto |\langle v|H_{\text{int}}|c\rangle|^2\, \delta\big(E_v(\mathbf{k}_v) - E_c(\mathbf{k}_c) - E)\big), \tag{3.121}$$

where E_v and E_c are the energies of the initial and final state, respectively, and H_{int} is the interaction hamiltonian between light and the studied system, usually written in the dipole approximation. If we denote by index i the electronic subbands in the conduction band and by j the hole subbands in the valence band, the total luminescence intensity $\mathcal{L}$ is then determined as a summation over all initial and final states, i. e. over indices i, j and momenta $\mathbf{k}_v$, $\mathbf{k}_c$:

$$\mathcal{L}(E) \propto \sum_{i,j} \sum_{\mathbf{k}_v, \mathbf{k}_c} f^c_{FD}\big(E_{c_i}(\mathbf{k}_c)\big)\big[1 - f^v_{FD}\big(E_{v_j}(\mathbf{k}_v)\big)\big]\, |\langle c_i|H_{\text{int}}|v_j\rangle|^2$$
$$\cdot\, \delta\big(E_{c_i}(\mathbf{k}_c) - E_{v_j}(\mathbf{k}_v) - E)\big). \tag{3.122}$$

In the latter formula, we have included the population of valence ($\propto 1 - f^v_{FD}$) and conduction ($\propto f^c_{FD}$) band states, usually described by the Fermi-Dirac distribution function $f^{c(v)}_{FD}(E) = \big[1 + \exp\big((E - E_F^{c(v)})/k_B T\big)\big]^{-1}$, if $E_F^{c(v)}$ denotes the quasi-Fermi level in the conduction (valence) band, k_B is the Boltzmann constant, and T temperature. To simplify Eq. (3.122), it is essential to calculate the matrix element of the interaction hamiltonian, $\langle c_i|H_{\text{int}}|v_j\rangle$. In the envelope function approximation, we have

$$\begin{aligned} \langle \mathbf{r}\,|c_i\rangle &\propto \chi^i_{e,\mathbf{k}_{e\parallel}}(z) u_c(\mathbf{r}) \exp\big(\mathrm{i}\,\mathbf{k}_{e\parallel}\cdot\mathbf{r}_\parallel\big), \\ \langle \mathbf{r}\,|v_j\rangle &\propto \sum_\nu \chi^j_{\nu,\mathbf{k}_{h\parallel}}(z) u_\nu(\mathbf{r}) \exp\big(\mathrm{i}\,\mathbf{k}_{h\parallel}\cdot\mathbf{r}_\parallel\big), \end{aligned} \tag{3.123}$$

where the summation over ν runs over light- and heavy-hole states, $|\frac{3}{2},\pm\frac{1}{2}(\frac{3}{2})\rangle$. Assuming that the envelope function varies slowly in comparison to the rapid-oscillating periodic

parts of the Bloch functions, one can further write

$$\langle c_i | H_{\text{int}} | v_j \rangle \propto \sum_{\nu} \langle u_c | H_{\text{int}} | u_\nu \rangle \, \delta_{\mathbf{k}_{e\parallel}, \mathbf{k}_{h\parallel}} \int_{-\infty}^{+\infty} \left(\chi^i_{e,\mathbf{k}_{e\parallel}}(z) \right)^* \chi^j_{\nu,\mathbf{k}_{h\parallel}}(z) \, \mathrm{d}z. \tag{3.124}$$

The first term in Eq. (3.124) determines the strength of the corresponding optical transition. It can be found in [13] that for the light propagation parallel to the z axis, the intensity of light polarized in the x, y direction is three times higher for the heavy hole-electron transitions than for the light hole-electron transitions, hence we take:

$$\begin{aligned}
\mathcal{I}_{|\frac{3}{2}, \pm\frac{3}{2}\rangle} &= \langle u_c | H_{\text{int}} | u_{|\frac{3}{2}, \pm\frac{3}{2}\rangle} \rangle = \frac{1}{\sqrt{2}}, \\
\mathcal{I}_{|\frac{3}{2}, \pm\frac{1}{2}\rangle} &= \langle u_c | H_{\text{int}} | u_{|\frac{3}{2}, \pm\frac{1}{2}\rangle} \rangle = \frac{1}{\sqrt{6}}.
\end{aligned} \tag{3.125}$$

These quantities will be used later in the computation of the optical spectra. The second term in Eq. (3.124) demonstrates the momentum conservation in the optical transition. Finally, the last term is the electron-hole overlap integral. To calculate it, we have to write formulae for $\chi^i_{e,\mathbf{k}_{e\parallel}}$ and $\chi^j_{\nu,\mathbf{k}_{h\parallel}}$. In the tight-binding approximation, these are given by

$$\chi^i_{e,\mathbf{k}_{e\parallel}}(z) = c^{1,i}_{e,\mathbf{k}_{e\parallel}} \varphi^1_e(z) + c^{2,i}_{e,\mathbf{k}_{e\parallel}} \varphi^2_e(z),$$

$$\chi^j_{\nu,\mathbf{k}_{h\parallel}}(z) = \begin{cases} c^{1,j,\pm}_{h0,\mathbf{k}_{h\parallel}} \varphi^1_{h0}(z) + c^{2,j,\pm}_{h0,\mathbf{k}_{h\parallel}} \varphi^2_{h0}(z) + c^{1,j,\pm}_{h1,\mathbf{k}_{h\parallel}} \varphi^1_{h1}(z) + c^{2,j,\pm}_{h1,\mathbf{k}_{h\parallel}} \varphi^2_{h1}(z) & \text{if } \nu = |\frac{3}{2}, \pm\frac{3}{2}\rangle, \\ c^{1,j,\pm}_{l,\mathbf{k}_{h\parallel}} \varphi^1_l(z) + c^{2,j,\pm}_{l,\mathbf{k}_{h\parallel}} \varphi^2_l(z) & \text{if } \nu = |\frac{3}{2}, \pm\frac{1}{2}\rangle. \end{cases} \tag{3.126}$$

For the functions $\varphi_{e(h0(1),l)}(z_{e(h)})$, see Eqs. (3.48) and (3.49). If we substitute the latter formula together with (3.124) into (3.122), after some trivial math, one can find that

$$\begin{aligned}
\mathcal{L}(E) \propto \sum_{i,j} \sum_{\mathbf{k}} f_{FD}\big(E^i_e(\mathbf{k})\big) \big[1 - f_{FD}\big(E^j_h(\mathbf{k})\big)\big] \Bigg| \sum_{\sigma=\pm} \mathcal{I}_{|\frac{3}{2}, \frac{3}{2}\sigma\rangle} \big(c^{1,i}_{e,\mathbf{k}} c^{1,j,\sigma}_{h0,\mathbf{k}} + c^{2,i}_{e,\mathbf{k}} c^{2,j,\sigma}_{h0,\mathbf{k}} \big) \\
+ \mathcal{I}_{|\frac{3}{2}, \frac{1}{2}\sigma\rangle} \big(c^{1,i}_{e,\mathbf{k}} c^{1,j,\sigma}_{l,\mathbf{k}} + c^{2,i}_{e,\mathbf{k}} c^{2,j,\sigma}_{l,\mathbf{k}} \big) \Bigg|^2 \delta\big(E^i_e(\mathbf{k}) - E^j_h(\mathbf{k}) - E\big).
\end{aligned} \tag{3.127}$$

It can be seen that by the rules of tight-binding approximation, the overlap integral between the ground electronic QW bound state and the first excited heavy-hole state equals zero.

Since the products $c^{r,i}_{e,\mathbf{k}} c^{s,j,\sigma}_{\eta,\mathbf{k}}$ are described by the expansion coefficients $a^{\pm}_{r\beta(\gamma)s}$, $d^{\pm}_{r\alpha s}$ of Eqs. (3.44)–(3.47), replacing $E^i_e(\mathbf{k}) - E^j_h(\mathbf{k})$ by the nth excitonic energy level $E_n(\mathbf{k})$ and substituting the distribution functions f_{FD} in (3.127) with the Boltzmann exponential factor $\mathrm{e}^{-E_n(\mathbf{k})/k_B T}$, finally it is obtained

$$\mathcal{L}(E) \propto \sum_n \sum_{\mathbf{k}} \mathrm{e}^{-E_n(\mathbf{k})/k_B T} \Bigg| \sum_{\sigma=\pm} \mathcal{I}_{|\frac{3}{2}, \frac{3}{2}\sigma\rangle} \big(a^{\sigma,n\mathbf{k}}_{1\beta 1} + a^{\sigma,n\mathbf{k}}_{2\beta 2} \big) + \mathcal{I}_{|\frac{3}{2}, \frac{1}{2}\sigma\rangle} \big(d^{\sigma,n\mathbf{k}}_{1\alpha 1} + d^{\sigma,n\mathbf{k}}_{2\alpha 2} \big) \Bigg|^2 \delta\big(E_n(\mathbf{k}) - E\big). \tag{3.128}$$

The meaning of $\mathbf{k}$ will be clarified later. It is usual to describe the inhomogeneous broadening of the spectral line using either Lorentz-shaped line or Gaussian function, or the convolution of Lorentz-shaped line with the Boltzmann distribution function, instead of the delta function in Eq. (3.128). We use the second approach, having

$$\mathcal{C}_m(E) = \frac{\Delta_m}{\pi k_B T} \int_0^{+\infty} \frac{\mathrm{e}^{-E'/k_B T} \, \mathrm{d}E'}{(E - E_m - E')^2 + \Delta_m^2} \tag{3.129}$$

analogously to [8]. Therefore, the resulting formula, luminescence spectra will be calculated with, reads

$$\mathcal{L}(E) \propto \sum_n \sum_{\mathbf{k}} \mathrm{e}^{-E_n(\mathbf{k})/k_B T} \left| \sum_{\sigma=\pm} \mathcal{I}_{|\frac{3}{2},\frac{3}{2}\sigma\rangle} \left(a_{1\beta1}^{\sigma,n\mathbf{k}} + a_{2\beta2}^{\sigma,n\mathbf{k}} \right) + \mathcal{I}_{|\frac{3}{2},\frac{1}{2}\sigma\rangle} \left(d_{1\alpha1}^{\sigma,n\mathbf{k}} + d_{2\alpha2}^{\sigma,n\mathbf{k}} \right) \right|^2 \mathcal{C}_{n\mathbf{k}}(E). \tag{3.130}$$

Since the Boltzmann exponential factor in Eqs. (3.129), (3.130) is redundant for the computation of absorption spectra as all states are assumed to be unoccupied, $\mathcal{C}_m(E)$ reduces to

$$L_m(E) = \frac{\Delta_m}{\pi} \frac{1}{(E - E_m)^2 + \Delta_m^2}. \tag{3.131}$$

If we then replace $\mathcal{C}_{n\mathbf{k}}(E)$ in (3.130) by (3.131) with $m = n\mathbf{k}$, the final formula, absorption spectra computation will be driven by, arises:

$$\mathcal{A}(E) \propto \sum_n \sum_{\mathbf{k}} \left| \sum_{\sigma=\pm} \mathcal{I}_{|\frac{3}{2},\frac{3}{2}\sigma\rangle} \left(a_{1\beta1}^{\sigma,n\mathbf{k}} + a_{2\beta2}^{\sigma,n\mathbf{k}} \right) + \mathcal{I}_{|\frac{3}{2},\frac{1}{2}\sigma\rangle} \left(d_{1\alpha1}^{\sigma,n\mathbf{k}} + d_{2\alpha2}^{\sigma,n\mathbf{k}} \right) \right|^2 L_{n\mathbf{k}}(E). \tag{3.132}$$

Achieved results will be presented in Chapter 4.

3.3.8 Probability density

Nice figures demonstrating the real-space charge density distribution can be obtained computing the probability density. By the rules of quantum mechanics, it is achieved by evaluating the square of the absolute value of the wavefunction describing the studied system. Important details concerning our excitonic wavefunction were summarized in Sec. 3.3.6. From the facts shown there, we can easily derive that in the envelope function approximation, the radial[6] charge density is given by

$$|\Psi(x,y)|^2 = \sum_{i,j=1}^{2} \sum_{\sigma=\pm} \left(|a_{i\beta j}^{\sigma}|^2 + |a_{i\gamma j}^{\sigma}|^2 + |d_{i\alpha j}^{\sigma}|^2 \right), \tag{3.133}$$

where one must not forget to construct the coefficients $a(d)_{i\beta(\gamma,\alpha)j}^{\pm}$ from the expansions discussed in Sec. 3.3.6.

---

[6]It means written in in-plane coordinates x, y.

3.3.9 Numerical treatment

As the complexity of the problem does not enable us to find the solution analytically, we are thrown upon the use of numerical methods. These have been developing for years by mathematicians all over the world and now a lot of the common mathematical tasks we can come across during solving physical problems are solved. The only question that is to be answered is the choice of the proper method, keeping in mind the requirements for numerical precision or time consumption.

Most of the optimized codes are available on-line, e. g. a large collection of Fortran subroutines that compute the eigenvalues and eigenvectors for special types of matrices is contained in the EISPACK library. Other important codes can be found in [23].

The three most important tasks that our problem contains are: (1) the variational computation of the optimal basis parameters, (2) the construction of the matrix hamiltonian in the chosen basis of the Hermite-Gauss functions (3.114), and (3) the diagonalisation of the resulting matrix.

For one-dimensional variational method, the Brent algorithm is used, two-dimensional one is performed using AMOEBA subroutine. Details for both methods are to be found in [23]. The computation of matrix terms is performed using Romberg integration method, details can be found in [23]. The upper limits n_{max}, m_{max} of the expansions (3.117) and (3.118) fulfil the conditions $n_{max} \leq 9$, $m_{max} \leq 9$, since greater values would prolong the computation too much. To diagonalise the matrix hamiltonian, we used the EISPACK CH-subroutine, designed for complex hermitian matrices. This method calls the recommended sequence of subroutines to find the eigenvalues and eigenvectors: first of all, the input matrix is reduced to a real symmetric tridiagonal matrix. In the next step, the tridiagonal matrix is diagonalised using the QL method, the eigenvalues are written on output. As the last operation, the eigenvectors are formed by back transforming the corresponding real symmetric tridiagonal matrix from the previous step. On output, the eigenvalues and eigenvectors are provided.

Chapter 4

Results and discussion

In this chapter, the calculated results will be demonstrated. We start with the dispersion relations, showing the energy dependence on the centre-of-mass momentum. On the simplest possible model, an exciton located in a DQW when no external fields are present, the most important effects are illustrated, giving us an opportunity to predict the behaviour when more precise calculations are performed. The effect of an electric field in the growth direction and a magnetic field in both perpendicular and parallel orientations is discussed. Finally, absorption and photoluminescence spectra are computed and illustrated on relevant figures.

It could be found in [5] that the energy minimum is always located at $K_x = 0$. Hence we do not discuss the K_x dependency in detail. The following parameters are used in all calculations throughout the work:

$$m_e = 0.067m_0, \qquad \gamma_1 = 6.85, \qquad \gamma_2 = 2.10, \qquad \gamma_3 = 2.90,$$

from which it follows that

$$m_{hh\parallel} = 0.112m_0, \quad m_{hh\perp} = 0.377m_0, \quad m_{lh\parallel} = 0.211m_0, \quad m_{lh\perp} = 0.090m_0,$$

where $m_0 = 9.109 \times 10^{-31}$ kg is the free-electron mass. For electron, the "in-plane" and the "perpendicular" masses are assumed to be equal. Moreover, for both electrons and holes, we suppose that the masses are the same both in the well and the barrier. Notice that the in-plane heavy-hole mass is less that the in-plane light-hole mass (so called *mass reversal*).

The permittivity of GaAs/AlGaAs, the well width, and the distance between QWs forming the DQW are as follows:

$$\epsilon_r = 12.9, \qquad L = 10 \text{ nm}, \qquad d = 10 \text{ nm},$$

assuming $\epsilon_0 = 8.854 \times 10^{-12}$ F/m. The bandgap width and the energies of bound states in separate QWs are

$$E_g = 1.5 \text{ eV}, \qquad E_{e0} = 42 \text{ meV}, \qquad E_{l0} = 22 \text{ meV},$$
$$E_{h00} = 4 \text{ meV}, \qquad E_{h10} = 29 \text{ meV},$$

while for the tunneling matrix elements, we have

$$t_e = 3 \text{ meV}, \qquad\qquad t_l = 2 \text{ meV},$$
$$t_{h0} = 0.010 \text{ meV}, \qquad\qquad t_{h1} = -0.012 \text{ meV}.$$

The minus sign in t_{h1} originates from the definition of the corresponding matrix term.

Throughout the whole previous chapter, we paid attention to derived equations, looking for a chance to simplify them by setting the parameters μ, λ of the transformation (3.87) properly. However, no advantageous choice satisfying the condition $\mu + \lambda = 1$ was discovered. Thus, we chose the symmetric gauge $\mu = \lambda = \frac{1}{2}$.

4.1 Energy dependencies

Dispersion relations both with and without external fields, the effect of the valence-subband mixing on expansion coefficients, the shift of energy levels in external fields, and a comparison between bases of different extensions are studied in this section.

4.1.1 Dispersion relations

Basic information about the excitonic energy levels is provided by dispersion relations. These show the energy dependence on the "generalized" centre-of-mass momentum introduced by Eq. (3.87). As mentioned above, since the K_x dependence is not of our main interest, only the $E = E(K_y)$ dependence is discussed.

4.1.1.1 Dispersion relations in the absence of external fields

Starting with 1×1 basis,[1] which means that the results will be more qualitative than quantitative, the situation for no external fields is shown in Fig. 4.1. The relations are even in K_y and four important effects that play the main role for the form of depicted lines are illustrated: band anti-crossing, valence-subband mixing, mass reversal, and light-hole negative effective mass near the origin. Let us inspect them in detail.

As mentioned in the previous chapter, the presence of non-zero matrix elements originating from Luttinger $\hat{b}$ and $\hat{c}$ terms modifies the energy spectrum. If these terms are neglected, the anti-crossing effect does not take place, the dispersion relations intersect each other and the situation is similar to that depicted in Fig. 4.1 with dashed lines. Solid lines show the situation when $\hat{b}$ and $\hat{c}$ terms are considered. It is obvious that though the degeneracy of most levels is partially lifted, all levels remain twofold degenerate. This "spin" degeneracy, which cannot be lifted when no external fields are applied, corresponds to $m_J = \pm \frac{1}{2}$ and $m_J = \pm \frac{3}{2}$ hole subbands.

The valence-subband mixing is also obvious in Fig. 4.1 at first sight, if we take a look at the two lowest-lying levels. Although it may seem that they are degenerate at the origin,

---

[1]Expansions (3.117) of the matrix hamiltonian are restricted to the lowest level separately in both the x and the y directions.
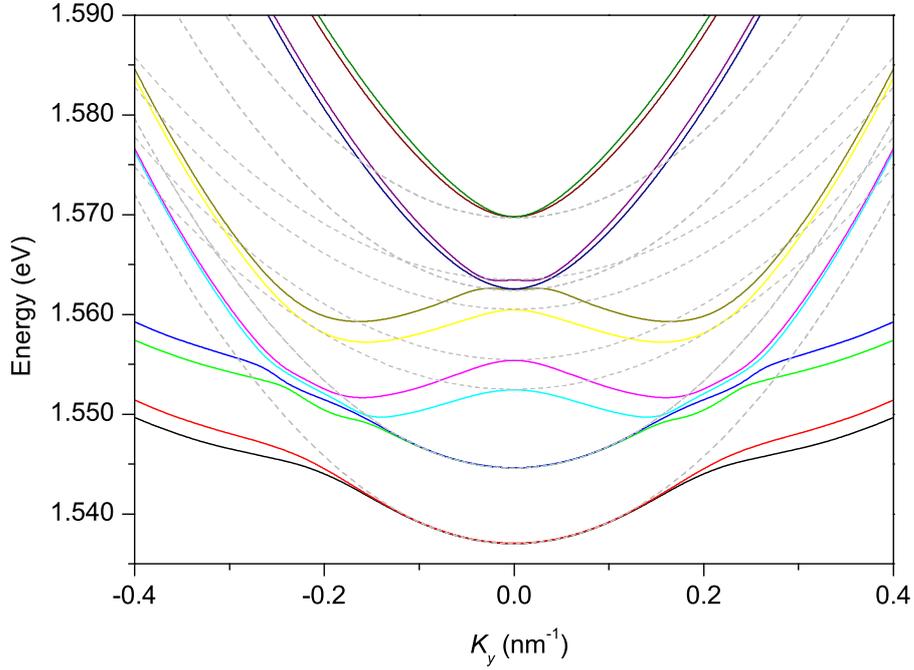
Figure 4.1: Dispersion relations of an exciton in a DQW without external fields. Solid lines show the situation when $\hat{b}$ and $\hat{c}$ terms are non-zero whilst dashed lines illustrate the situation when these vanish.

they are actually not. This arises from the energy axis scale that is too large to realize the gap between them, approximately given by $2t_{h0} = 2 \times 0.01$ meV $= 0.02$ meV, since both these levels correspond to heavy-hole excitonic states. However, farther from the origin, starting approximately at $K_y \approx 0.2$ nm^{-1} and from there on, the character of these levels changes. The strength of heavy-hole contributions falls as the strength of light-hole ones rises. This can be seen in Fig. 4.2 on the K_y dependence of the expansion coefficients (square of their absolute values) associated with light- and heavy-hole excitonic states of the tight-binding expansions (3.44)–(3.47).

Since the heavy-hole contribution weakens whereas the light-hole one becomes more important with increasing K_y, the gap between the two lowest-lying levels, given in the first case approximately by $2t_{h0}$, changes to $2t_l = 2 \times 2$ meV $= 4$ meV, a significantly greater value, in the second case, as can been seen directly from Fig. 4.1.

If we are concerned about the excitonic binding energies, a simple estimate can be made from Fig. 4.1 using parameters introduced at the beginning of this chapter. If we denote by $\Delta E = E_g + E_{e0} + E_{h00} = 1.546$ eV the energy separation of the ground levels in a single QW and since the energy E_{hh}^{d} of the direct heavy-hole excitonic level with $K_y = 0$ is $E_{hh}^{\text{d}} = 1.5370$ eV, the corresponding binding energy B_{hh}^{d} is approximately given by $B_{hh}^{\text{d}} = \Delta E - t_e - E_{hh}^{\text{d}} = 6.0$ meV, if the value t_{h0} of the heavy-hole tunneling matrix element has been neglected in comparison to t_e. Analogously, as the energy E_{hh}^{ind} of the
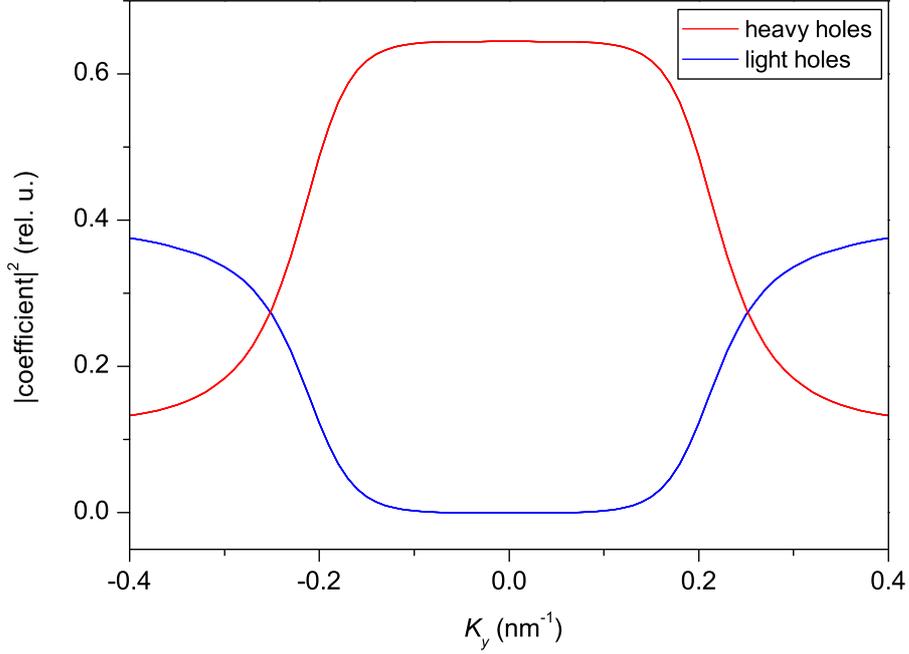
Figure 4.2: The effect of the valence-subband mixing on the tight-binding expansion coefficients when no external fields are applied.

indirect heavy-hole exciton is $E_{hh}^{\text{ind}} = 1.5446$ eV, using the formula $B_{hh}^{\text{ind}} = \Delta E + t_e - E_{hh}^{\text{ind}}$, the corresponding binding energy reads $B_{hh}^{\text{ind}} = 4.4$ meV. Discussion of these values, as well as a comparison with existing results, will be given in Chapter 5.

The change in the dispersion relations character is also accompanied by the change in the slope of the corresponding curves. The curvature near the origin determines the effective mass. The greater the mass is, the less slope obtained. Comparing slopes of the two lowest-lying levels near the origin and for $K_y > 0.2$ nm^{-1}, one can conclude that the effective mass for smaller K_y is less than that for greater K_y: another nice illustration of the described phenomenon, the valence-subband mixing, now demonstrated by the mass reversal effect, as $m_{hh\parallel} < m_{lh\parallel}$.

Finally, the last effect we are about to discuss is the negative light-hole effective mass. This effect, connected to Luttinger $\hat{b}$ and $\hat{c}$ terms (see Fig. 4.1), demonstrates once again the strong coupling between valence subbands. The dispersion lines of light-hole excitons, influenced by near-located heavy-hole excitonic levels with a hole in the first excited state, turn down and fall until they are far enough that the interaction with heavy-hole excitonic levels with a hole in the ground state turns them up again.

It may seem that the proximity of the light-hole excitonic states and the heavy-hole excitonic levels with an excited hole is a real effect. However, this situation is just accidental, resulting from the chosen set of parameters used for variational computation. Expanding the solution to the larger basis, this effect would vanish, leaving the levels distant enough.

Table 4.1: Dependence of the variational parameter C, the related quantity A, and the excitonic radius R on K_y for 1×1 basis.

K_y (nm^{-1})	-0.4	-0.3	-0.2	-0.1	0.0	0.1	0.2	0.3	0.4
C (10^{-6} kg/s^2)	3.796	3.733	3.443	3.269	3.265	3.269	3.443	3.733	3.796
A (10^{-3} nm^{-2})	2.712	2.690	2.583	2.517	2.515	2.517	2.583	2.690	2.712
R (nm)	13.6	13.7	13.9	14.1	14.1	14.1	13.9	13.7	13.6

Let us take a look at the variational method itself. As the variational calculation is performed for each K_y from the selected interval, the optimal value of variational parameter C and the corresponding value of A (see Eq. (3.115)) may change. For some values of -0.4 nm$^{-1} \leq K_y \leq 0.4$ nm^{-1}, this can be found in Tab. 4.1; R is the radius of the ground-state exciton.[2] Since no external fields are present, the value of C varies very slowly. It will be demonstrated later that if an electric (or especially a magnetic field) is applied, the dependence is much stronger. Further discussion of obtained values of R will be given in Chapter 5.

4.1.1.2 Dispersion relations in the presence of an external electric field

Another very important situation, an exciton in a DQW in the presence of an external electric field, can be nicely illustrated on our simplified model, based on 1×1 basis expansion. Dispersion relations for the electric field $\mathcal{E} = 30$ kV/cm are depicted in Fig. 4.3. Evidently, there are more lines then in Fig. 4.1. If one tried to count them, the number of 24 would be achieved. The presence of an external electric field breaks the symmetry of our quantum-well system, resulting in the splitting of twofold degenerate energy levels for $K_y \neq 0$. The Kramer's degeneracy is lifted away off the origin.[3] Such a split off clearly originates from the term $\hat{H}_{hh}^2$ of the excitonic hamiltonian. As it is given by Eq. (3.64), the only way how to make it non-zero is to turn on the in-plane magnetic field, or — just like in this situation — to apply an electric field on the sample. Consequently, the excitonic hamiltonian, a 24×24 matrix in 1×1 basis, cannot be decomposed into two identical 12×12 non-interacting blocks as in the situation when no fields were applied. The matrix is irreducible, giving 24 different eigenvalues. However, as only the electric field is applied and there is no additional magnetic field, the dispersion relations remain even in K_y, $E(K_y) = E(-K_y)$.

Though an electric field is applied in the growth direction (along the z axis), it affects energy levels in x, y plane. The splitting for $K_y = \pm 0.4$ nm^{-1} reaches for the lowest-

---

[2]Though the quantity R, connected to the variational parameter A through the formula $R = 1/\sqrt{2A}$ (2 in the denominator comes from $|\Psi|^2$), does not exactly express the excitonic radius but the "width" of Gaussian functions used to construct a wavefunction, its increase would obviously rise the value of excitonic radius and we will use it in this sense.

[3]For more details about the Kramer's degeneracy, please see [13].
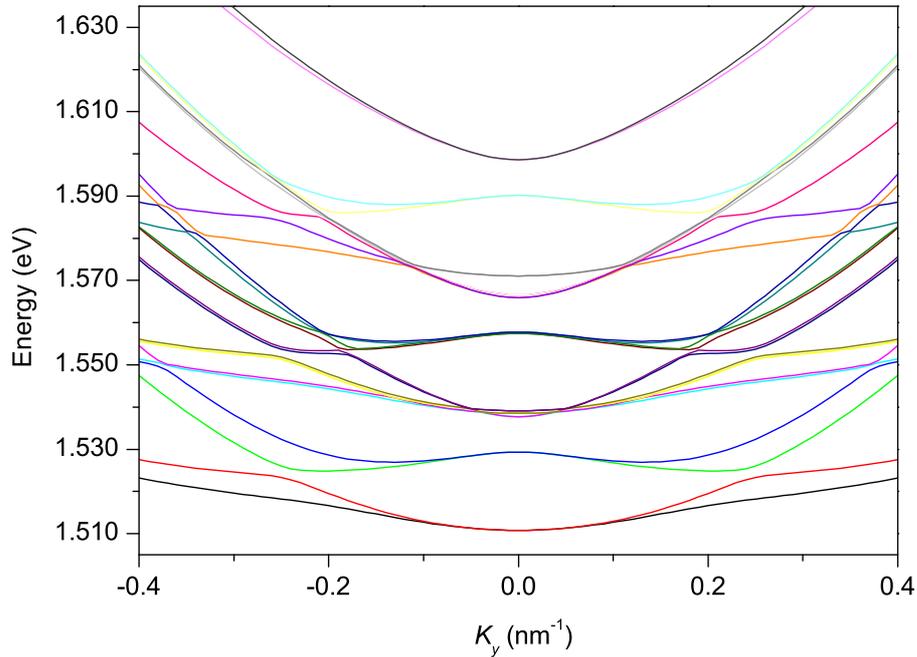
Figure 4.3: Dispersion relations of an exciton in a DQW for the electric field $\mathcal{E} = 30$ kV/cm in the growth direction.

lying levels approximately 4 meV. The character of several energy levels is summarized in Tab. 4.2, where the greatest contribution to eigenvectors for the corresponding eigenvalue is shown. Notice that for $K_y = 0$, all levels are twofold degenerate. Remember, we adopted notation α for light holes, β for the heavy-hole ground state, and finally, γ stands for the first excited heavy-hole state. The second line shows the energy of the level, the third line keeps the state of major contribution, correspondence to either direct (d) or indirect (i) exciton is to be read from the fourth line. The last line shows the absolute value of the greatest expansion coefficient. While for $K_y = 0$, the listed states are dominant as mixing is very weak, for non-zero K_y, the coupling strengthens, resulting in levels composed of both light- and heavy-hole excitons. This can be seen as the decrease of the absolute value of the strongest expansion coefficients shown in Tab. 4.2.

It is also notable that the lowest-lying states consist of indirect excitons, for the chosen orientation of the electric field with an electron in the left well and a hole in the right well. Moreover, we can conclude that an electric field applied on a DQW structure does not prefer any total angular momentum orientation since states with both $m_J = +\frac{1}{2}(\frac{3}{2})$ and $m_J = -\frac{1}{2}(\frac{3}{2})$ are represented in different eigenvectors equally.

Just like in previously discussed situation, we can take notice of variational calculations. As the dispersion relations are even in K_y, nothing different can be expected from the dependence of C and A on the centre-of-mass momentum. This is shown in Tab. 4.3. We tried the two-dimensional variational method as well. However, there was no significant

Table 4.2: The strongest contributions to eigenvector expansions for several selected energy levels for $\mathcal{E} = 30$ kV/cm and $K_y = 0$ (a), and $K_y = \pm 0.3$ nm^{-1} (b).

(a)

level	1	2	3
E (eV)	1.5108	1.5293	1.5377
state	$1\beta 2^{\pm}$	$1\alpha 2^{\pm}$	$1\gamma 2^{\pm}$
type	i	i	i
|coeff.|	0.9762	0.9918	0.9756

(b)

level	1	2	3	4	5	6
E (eV)	1.5196	1.5246	1.5316	1.5382	1.5473	1.5478
state	$1\alpha 2^{\pm}$	$1\alpha 2^{\pm}$	$1\beta 2^{\pm}$	$1\beta 2^{\pm}$	$1\alpha 1^{\pm}$	$2\alpha 2^{\pm}$
type	i	i	i	i	d	d
|coeff.|	0.4570	0.5295	0.5959	0.5612	0.4519	0.4542

Table 4.3: Dependence of the variational parameter C, the related quantity A, and the excitonic radius R on K_y for $\mathcal{E} = 30$ kV/cm in 1×1 basis.

K_y (nm^{-1})	-0.4	-0.3	-0.2	-0.1	0.0	0.1	0.2	0.3	0.4
C (10^{-6} kg/s^2)	0.551	0.515	0.460	0.454	0.459	0.454	0.460	0.515	0.551
A (10^{-3} nm^{-2})	1.033	0.999	0.944	0.938	0.943	0.938	0.944	0.999	1.033
R (nm)	22.0	22.4	23.0	23.1	23.0	23.1	23.0	22.4	22.0

effect on dispersion relations. The only effect observed was the slight change in the value of expansion coefficients as C_x and C_y parameters were almost equal. Furthermore, the two-dimensional procedure is more time-consuming than the one-dimensional. Therefore, we chose faster method and performed the calculations using one-dimensional algorithm.

The binding energy B_{hh}^{ind} of the ground indirect heavy-hole exciton with $K_y = 0$ is evaluated using the same procedure as in the previous paragraph, giving $B_{hh}^{\text{ind}} = \Delta E - t_e - ed\mathcal{E} - E_{hh}^{\text{ind}} = 2.2$ meV, where $ed\mathcal{E} = 30$ meV and E_{hh}^{ind} is the energy of level 1 in Tab. 4.2a. The decrease in binding energy of the ground excitonic level in an electric field in comparison to the situation when no fields were present is comprehensible: while in the currently-studied situation, the ground level is formed from indirect states, in the second case it is composed of direct ones. Since the binding energy is lower, the excitonic radius is larger, see Tabs. 4.1 and 4.3.
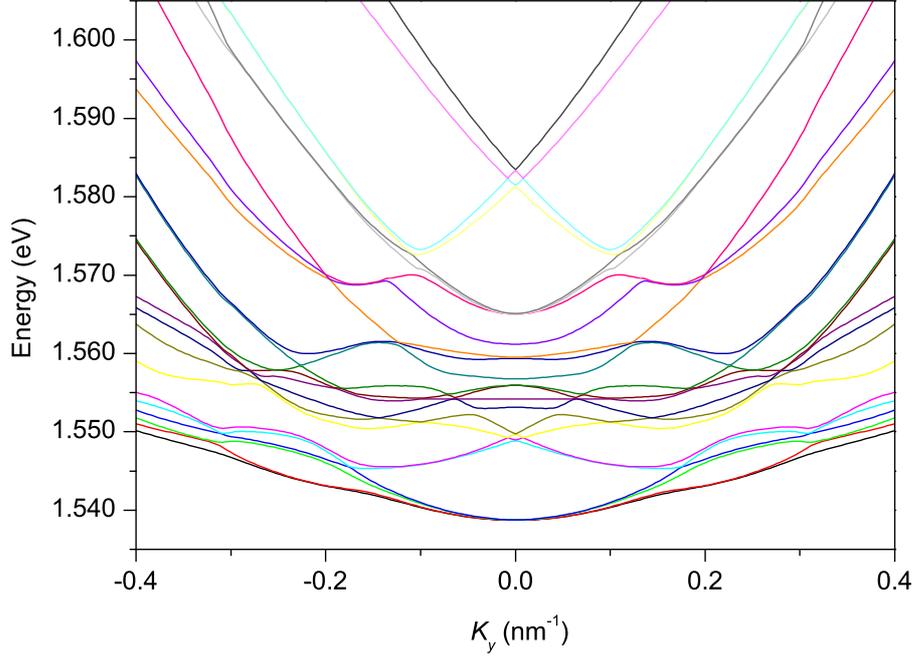
Figure 4.4: Dispersion relations of an exciton in a DQW for the situation when the in-plane magnetic field of magnitude $B_\parallel = 10$ T is applied.

4.1.1.3 Dispersion relations in the presence of the in-plane magnetic field

To demonstrate the effect of the in-plane magnetic field on our system, the dispersion relations were calculated for 1×1 basis. In Fig. 4.4, the situation for $B_\parallel = 10$ T is shown.

There is no doubt that the degeneracy splitting takes place. Thus instead of 12 lines as in the absence of external fields (see Fig. 4.1), the situation is similar to that discussed above (see Fig. 4.3): 24 lines showing the energy dependence exist. However, for the lowest energy levels, the splitting does not reach such values as it did in the presence of an electric field. For $K_y = \pm 0.4$ nm^{-1}, it is at about 1 meV, the lines are close to each other.

Just like in all forementioned situations, we can identify energy levels of our choice. The results achieved for $K_y = 0$ can be found in Tab. 4.4, those for $K_y = \pm 0.24$ nm^{-1} are listed in Tab. 4.5. It should be noted that for $K_y = 0$, the four lowest-lying levels associated with direct heavy-hole excitons are almost degenerate while for non-zero K_y, this "degeneracy" disappears. Strong valence-subband mixing takes place, resulting in the change of character of the lowest levels. For $K_y = \pm 0.24$ nm^{-1}, the two states of minimal energy are created predominantly from indirect excitons, which is clearly demonstrated in the increase of excitonic radius depicted in Fig. 4.5a.

It was derived in Chapter 3 that if the in-plane magnetic field of magnitude $B_\parallel$ is applied, the indirect-exciton dispersion branches are shifted away off the origin by $\pm deB_\parallel/\hbar$, giving rise to two lateral local extrema. For $B_\parallel = 10$ T, this quantity equals approximately

Table 4.4: The strongest contributions to eigenvector expansions for lowest energy levels for $B_\parallel = 10$ T and $K_y = 0$.

level	1	2	3	4	5	6
E (eV)	1.5387	1.5387	1.5387	1.5388	1.5487	1.5490
state	$1\beta1^\pm$ $2\beta2^\pm$	$1\beta1^\pm$ $2\beta2^\pm$	$1\beta1^\pm$ $2\beta2^\pm$	$1\beta1^\pm$ $2\beta2^\pm$	$1\beta2^\pm$ $2\beta1^\pm$	$1\beta2^\pm$ $2\beta1^\pm$
type	d	d	d	d	i	i
|coeff.|	0.4913	0.4915	0.4919	0.4921	0.4534	0.4658

Table 4.5: The strongest contributions to eigenvector expansions for several selected energy levels for $B_\parallel = 10$ T and $K_y = \pm 0.24$ nm^{-1}.

level		1	2	3	4	5	6
E (eV)		1.5442	1.5443	1.5476	1.5480	1.5495	1.5499
state $\{$	$K_y = -0.24$ nm^{-1}	$1\beta2^\pm$	$1\beta2^\pm$	$1\beta1^\pm$	$2\beta2^\pm$	$1\beta1^\pm$	$2\beta2^\pm$
	$K_y = +0.24$ nm^{-1}	$2\beta1^\pm$	$2\beta1^\pm$	$2\beta2^\pm$	$1\beta1^\pm$	$2\beta2^\pm$	$1\beta1^\pm$
type		i	i	d	d	d	d
|coeff.|		0.6862	0.6985	0.5061	0.4966	0.3909	0.4029

± 0.15 nm^{-1}. Such an effect could be seen for higher energy levels (e. g. on a bunch of lines between 1.55 and 1.56 eV in Fig. 4.4), but for the lowest-lying levels, it is not so demonstrated because of the strong mixing and influence of adjacent states.

It the text above, we have likened the degeneracy splitting in a DQW subject to the in-plane magnetic field to the situation when the electric field in the growth direction is applied. However, there is one difference worth mentioning: while for $\mathcal{E} \neq 0$, $B_\parallel = 0$, it does not depend on the sign of K_y (see Tab. 4.2b), when $\mathcal{E} = 0$, $B_\parallel \neq 0$, the parity of states is different for $K_y > 0$ and $K_y < 0$. This is nicely illustrated in Tab. 4.5 and Fig. 4.5b: for $K_y < 0$, states with an electron in the left QW and a hole in the right QW are preferred, whereas for $K_y > 0$, states with a hole in the left QW and an electron in the right QW are of advantage. For the opposite sign of K_y than it is preferred, the value of corresponding coefficients decreases rapidly. However, such behaviour should not be surprising. The Lorentz force $\mathbf{F}_L$, the force of main importance when studding electrically charged moving particles, is given by

$$\mathbf{F}_L = q\mathbf{v} \times \mathbf{B}, \tag{4.1}$$

where q marks the electric charge of a particle moving with speed $\mathbf{v}$ in the magnetic field $\mathbf{B}$. As we are concerned in excitons moving in the direction of the y axis, only the second coordinate of $\mathbf{v}$ is non-zero, $\mathbf{v} = v\mathbf{e}_y$. Hence, assuming that $\mathbf{B} = B_\parallel \mathbf{e}_x$, after substitution
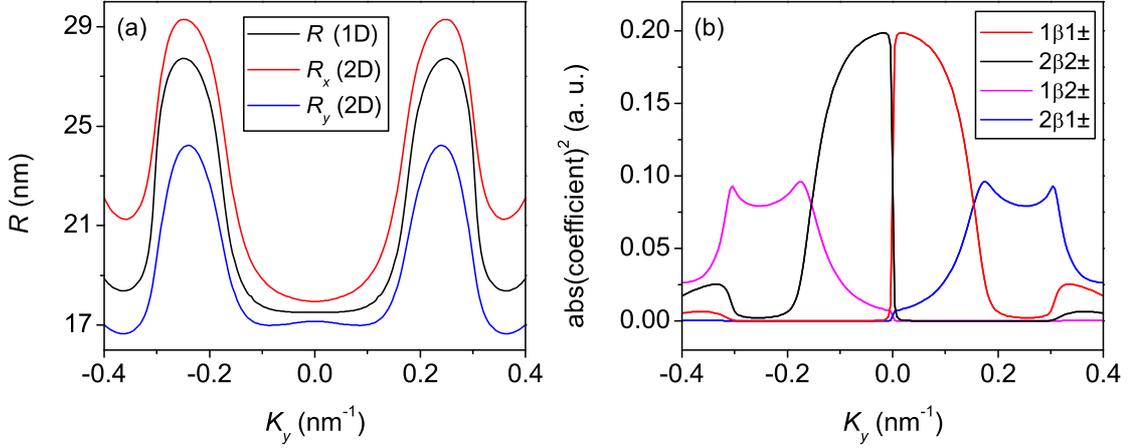
Figure 4.5: Excitonic radii from both one- and two-dimensional variational methods (a) and the squares of the absolute values of the greatest expansion coefficients (b) as functions of K_y for $B_\parallel = 10$ T in 1×1 basis.

to Eq. (4.1), it follows that the Lorentz force exerts in the z direction. Changing the orientation of the magnetic field or K_y direction, $\mathbf{B} \leftrightarrow -\mathbf{B}$ or $K_y \leftrightarrow -K_y$, the Lorentz force changes its orientation, too: if it exerted in the z^+ direction, now it is in the direction of z^-, and vice versa. Thus, the change of parity is a simple effect of the Lorentz force.

Detailed inspection would bring us the identification of matrix-hamiltonian terms responsible for observed splitting. Since it obviously comes from the valence-subband mixing, one can conclude that Luttinger $\hat{b}$ and $\hat{c}$ terms are of effect. Actually, because of the substitution $K_y \leftrightarrow K_y \pm deB_\parallel/\hbar$ applied on indirect excitonic states in the presence of the in-plane magnetic field, many matrix terms, which vanish in the absence of external fields, are now non-zero, enabling the mixing. Through the tunneling matrix elements, all terms of the hamiltonian (3.77) are then coupled. However, there is just one more effect that comes into question. The Lorentz force. Its effect on the system is similar to the effect of the electric field in the growth direction. As it exerts along the z axis, it leaves the matrix $\hat{H}_{hh}^2$ term non-zero, allowing the coupling as well.

As the effect of the magnetic field is stronger than that of the electric field, bringing along the change in parity of eigenfunctions for $K_y \gtrless 0$, one can assume that some effect on the polarisation of an exciton could take place, too.[4] Two-dimensional variational method used for the computation of optimal values of basis parameters gives us a good tool for this as excitonic radii in perpendicular directions are provided on output. The results of such calculations are depicted in Fig. 4.5a, where R_x denotes the radius along the x axis while R_y marks the corresponding quantity in the direction of the axis y. For comparison, the value of one-dimensional variational parameter R is shown. We see that the exciton affected by the in-plane magnetic field is squeezed in the propagation direction whereas

---

[4]By this we understand stretching in one direction while shrinking in the other.
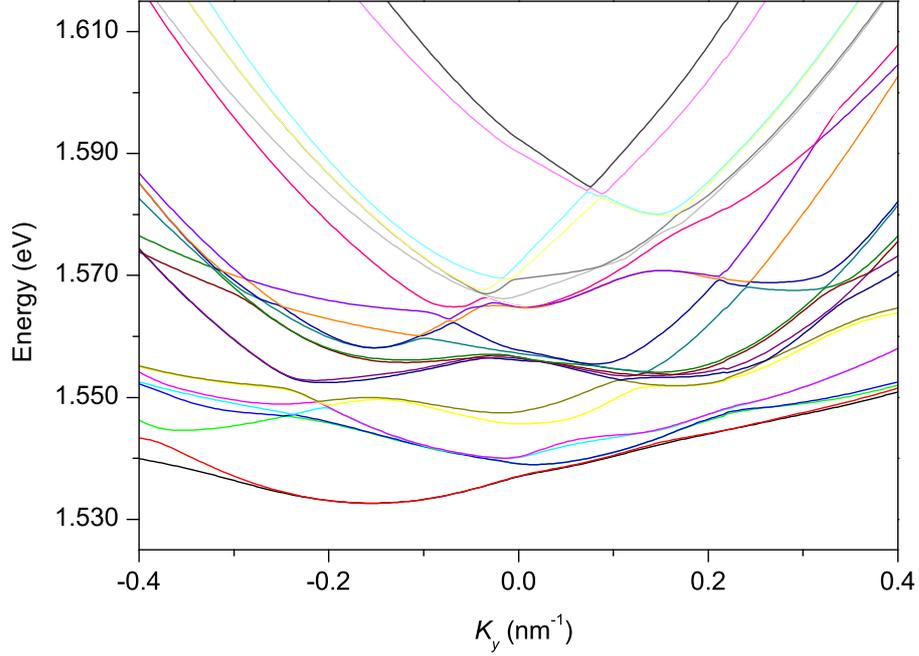
Figure 4.6: Dispersion relations of an exciton in a DQW subject to both the in-plane magnetic field of magnitude $B_\parallel = 10$ T and the electric field $\mathcal{E} = 10$ kV/cm in the growth direction.

spread along the axis showing field orientation, and the following relation evidently holds: $R_x > R > R_y$.

4.1.1.4 Dispersion relations in the presence of both the electric and the in-plane magnetic field

All results presented so far had one feature in common: dispersion relations were even in K_y, $E(K_y) = E(-K_y)$. To get rid of such behaviour, both electric and magnetic fields have to be applied on a DQW structure. The decrease in symmetry renders dispersion relations asymmetric in K_y, as depicted in Fig. 4.6. As the electric field separates direct and indirect excitonic states in energy and the in-plane magnetic field shifts the dispersion branches of indirect excitons away off the origin by $\pm deB_\parallel/\hbar$, the ground level is formed from indirect excitonic states with an electron and a hole spatially separated in opposite QWs in accordance with the orientation of the electric field, see Tabs. 4.6–4.7. Moreover, $B_\parallel = 10$ T gives $deB_\parallel/\hbar \approx 0.15$ nm^{-1} in excellent agreement with the position of the ground level global minimum. In the absence of an electric field, the energies of lateral minima of indirect-exciton dispersion lines would be equal (see Fig. 4.4). On the contrary, when an external electric field is applied, one of these minima lowers while the second one rises, leaving the energy separation $\Delta\epsilon$ among them proportional to the magnitude of the

Table 4.6: The strongest contributions to eigenvector expansions for several energy levels for $B_\parallel = 10$ T, $\mathcal{E} = 10$ kV/cm, and $K_y = 0$.

level	1	3	5	7	9	11
E (eV)	1.5370	1.5391	1.5401	1.5456	1.5561	1.5566
state	$1\beta2^\pm$	$1\beta1^\pm$	$2\beta2^\pm$	$1\alpha2^\pm$	$2\alpha2^\pm$	$1\alpha1^\pm$
type	i	d	d	i	d	d
|coeff.|	0.5823	0.7030	0.5920	0.5677	0.4443	0.5571

Table 4.7: The strongest contributions to eigenvector expansions for several energy levels for $B_\parallel = 10$ T, $\mathcal{E} = 10$ kV/cm, and $K_y = -0.15$ nm^{-1} (a) or $K_y = 0.15$ nm^{-1} (b).

(a)	level	1	3	5	7	9	10
	E (eV)	1.5326	1.5440	1.5449	1.5496	1.5531	1.5537
	state	$1\beta2^\pm$	$1\beta1^\pm$	$1\beta1^\pm$	$1\alpha2^\pm$	$2\alpha2^\pm$	$1\alpha1^\pm$
	type	i	d	d	i	d	d
	|coeff.|	0.7045	0.6517	0.7003	0.6493	0.5511	0.5092

(b)	level	1	3	5	7	9	10
	E (eV)	1.5424	1.5436	1.5447	1.5519	1.5533	1.5536
	state	$2\beta2^\pm$	$1\beta1^\pm$	$2\beta2^\pm$	$2\alpha2^\pm$	$1\alpha1^\pm$	$2\alpha2^\pm$
	type	d	d	d	d	d	d
	|coeff.|	0.4480	0.6759	0.4864	0.5363	0.4384	0.5312

intensity of an electric field, $\mathcal{E}$. For the chosen parameters, we have $\Delta\epsilon = ed\mathcal{E} = 0.01$ eV, just like found in Fig. 4.6.

Although there are only 24 lines shown in Fig. 4.6 as restricted to the smallest basis, determination of their character by sight would cause some problems. There is no doubt that the two lowest-lying ones describe the indirect excitons with an electron in the left QW and a hole in the right QW for $K_y < 0$ and in the vicinity of the origin. However, even for the ground state for $K_y > 0$, the character of levels changes with varying K_y as strong coupling mixes the states. For some values of K_y, it is illustrated in Tabs. 4.6–4.7. To distinguish between direct and indirect excitonic states experimentally, one would have to perform a series of measurements in electric fields of different magnitudes. Through the shift of levels, one could easily identify the indirect excitons. This will be of our interest in the following section.

4.1.2 Energy levels shift in external fields

We have studied the dependence of energy on the centre-of-mass momentum so far. Another interesting field of interest, one step closer to the calculation of optical spectra, would surely be the energy dependence on applied external fields. We will focus our attention on such a problem in this section.

4.1.2.1 Energy levels shift in an external electric field

Because it is necessary to obey both the energy and the momentum conservation laws, optically active excitons are those with $K_y \approx 0$. To construct the demanded dependencies, we have to compute the system of energy levels just once for one particular set of external fields, however, this has to be repeated many times with varying values of $\mathcal{E}$, $B_\perp$, or $B_\parallel$ from the chosen interval. To demonstrate some effects, which are typical for excitons in DQWs and which arise from the substance of the problem itself, in the simplest possible form, energy dependence on an external electric field from 0 to 30 kV/cm was calculated for 1×1 basis. The results are depicted in Fig. 4.7.

For $\mathcal{E} = 0$, one can notice that the level positions correspond to that shown in Fig. 4.1 for $K_y = 0$. But if an electric field is applied on a structure, levels shift: some of them increase, some of them lower in energy. Field-induced splitting of several levels is also notable. To understand the processes we are facing, a little help of Fig. 4.8 would be appreciated. In a simple model of a DQW structure with only two levels both in the conduction and valence bands,[5] four transitions are possible. Two correspond to direct (2, 3) and two are associated with indirect (1, 4) excitons. In the absence of external fields, all levels would be flat-banded. However, the presence of an electric field slants the energy levels structure, resulting in preferable localization of electrons and holes. As the electric field in Fig. 4.8 points from left to right, electrons are localized more in the left QW (level E1), whereas holes are preferred to be in the right one (level H1). The population of higher states (levels E2, H2) is lower. The localization strengthens with increasing field. Transitions 1, 2, 3, and 4 in the figure are numbered by the increasing energy of transition. The lowest energy (1, E1–H1) marks the indirect exciton composed of an electron and a hole both in the ground states, the second-lowest energy (2, E1–H2) corresponds to the direct exciton with an electron in the ground state but a hole on the higher level, the third energy level (3, E2–H1) is associated with direct exciton as well, but now with an electron in the higher state and a hole on the ground level, and finally the highest-energy level (4, E2–H2) represents the bounding state between an electron and a hole both in excited states. Because of the Coulomb interaction, the energy of a transition is less than the gap between particular levels in a DQW.

Looking at Fig. 4.8 once again, it is easy to realize that whereas the energy of direct excitons is nearly unaffected by an electric field, the energy of indirect excitons shifts

---

[5]If QWs forming the DQW were separate, only one energy level (the ground level) both in the valence and the conduction band would exist. As the wells are close to each other, the tunneling effect gives rise to two levels in the valence band and two levels in the conduction band of a DQW structure.
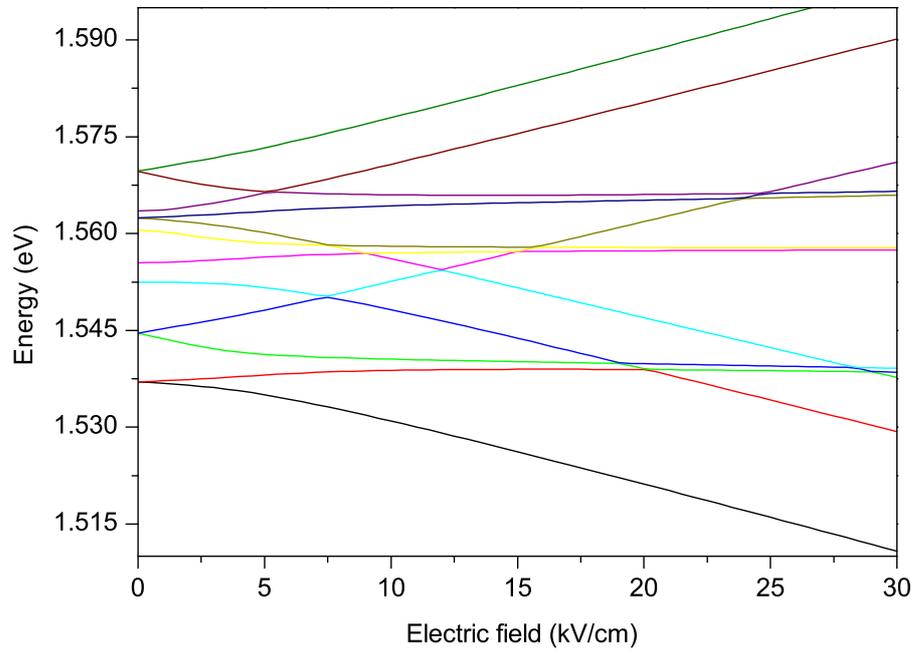
Figure 4.7: Shift of energy levels in an external electric field calculated for 1×1 basis.
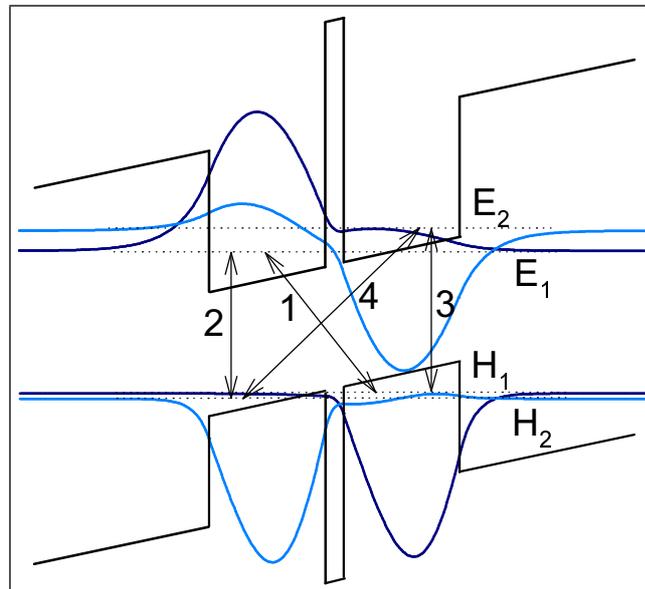
Figure 4.8: Transitions in a DQW structure subject to an external electric field, [22].

Table 4.8: Character of particular excitonic levels in a DQW for $\mathcal{E} = 14$ kV/cm and $K_y = 0$ calculated in 1×1 basis.

level	1	2	3	4	5	6
E (eV)	1.5272	1.5390	1.5402	1.5447	1.5525	1.5563
state	$1\beta2^{\pm}$	$1\beta1^{\pm}$	$2\beta2^{\pm}$	$1\alpha2^{\pm}$	$1\gamma2^{\pm}$	$2\beta1^{\pm}$
type	i	d	d	i	i	i
|coeff.|	0.9682	0.9796	0.9668	0.9593	0.9699	0.9778

level	7	8	9	10	11	12
E (eV)	1.5572	1.5579	1.5647	1.5659	1.5745	1.5819
state	$1\alpha1^{\pm}$	$2\alpha2^{\pm}$	$1\gamma1^{\pm}$	$2\gamma2^{\pm}$	$2\alpha1^{\pm}$	$2\gamma1^{\pm}$
type	d	d	d	d	i	i
|coeff.|	0.9610	0.9443	0.9796	0.9685	0.9773	0.9778

linearly: E1–H1 decreases with increasing electric field, E2–H2 linearly increases. If we take a look back at Fig. 4.7, we see that the actual situation is more complicated than in the simplified model. There are more than four levels, but the structure remains unchanged. It is easy to identify direct and indirect levels. If one would not be sure, Tab. 4.8 is of use. Remember, since $K_y = 0$ and no magnetic field is present, all levels are twofold degenerate.

The reason for why the energy of direct excitons nearly does not change can be found by analyzing the form of Eqs. (3.60)–(3.76). Since $\hat{H}_e^{1(3)}$ and $\hat{H}_{lh}^{1(3)}$ or $\hat{H}_{hh}^{1(4,6,7)}$ are linear in $\mathcal{E}$ and $z_{1(2)} = \pm\frac{d}{2}$, for direct excitons the linear contribution vanishes whereas for indirect ones is added.

4.1.2.2 Energy levels shift in both the electric and the in-plane magnetic field

The effect of the in-plane magnetic field on $E = E(\mathcal{E})$ dependence is demonstrated in Fig. 4.9. The decrease in symmetry induces the degeneracy splitting. For $\mathcal{E} = 0$, energy level positions are in agreement with energies depicted in Fig. 4.4 for $K_y = 0$. With increasing electric field, the degeneracy is lifted although the corresponding levels (those that were degenerate for $B_\parallel = 0$) keep going close to each other. If we take a look at Tab. 4.9, one might think that these lines are still degenerate and the "splitting" originates from numeric errors. However, detailed inspection proved that although predominant expansion coefficients are almost equal, these levels correspond to different eigenvalues since the matrix hamiltonian is irreducible and cannot be decomposed into non-interacting blocks.[6]

---

[6]In some other cases, e. g. for $K_y = 0$, $\mathcal{E} = 0$, but $B_\perp \neq 0$, the hamiltonian written in greater than 1×1 basis (2×2, etc.) is formed of two blocks. However, these are not identical, giving different eigenvalues.
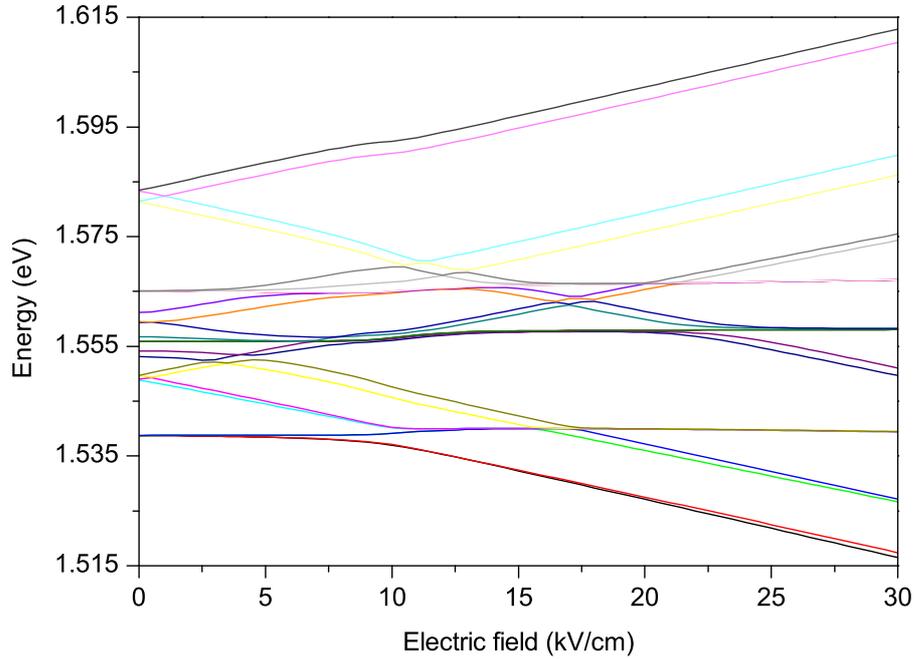
Figure 4.9: Shift of energy levels in an external electric field in the presence of the in-plane magnetic field $B_\parallel = 10$ T calculated for 1×1 basis.

Analogously to previously discussed situation ($B_\parallel = 0$), the lowest-lying levels are created mostly from indirect excitonic states. But as all levels are split, the absolute values of expansion coefficients are not as high as in Tab. 4.8. Nevertheless, the strongest contributions displayed in Tab. 4.9 are still predominant in all cases. Higher levels are associated with direct excitons, at first in accordance with the field orientation (an electron in the left QW and a hole in the right QW), then in the opposite order. The highest energy levels are composed of indirect excitons of the opposite arrangement than the lowest-level excitons.

To summarize results achieved in this section, it is necessary to highlight the degeneracy splitting for $\mathcal{E} > 0$, $B_\parallel > 0$. This effect originates from non-zero off-diagonal matrix terms associated with Luttinger $\hat{b}$ and $\hat{c}$ operators calculated in the chosen basis (see Eqs. (3.107)–(3.110)).[7] If these terms were neglected, it would be possible to decompose the matrix hamiltonian to four blocks, two of which would correspond to heavy-hole excitons ($m_J = \pm\frac{3}{2}$) and the other two to light-hole ones ($m_J = \pm\frac{1}{2}$), leaving all levels in Fig. 4.9 twofold degenerate. As they are included, the decomposition is not possible and the degeneracy is lifted.

---

[7]Though the presented results were computed in 1×1 basis, this conclusion holds true even if expanded to a larger basis set.

Table 4.9: Character of several excitonic levels in a DQW for $\mathcal{E} = 28$ kV/cm, $B_\parallel = 10$ T, and $K_y = 0$ calculated in 1×1 basis.

level	1	2	3	4	5	6
E (eV)	1.5186	1.5194	1.5285	1.5292	1.5395	1.5395
state	$1\beta2^\pm$	$1\beta2^\pm$	$1\alpha2^\pm$	$1\alpha2^\pm$	$1\beta1^\pm$	$1\beta1^\pm$
type	i	i	i	i	d	d
|coeff.|	0.6648	0.7026	0.5568	0.5961	0.6945	0.6945

level	19	20	21	22	23	24
E (eV)	1.5725	1.5737	1.5842	1.5878	1.6083	1.6107
state	$2\beta1^\pm$	$2\beta1^\pm$	$2\alpha1^\pm$	$2\alpha1^\pm$	$2\gamma1^\pm$	$2\gamma1^\pm$
type	i	i	i	i	i	i
|coeff.|	0.6401	0.6720	0.5935	0.5850	0.6044	0.5800

It is well-known that the presence of the perpendicular magnetic field enables the creation of Landau levels, [24]. To describe this effect in our model, at least 2×2 basis has to be used. With a larger basis, more energy levels are obtained from diagonalisation, making relevant figures much more complicated. Thus, no results for $B_\perp \neq 0$ will be given here. The situation will be studied later in Sec. 4.2.

4.1.3 Comparison of different bases

Before we proceed to optical spectra computation, it is very important to compare the results that bases of various sizes can provide, with the biggest attention paid to differences in energy. As variational method is used to determine the best value(s) of basis parameter(s) by minimizing the energy of the ground level,[8] it is clear that the larger basis we take, the lower ground level energy will be achieved. The question is: does the change of basis size affect qualitative and/or quantitative results, and if the answer is positive, how much? To answer the first question, the help of Figs. 4.10–4.11 will be of use. In the first one, the dispersion relations of the ground excitonic level in the absence of external fields for various bases are depicted, the second figure shows the same when the perpendicular magnetic field is applied on a DQW.

Let us focus on Fig. 4.10 for a start. We see that there is a huge qualitative difference between the results achieved for 1×1 and 3×3 bases. There are no lateral minima for 1×1 basis, whereas two minima exist for 3×3 basis set. On the contrary, for larger bases, the qualitative difference of particular lines vanishes. Quantitatively, for $K_y \approx 0$, the energies

---

[8]To remind to those who do not remember, one parameter C is used for one-dimensional variational method; two parameters C_x, C_y are used for two-dimensional one. Both C and C_x, C_y are related to the excitonic radius R.
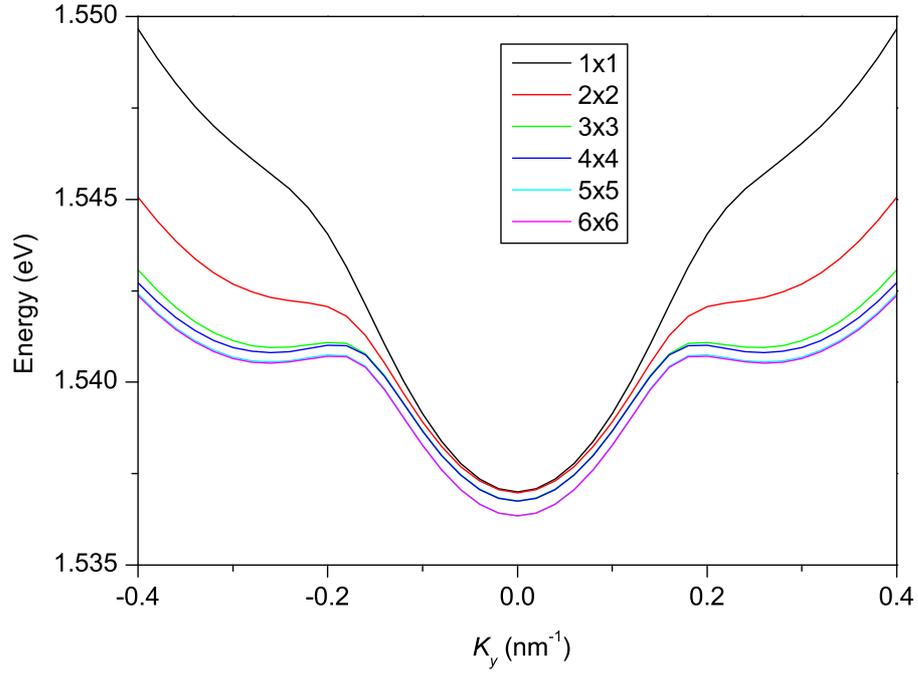
Figure 4.10: Dispersion relations of the ground excitonic level in the absence of external fields calculated for various bases.
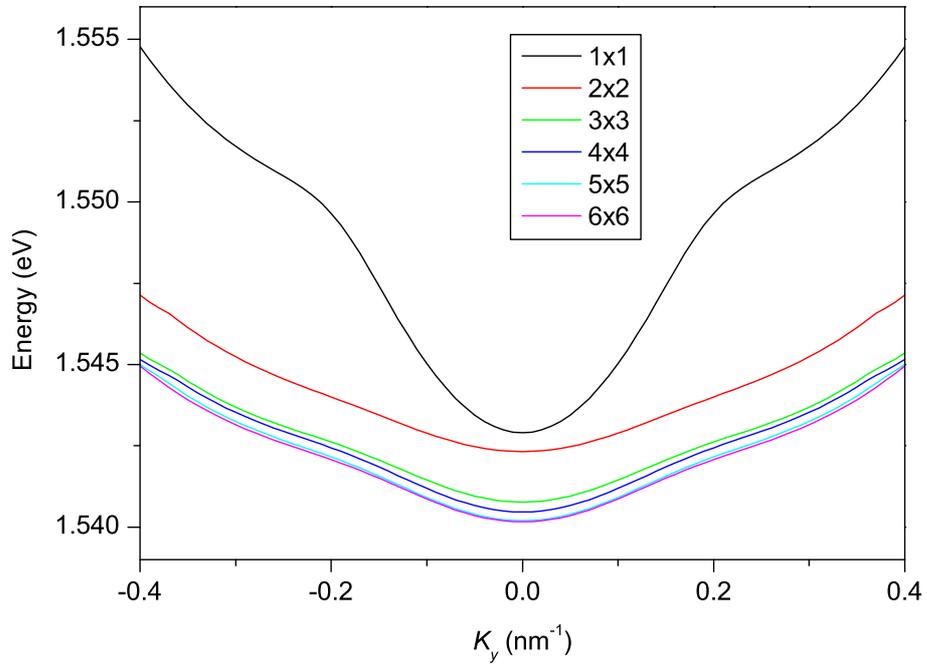
Figure 4.11: Dispersion relations of the ground excitonic level in the presence of the perpendicular magnetic field $B_\perp = 10$ T calculated for various bases.
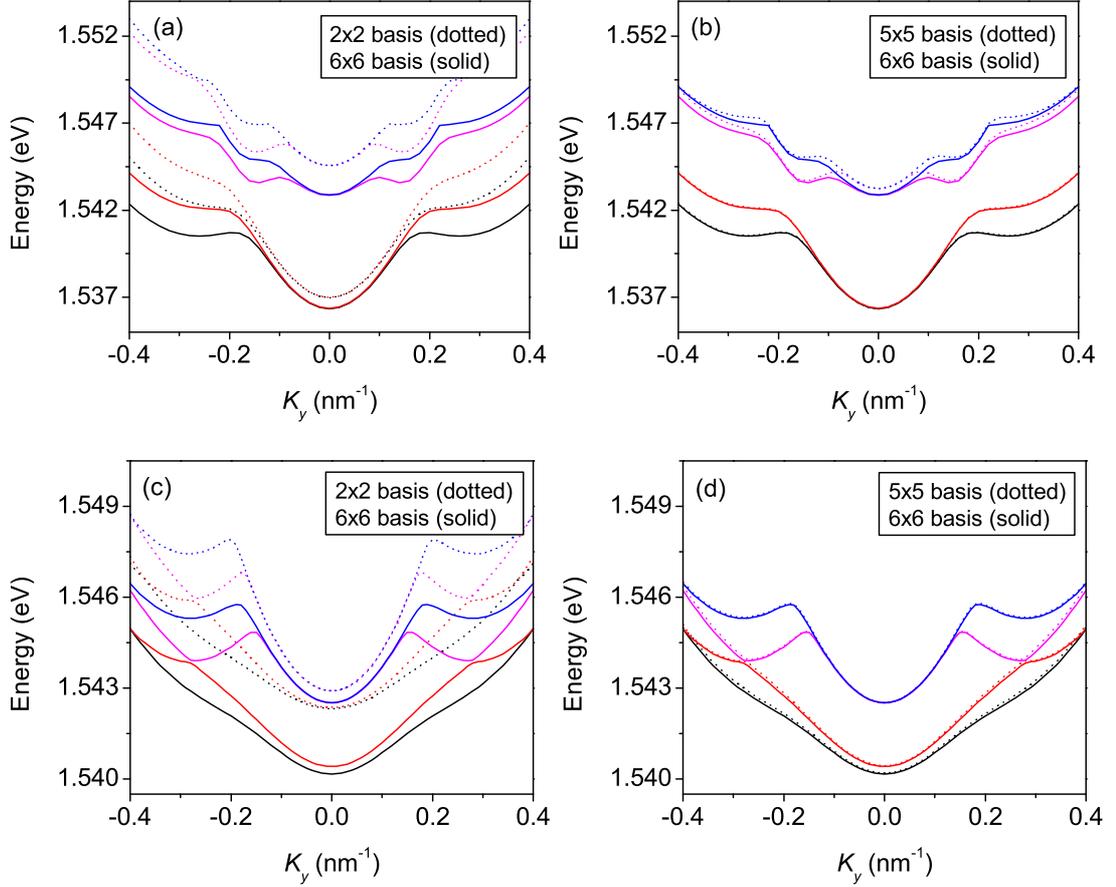
Figure 4.12: Comparison between dispersion relations of several lowest-lying energy levels in the absence of external fields calculated for 2×2 and 6×6 bases (a) and 5×5 and 6×6 bases (b), and in the presence of the perpendicular magnetic field of magnitude $B_\perp = 10$ T computed for 2×2 and 6×6 bases (c) and 5×5 and 6×6 bases (d).

of 1×1 and 2×2 calculations nearly coincide and the same is true for 3×3, 4×4 and 5×5, 6×6 ground levels. However, there is always a little gap between these pairs of lines as variational method finds the better values of basis parameters always when the basis extension increases to be given by two odd numbers. We can suppose that for larger bases, the qualitative character of obtained levels will not change and the energy difference between them will decrease. This can be seen in Figs. 4.12a, b even for higher levels.

Analogous discussion can be performed for what is depicted in Fig. 4.11 and nearly all conclusions can be reproduced. Once again, we see that the biggest qualitative difference appears between 1×1 and 2×2 bases as smaller bases are not a proper choice for calculations when the perpendicular magnetic field is applied (since the Landau levels are not involved). With larger bases, the situation improves: various lines in Fig. 4.11 differ less and less and

Table 4.10: Energy of the ground excitonic level computed for various bases in the presence of the in-plane magnetic field $B_\parallel = 10$ T for $K_y = 0$.

basis	1×1	2×2	3×3	4×4	5×5
E (eV)	1.5387	1.5385	1.5383	1.5382	1.5378
basis	6×6	7×7	8×8	9×9	10×10
E (eV)	1.5378	1.5377	1.5377	1.5376	1.5376

starting from 6×6 basis, the difference is small even between higher levels. To experience this, see Figs. 4.12c, d.

Later, as we will be computing optical spectra, $K_y \approx 0$ will be used. Therefore, it will be helpful if we take a look at the results we can obtain for different bases when K_y is supposed to be zero. These are listed in Tab. 4.10 for such a case when the in-plane magnetic field is applied. Whereas the energies of the ground level obtained for smaller bases differ in the fifth significant digit, for larger bases, it is one order better, providing us satisfactory precision. Thus, it is not surprising that the data in Tab. 4.10 illustrate the same findings as before: the larger bases, the better results that differ the less.

Now we have enough knowledge to conclude: to show the qualitative character of studied dependencies, smaller bases (4×4, 5×5, etc.) are sufficient. However, to provide results able to explain the experimental data both qualitatively and quantitatively, the larger basis used, the better agreement can be expected. That is why we will perform optical spectra calculations in the largest possible basis that our program allows: 10×10 basis composed of the Hermite-Gauss functions (3.114) up to the 9th order in x, y.

4.2   Optical spectra

In this section, we will present calculations of optical spectra obtained from our model. Starting with the situation in the absence of external fields, absorption and PL spectra in the presence of an external electric field and a magnetic field of in-plane and perpendicular orientations will be shown. But as it will be depicted in all studied situations, let us start with the calculation of optical spectra when no fields are applied on a DQW.

4.2.1   Optical spectra in the absence of external fields

It is true that because both the energy and the momentum conservation laws have to be obeyed, optically active excitons are those with $K_y \approx 0$. In foregoing chapters, we have studied dispersion relations and discussed the effects of bases of different extensions on various quantities. In Sec. 3.3.7, short theory of absorption and photoluminescence was given and two important formulae, Eq. (3.130) and (3.132), were derived. We will

use them now to calculate optical spectra from the corresponding dispersion relations, assuming $K_y = 0$.

For bases from 2×2 to the largest possible 10×10 basis, absorption spectra were computed using Eq. (3.132). It is clear that the larger basis we take, the better results we achieve, but it turned out that for larger bases, levels of excited excitons appear in spectra as well. These are analogues to the excited states of the hydrogen atom and their presence originates from the larger number of basis functions used for calculations. However, for greater energies, eigenvectors constructed mainly from excited states (those with large indices of basis functions) appear, causing that calculations with various bases slightly differ. To handle this, we tried to restrict the computation only to those energy levels, eigenvectors of which have the strongest contributions from basis functions of the lowest indices.[9] Absorption spectra computed for various bases but restricted only to the ground levels ($n = m = 0$ in Eq. (3.114)) are depicted in Fig. 4.13a, Fig. 4.13b illustrates the situation when no restrictions are assumed.

Let us give some remarks on these figures. The "width" of all peaks was chosen to be $\Delta = 0.5$ meV, intensities of heavy-hole excitonic transitions are three times higher than those of light-hole ones, just according to Eq. (3.125). There is a little shift in positions of dominant peaks with increasing basis extension for both cases (a) and (b), but it should not amaze us since it has already been discussed. As minimum energy levels are included, the spectrum is the simplest in the first case (a), where excited levels are suppressed. On the contrary, the richest spectrum corresponds to the situation when all energy levels are included into calculations (b). In Fig. 4.13, the character of transitions corresponding to major peaks is shown: from left to right, the three peaks of the lowest energy are associated with direct heavy-hole excitons, indirect heavy-hole excitons and direct light-hole excitons, respectively, both heavy-hole ones with a hole in the ground state. The studied cases have one feature in common: the intensity of the first peak is the highest, intensities of another two are almost equal. In Fig. 4.13a, the following two peaks (for 10×10 basis) originate from indirect light-hole excitonic states. It is notable that for smaller bases, there is only one peak instead of these two. However, in Fig. 4.13b, the situation differs. There are several small peaks between the peaks of direct and indirect light-hole excitons. Since they are not present in Fig. 4.13a, they evidently come from higher (excited) states whose strongest eigenvector contributions correspond to basis functions with $n + m \geq 1$. Some of these peaks are marked with an asterisk in Fig. 4.13b. Two peaks of indirect light-hole excitons are also visible at the same position as in Fig. 4.13a (≈ 1.56 eV).

Let us mention just one curious thing: in Fig. 4.13a (and a little in Fig. 4.13b as well), there are two peaks in the position of the direct light-hole excitonic level in the absorption spectrum calculated for 6×6 basis, whereas for other basis extensions, only one peak appears. We suppose that such behaviour is just accidental, caused by some random effects

---

[9]To make it clear, two steps are carried out: (1) matrix hamiltonian is constructed in any basis, eigenvalues and eigenvectors are obtained, (2) only those eigenvalues and eigenvectors, which fulfil the above-mentioned conditions, are used to calculate optical spectra.
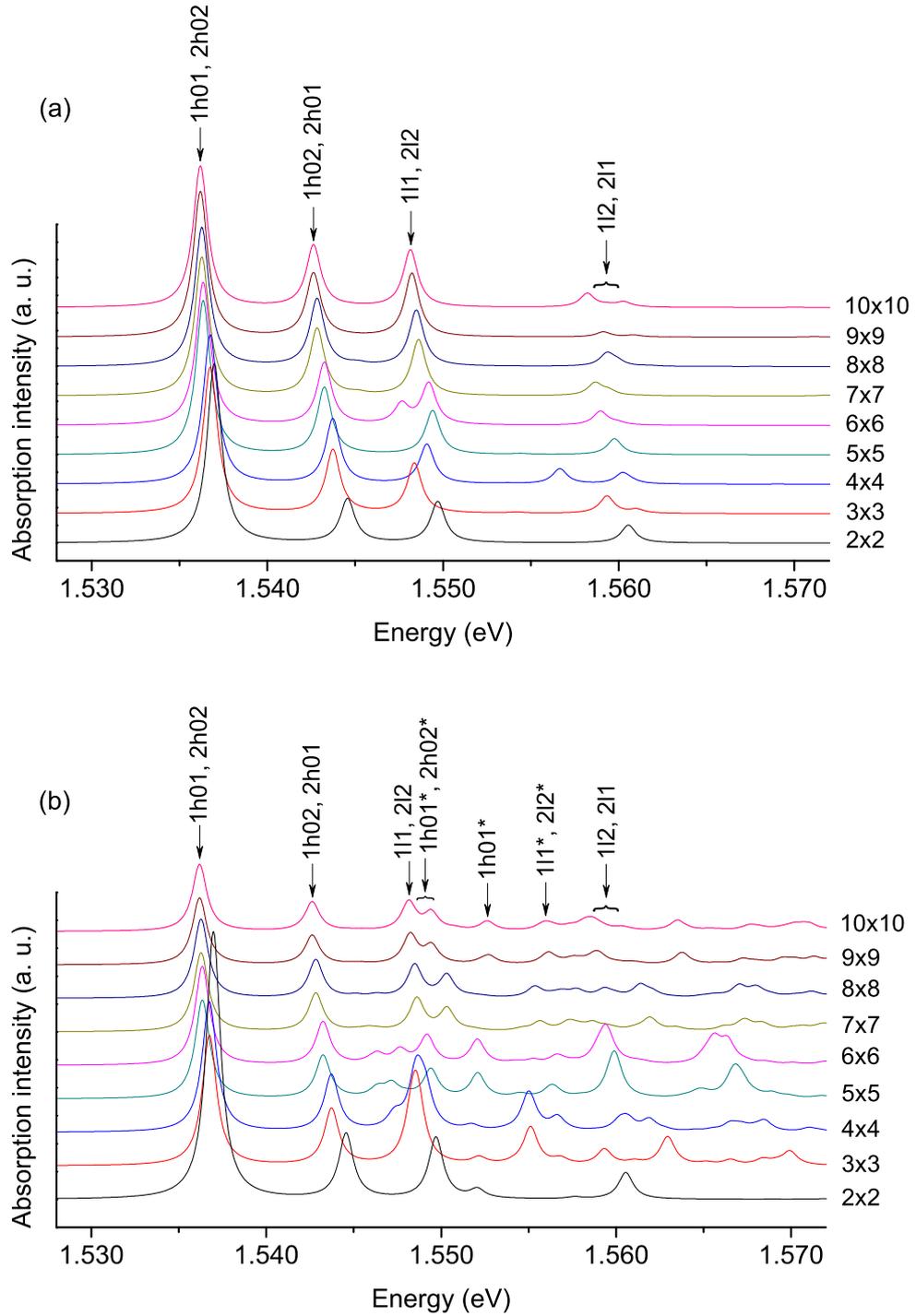
Figure 4.13: Comparison of absorption spectra in the absence of external fields computed for different bases and restricted to the ground states (a) and with no restrictions assumed (b), $\Delta = 0.5$ meV.
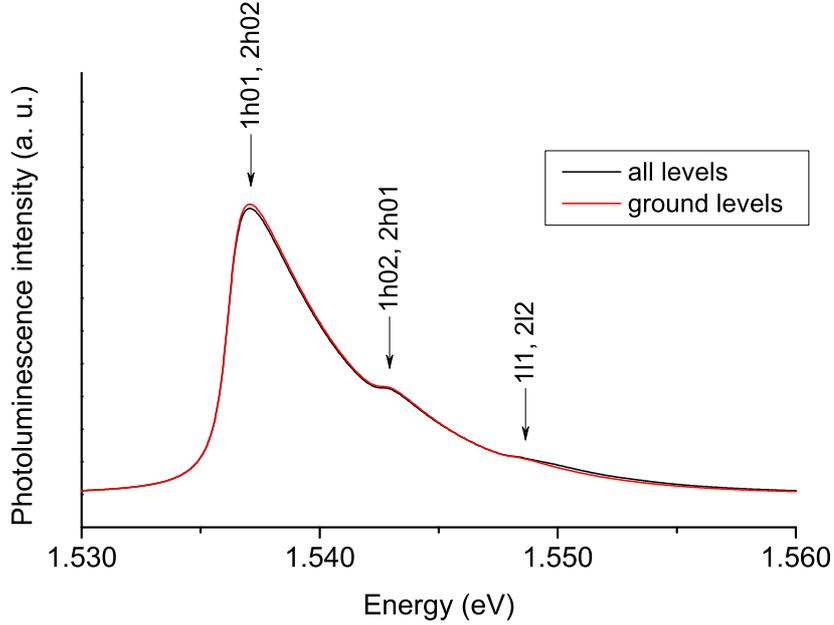
Figure 4.14: Photoluminescence spectrum calculated for 10×10 basis considering only ground levels and when all levels are included, $\Delta = 0.5$ meV, $T = 45$ K.

which we are not able to trace up and which cause the increase in transition probability of a peak that is not significant otherwise.

To summarize: in the absence of external fields, the presence of excited levels in higher energies affects absorption spectra calculated for larger bases. In actual, experimentally measured, spectra, these levels are localized below the absorption edge of the two-dimensional electron-hole gas. The absorption edge is determined by the bandgap width and the energies of ground states in DQWs in the valence and conduction bands: for our set of parameters, it is approximately 1.543 eV. However, the first excited states in Fig. 4.13 are localized higher. This is the natural consequence of the chosen method, variational computation, which is well applicable for the ground level, but gives worse results for higher states. Nevertheless, up to 1.550 eV, there is no doubt that our theoretical absorption spectra are prepared to be compared with available experimental data.

We must not forget to mention photoluminescence spectra. These are shown in Fig. 4.14, where a comparison between the "full" spectrum and the spectrum constructed from the ground levels only is to be found. Just like in the text above, the broadening of PL peaks equals $\Delta = 0.5$ meV, temperature was set to $T = 45$ K (this choice will be clarified later). Whereas the absorption spectra in Fig. 4.13 were slightly different, the PL spectra in Fig. 4.14 are almost identical. The reason for this can be found in Eq. (3.130): the Boltzmann exponential factor $e^{-E/k_B T}$ strongly reduces the magnitude of a corresponding contribution to PL spectrum for higher energies. That is why only the first three peaks are

recognizable while another are suppressed. Apparently, visible peaks must be associated with the same transitions as in Fig. 4.13, so that from left to right, the peaks of direct heavy-hole excitons, indirect heavy-hole excitons, and direct light-hole excitons, respectively, appear in Fig. 4.14. Since the strength of transition is not determined by expansion coefficients only but the exponential weight factor affects it, too, the first peak, the highest in magnitude in absorption spectra, remains dominant in PL spectra as well. The another two peaks vanish in the tail of the first one.

4.2.2 Optical spectra in the perpendicular magnetic field

After we have studied optical spectra in the absence of external fields, we can proceed further and have a look at the situation when the perpendicular magnetic field is applied on a DQW structure. We know from the theoretical part of this work that the magnetic field lowers the symmetry. It implies that the degeneracy is being lifted, as proven on splitting of dispersion lines (see Sec. 4.1.1). In the corresponding section, we have demonstrated the effect of the in-plane magnetic field, however, the perpendicular magnetic field has not been studied yet since it requires more precise calculations with larger basis than in the field of interest there.

For the introduction of the perpendicular magnetic field, associated with the substitution (2.35), bases from 2×2 on are necessary since $\mathbf{A}$, given by Eq. (3.30), is linear in x, y for homogeneous magnetic field. In our calculations, we use 10×10 basis to show changes in absorption spectra when varying the strength of a magnetic field from 0 to 20 T. A comparison between 5×5 basis and 10×10 basis calculations will be given as well. Without further hesitation, let us take a look directly at Fig. 4.15.

As we face a figure of this type for the first time, let us describe its structure at first. On the horizontal axis, the magnitude of the applied external magnetic field is shown; on the vertical axis, the energy could be read. Such a figure actually consists of many absorption spectra ranged vertically side by side and is very useful to illustrate field-induced effects. The colour scale determines the strength of transition (the more red, the stronger it is) and will be used in all similar figures from now on. The absorption spectrum obtained in the absence of external fields coincides with the vertical axis on the left of each figure.

The top left Fig. 4.15a is the most important result of this section as it contains the absorption spectrum in the presence of the perpendicular magnetic field computed for 10×10 basis using the whole set of energy levels obtained from diagonalisation. Once again, $\Delta = 0.5$ meV. The top right Fig. 4.15b depicts the absorption spectrum constructed with an additional condition $n = m = 0$ for energy levels, which means that only the ground states are considered. Figs. 4.15a and 4.15b differ only for higher energy, the structure of low-energy transitions is the same. To give a comparison to Fig. 4.15a, the bottom left Fig. 4.15c showing 5×5 basis calculations from all levels is presented. It is of major interest to demonstrate effects associated with the off-diagonal Luttinger hamiltonian terms as well. For that case, the help of the bottom right Fig. 4.15d will be useful since it reflects calculations with $\hat{b} = \hat{c} \equiv 0$.
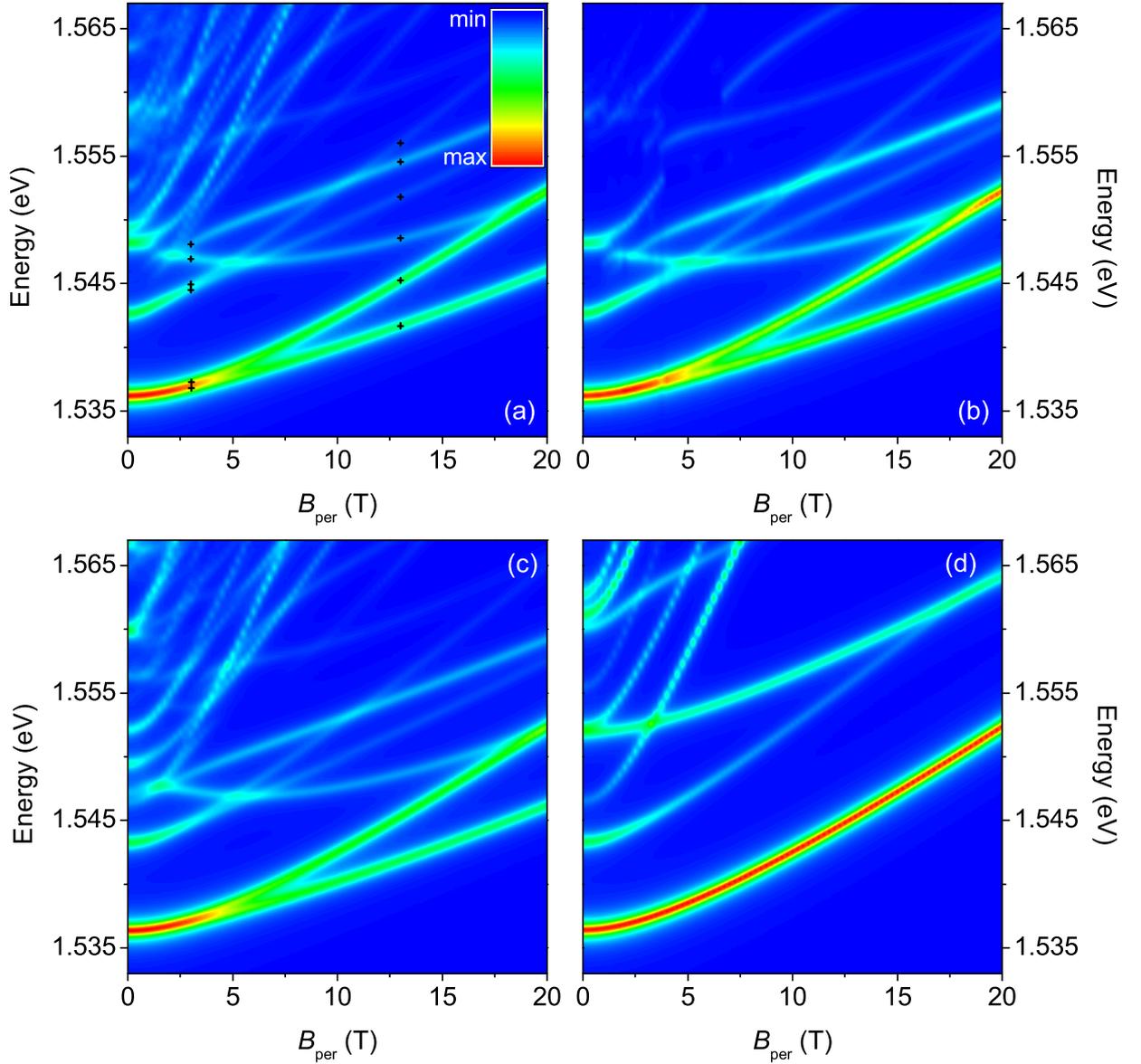
Figure 4.15: Absorption spectra in the presence of the perpendicular magnetic field computed for 10×10 basis from all energy levels (a) and with restriction to the ground levels only (b). Calculations for 5×5 basis including all levels (c) and the same situation when neglecting Luttinger $\hat{b}$ and $\hat{c}$ terms (d), $\Delta = 0.5$ meV.
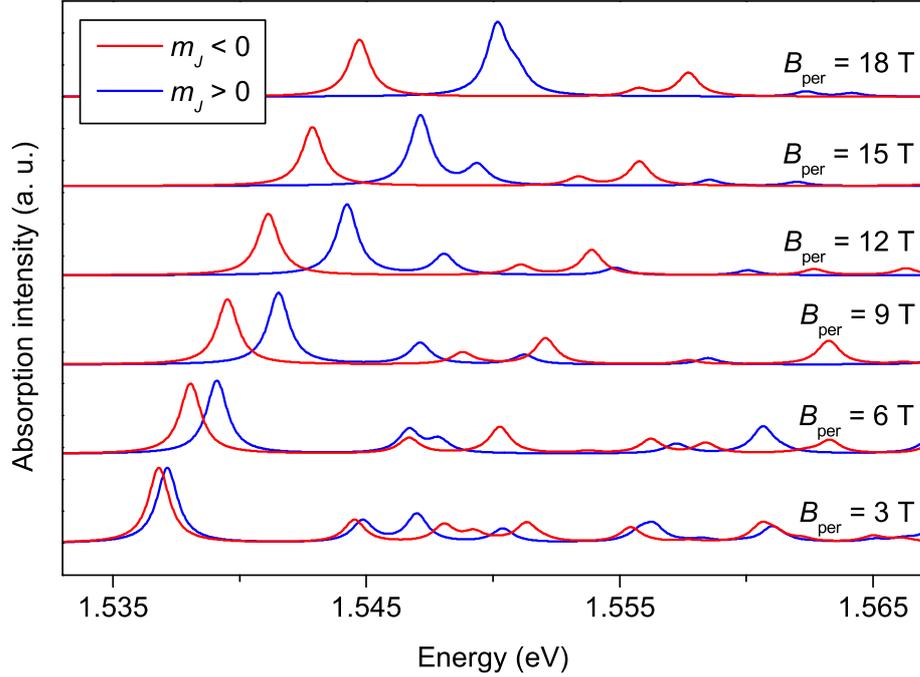
Figure 4.16: Absorption spectra in the presence of the perpendicular magnetic field computed in 10×10 basis for $m_J > 0$ and $m_J < 0$ states separately, $\Delta = 0.5$ meV.

There is no doubt that Figs. 4.15a, c obtained for different bases are almost identical. We see that if we are concerned about the lowest energy levels only (with energies up to 1.560 eV), 5×5 basis is sufficient to provide both qualitative and quantitative results. Just a small difference at around 1.548 eV is not interesting since our goal is to describe ground levels for strong fields.

Looking at Figs. 4.15a, d, there is one distinction apparent at first sight. If the full-structure excitonic hamiltonian is considered (including all terms originating from $\hat{b}$ and $\hat{c}$ operators), the ground level is being split for $B_\perp \gtrsim 5$ T. On the contrary, nothing happens when the off-diagonal Luttinger terms are neglected. When split, the lower level is associated with the direct heavy-hole exciton with a hole in the ground state. However, in contrast to situations without magnetic field, the total angular momentum comes into play as the strongest contributions are created from states with $m_J = -\frac{3}{2}$, while for the upper level, direct heavy-hole excitonic states with $m_J = +\frac{3}{2}$ are dominant. To better illustrate such behaviour, absorption spectra computed separately for $m_J < 0$ and $m_J > 0$ states are shown in Fig. 4.16. More information about dagger-marked levels of Fig. 4.15a is summarized in Tab. 4.11.

The lowest levels correspond to direct heavy- and light-hole excitons, heavy-hole ones with a hole in the ground state since the first excited hole state lies much higher. For weak fields, indirect heavy-hole excitonic states are localized between the states of direct heavy- and light-hole excitons, but for stronger fields, the intensity of indirect transitions

Table 4.11: The strongest contributions to eigenvector expansions for several energy levels of the absorption spectrum in Fig. 4.15a for $B_\perp = 3$ T (a) and $B_\perp = 13$ T (b).

	level	1	2	3	4	5	6
(a)	E (eV)	1.5368	1.5371	1.5445	1.5449	1.5470	1.5481
	state	$1\beta1^-$ $2\beta2^-$	$1\beta1^+$ $2\beta2^+$	$1\beta2^-$ $2\beta1^-$	$1\beta2^+$ $2\beta1^+$	$1\alpha1^+$ $2\alpha2^+$	$1\alpha1^-$ $2\alpha2^-$
	|coeff.|	0.6347	0.6405	0.5923	0.6014	0.5455	0.4084

	level	1	2	3	4	5	6
(b)	E (eV)	1.5417	1.5452	1.5485	1.5518	1.5545	1.5561
	state	$1\beta1^-$ $2\beta2^-$	$1\beta1^+$ $2\beta2^+$	$1\alpha1^+$ $2\alpha2^+$	$1\beta2^-$ $2\beta1^-$	$1\alpha1^-$ $2\alpha2^-$	$1\beta2^+$ $2\beta1^+$
	|coeff.|	0.6198	0.6763	0.5824	0.5692	0.6079	0.6696

decreases due to the strong mixing around $B_\perp \approx 5$ T on behalf of light-hole excitonic states. Moreover, for fields $B_\perp \approx 5$ T, the two lowest levels start to draw apart. The splitting for $B_\perp = 13$ T reaches approximately 3.5 meV and increases with $B_\perp$. From Tab. 4.11 and Fig. 4.16, it is evident that for the chosen orientation of the perpendicular magnetic field, heavy-hole excitonic states with $m_J = -\frac{3}{2}$ are preferred whereas light-hole states with $m_J = +\frac{3}{2}$ are of advantage. It was proven that for the opposite orientation of the magnetic field (i. e. $B_\perp < 0$), the sign of m_J changes for corresponding levels as well.

4.2.3 Optical spectra in the perpendicular magnetic field when an external electric field is present

As we have successfully achieved results in the perpendicular magnetic field, we can naturally proceed and show how these spectra change when an additional external electric field in the growth direction is applied. To handle this, we set $\mathcal{E} = 10$ kV/cm and perform all the calculations in 10×10 basis once again. To construct the corresponding absorption spectra, the spectral line broadening of $\Delta = 0.3$ meV was used to illustrate more complicated structure of the lowest levels. The results are depicted in Fig. 4.17: in Fig. 4.17a, calculations with 10×10 basis are demonstrated, whereas Fig. 4.17b shows 5×5 basis calculations with the off-diagonal Luttinger terms being neglected.

If the valence-subband mixing is forbidden ($\hat{b} = \hat{c} \equiv 0$), the corresponding absorption spectra indicate simpler structure than in the case when it is allowed. In contrast to Fig. 4.15a, there are four lines in Fig. 4.17a for stronger field ($B_\perp \gtrsim 5$ T) instead of two, however, it should not be surprising: the presence of an electric field separates direct excitonic states with particles localized in the left/right QWs in accordance to what stated in Sec. 4.1.1, while the perpendicular magnetic field splits every peak to form levels composed
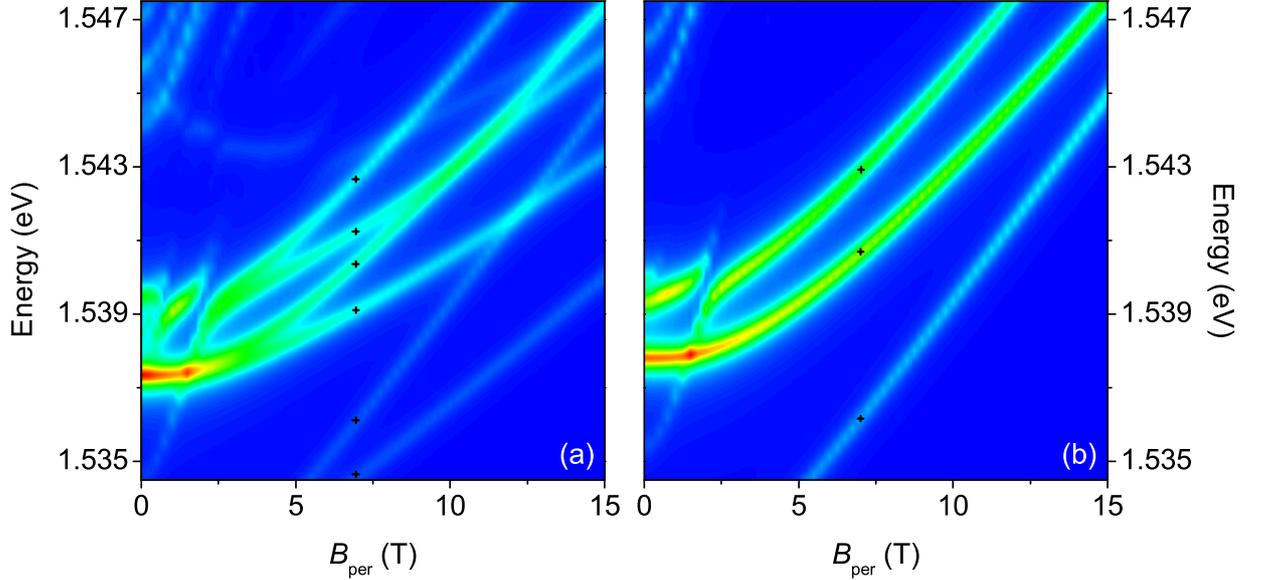
Figure 4.17: Absorption spectra in the presence of the perpendicular magnetic field and the electric field $\mathcal{E} = 10$ kV/cm in the growth direction computed for 10×10 basis (a) and 5×5 basis when the off-diagonal Luttinger $\hat{b}$ and $\hat{c}$ terms are neglected (b), $\Delta = 0.3$ meV.

mainly of $m_J = -\frac{3}{2}$ or $m_J = +\frac{3}{2}$ states. This is nicely illustrated just in Fig. 4.17a; in Tab. 4.12, detailed information about dagger-marked levels is available. With the increasing strength of a magnetic field, the direct heavy-hole excitonic levels $1\beta1^+$ and $2\beta2^-$ are getting closer since their slopes are different. As they are crossing over each other, it is accompanied by the increase in the intensity of transition. However, this effect originates from the normalization of spectra rather than from some physical reasons.

Although an electric field is present, giving rise to indirect excitonic states, indirect transitions are not as strong as direct ones and in Fig. 4.17a, they are hardly visible though marked with daggers. In weak magnetic fields, the strongest transition is associated with direct heavy-hole excitons. For energies around 1.539 eV, there are two peaks which exist only for the weakest field: they consist of $2\beta2^\pm$ states with indispensable contribution from $2\beta1^\pm$. When they separate out of the ground direct heavy-hole excitonic level, their intensity decreases fast. As lately as $1\beta1^\pm$ and $2\beta2^\pm$ levels start drawing apart (around $B_\perp \approx 2$ T), the major peak of $2\beta2^\pm$ remains dominant until it is split by the projection m_J of the hole total angular momentum in stronger magnetic field.

To conclude: the main difference in absorption spectra in the presence of an additional electric field in contrast to its absence is the splitting of dominant direct excitonic levels (with opposite values of m_J) into the peaks representing direct excitons with particles (i. e. an electron and a hole) localized in the left or right QWs.

Table 4.12: The strongest contributions to eigenvector expansions for several energy levels of the absorption spectra in Fig. 4.17 for $B_\perp = 7$ T, $\mathcal{E} = 10$ kV/cm when the off-diagonal Luttinger terms are present (a) and in the absence of these terms (b).

(a)

level	1	2	3	4	5	6
E (eV)	1.5345	1.5361	1.5391	1.5404	1.5413	1.5427
state	$1\beta2^-$	$1\beta2^+$	$1\beta1^-$	$1\beta1^+$	$2\beta2^-$	$2\beta2^+$
|coeff.|	0.8144	0.8524	0.9312	0.9682	0.8158	0.8351

(b)

level	1	2	3
E (eV)	1.5361	1.5406	1.5429
state	$1\beta2^\pm$	$1\beta1^\pm$	$2\beta2^\pm$
|coeff.|	0.8604	0.9708	0.8432

4.2.4 Optical spectra in an electric field when the perpendicular magnetic field is present

We have studied absorption spectra so far. Since we are concerned in the lowest energy levels only and we did not do it before, we can focus our attention on computation of photoluminescence spectra as well. Both absorption and PL spectra were calculated for 10×10 basis in the presence of the perpendicular magnetic field $B_\perp = 10$ T for various strengths of an external electric field from 0 to 20 kV/cm to illustrate the shift of indirect excitonic levels. Absorption spectra are depicted in Fig. 4.18, photoluminescence spectra are shown in Fig. 4.19. Just like in all previous situations, a comparison between the full-structure hamiltonian computation and the computation without the off-diagonal Luttinger terms is available, see Figs. 4.18a, b.

It is obvious that the presence of non-zero $\hat{b}$ and $\hat{c}$ terms makes the absorption spectrum more difficult. However, the substantial difference is the splitting of direct excitonic levels with holes of opposite total angular momentum projections: $1\beta1^+$, $1\beta1^-$ and $2\beta2^+$, $2\beta2^-$. For $\mathcal{E} = 5$ kV/cm, all the lowest-lying energy levels are composed of direct excitonic states (see Tab. 4.13), but in those which act like indirect levels in Fig. 4.18a (the position of which shifts in an electric field, e. g. dagger-marked levels 1 and 3), the strong contribution from indirect states appears. With the increasing magnitude of an electric field, these contributions are becoming more and more important until they are predominant for intensities from 10 kV/cm on.

In Figs. 4.18a, b, there is a nice demonstration of the anti-crossing effect. In the tight-binding approximation (see Sec. 3.3.2), non-zero off-diagonal matrix terms prevent some levels from crossing each other (e. g. $|1\beta1\rangle$ and $|1\alpha1\rangle$). However, the overlap integral of wavefunctions representing states in different QWs (e. g. $|1\beta1\rangle$ and $|2\alpha2\rangle$) equals zero as they are localized strictly inside the wells, rendering the off-diagonal terms, responsible for
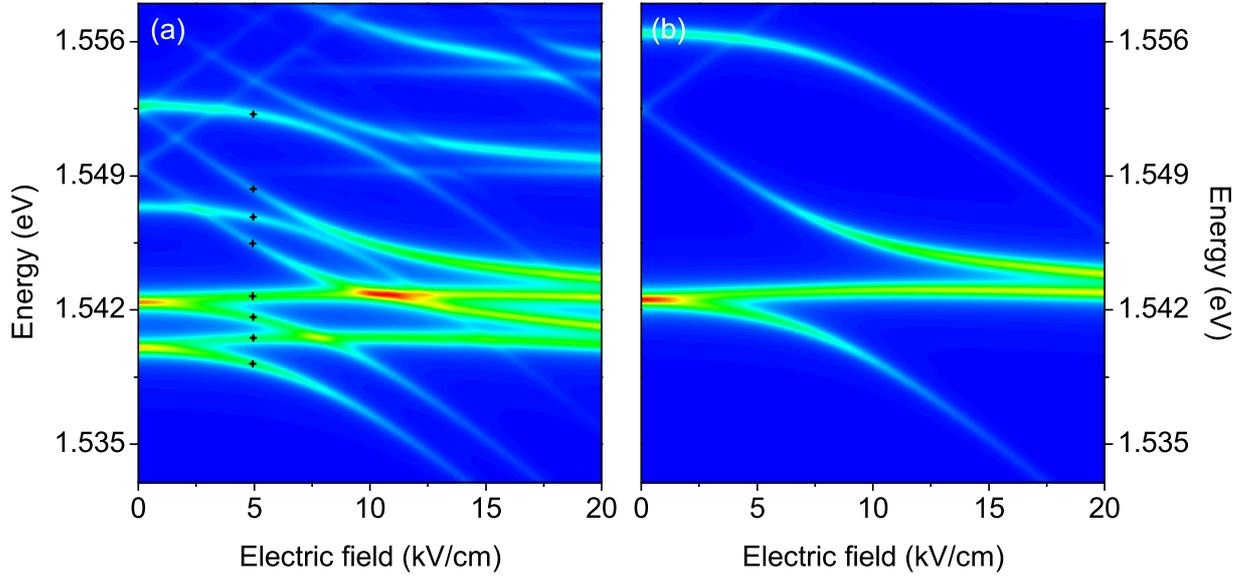
Figure 4.18: Absorption spectra in the presence of an electric field and the perpendicular magnetic field $B_\perp = 10$ T computed for 10×10 basis (a) and 5×5 basis when the off-diagonal Luttinger $\hat{b}$ and $\hat{c}$ terms are neglected (b), $\Delta = 0.3$ meV.
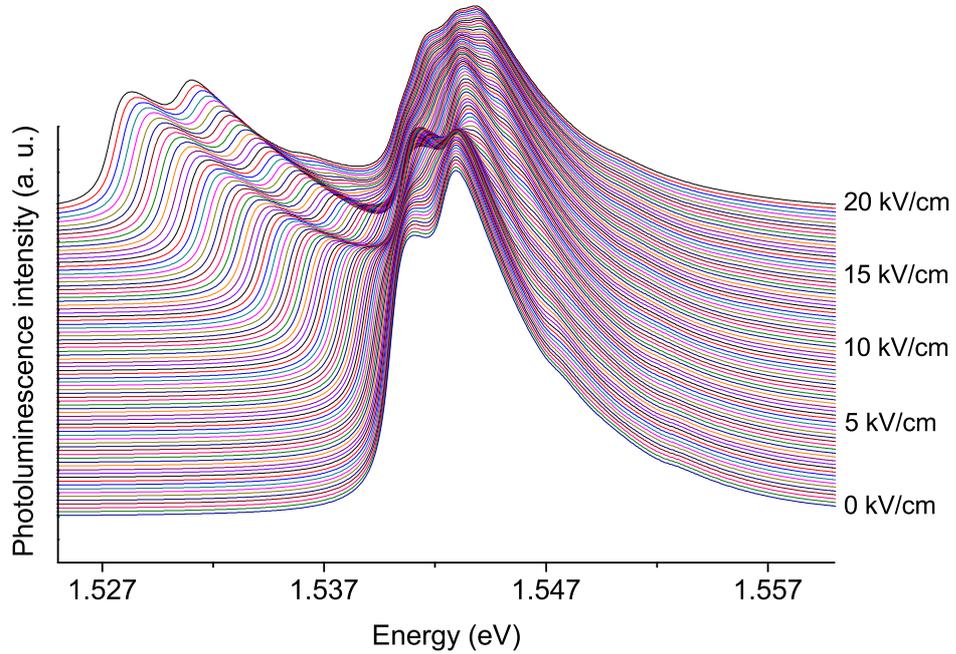
Figure 4.19: Photoluminescence spectra in the presence of an electric field and the perpendicular magnetic field $B_\perp = 10$ T computed for 10×10 basis, $T = 45$ K, $\Delta = 0.5$ meV.
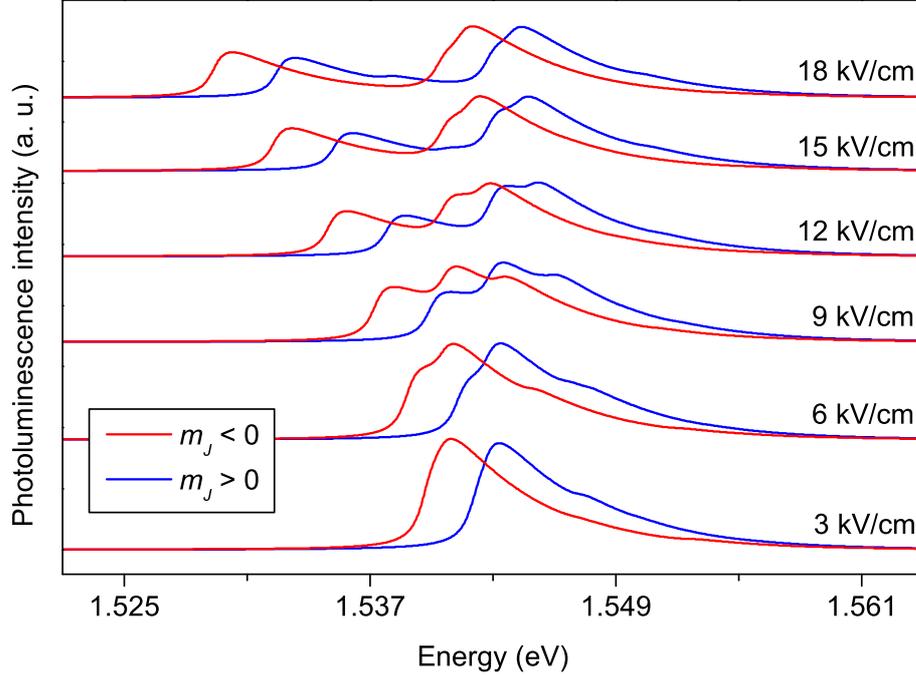
Figure 4.20: Photoluminescence spectra in the presence of the perpendicular magnetic field $B_\perp = 10$ T for various strengths of the electric field computed in 10×10 basis for $m_J > 0$ and $m_J < 0$ states separately, $T = 45$ K, $\Delta = 0.5$ meV.

the band anti-crossing, being zero as well. Thus, peaks associated with these levels can cross each other without any effect on the spectrum.

Except for more complicated structure of Fig. 4.18a, the substance remains the same as in Fig. 4.7, where the effect of an external electric field on excitonic levels was demonstrated for the smallest basis: levels corresponding to indirect excitons shift whereas direct excitonic levels stay unaffected by an external field, their position does not shift.

The additional information about excitonic levels in a DQW is provided by PL spectra. Because the level population is important for photoluminescence, only the lowest levels can contribute to measured signal: in our model, the population of a level of energy E is proportional to $e^{-E/k_B T}$, as can be seen from Eq. (3.130). The higher temperature, the more levels are populated. This is one reason for why we chose $T = 45$ K instead of low (helium) temperature. Computed PL spectra are depicted in Fig. 4.19, proving our notions of behaviour of direct and indirect excitons in external fields. As the two lowest levels correspond to indirect heavy-hole excitons (for $\mathcal{E} = 5$ kV/cm, the energy of $1\beta2^-$ peak is approximately 1.535 eV, that of $1\beta2^+$ is 1.538 eV) with an electron in the left QW and a hole in the right one, their energy decreases with increasing intensity of an electric field. Since the position of direct heavy-hole excitonic levels is around 1.540 eV and does not change, the distance between the levels of indirect and direct excitons increases, resulting in the decrease of direct excitonic PL peak intensity on behalf of the intensity of indirect

Table 4.13: The strongest contributions to eigenvector expansions for several energy levels of the absorption spectrum in Fig. 4.18a for $\mathcal{E} = 5$ kV/cm, $B_\perp = 10$ T.

level	1	2	3	4	5	6	7	8	9
E (eV)	1.5392	1.5405	1.5416	1.5427	1.5455	1.5468	1.5483	1.5522	1.5540
state	$2\beta2^-$	$1\beta1^-$	$2\beta2^+$	$1\beta1^+$	$1\beta2^-$	$2\alpha2^+$	$1\beta2^+$	$2\alpha2^-$	$1\alpha2^+$
|coeff.|	0.7761	0.9158	0.8536	0.9731	0.7297	0.6029	0.8482	0.6075	0.7207

ones, caused by the Boltzmann exponential factor. PL spectra calculated separately for $m_J < 0$ and $m_J > 0$ states are shown in Fig. 4.20.

4.2.5 Optical spectra in an electric field when the in-plane magnetic field is present

In the previous section, we have computed optical spectra in an electric field and an additional presence of the perpendicular magnetic field. To demonstrate that the orientation of the magnetic field is very important and that the system behaves differently if we change its direction, absorption and photoluminescence spectra in the presence of the in-plane magnetic field $B_\parallel = 10$ T were calculated for various values of $\mathcal{E}$. The results are shown in Figs. 4.21–4.22. Let us comment the situation in Fig. 4.21 at first.

It was proven before that optical spectra constructed in 10×10 basis do not differ from those achieved for 5×5 basis for lower energies and that the results of 5×5 basis calculations are applicable both qualitatively and quantitatively. Therefore, the following optical spectra were calculated using smaller basis for the benefit of faster computation and less hard-drive space requirements.[10] At first sight we see that the structure of the lowest levels is different than in the presence of the perpendicular field. The lowest levels are not split by the total angular momentum of a hole as they were in Fig. 4.18. There is only one dominant peak at around 1.537 eV associated with heavy-hole excitons and from which the indirect excitonic branch separates in stronger fields. Levels around 1.550 eV correspond to light-hole excitons and excited heavy-hole states, just like described in Sec. 4.2.1. For $\mathcal{E} = 15$ kV/cm, a large "bunch" of states is formed around 1.553 eV, dominant contributions arise from direct light-hole excitons with a little assistance of heavy-hole ones. For a comparison to the situation without the off-diagonal Luttinger terms, please refer to Fig. 4.21b.

In the PL spectra in Fig. 4.22, we see nearly non-shifting peak of direct heavy-hole excitons placed at 1.537 eV, from which indirect excitonic levels separate: in the presence of a magnetic field at first those, in the expansions of which the ground state eigenfunctions are predominant, then those with contributions from higher excited states as well. In

---

[10]Detailed information about the main program, several additional utilities and the ways how these programs work and treat with acquired data, is given in Appendix A.
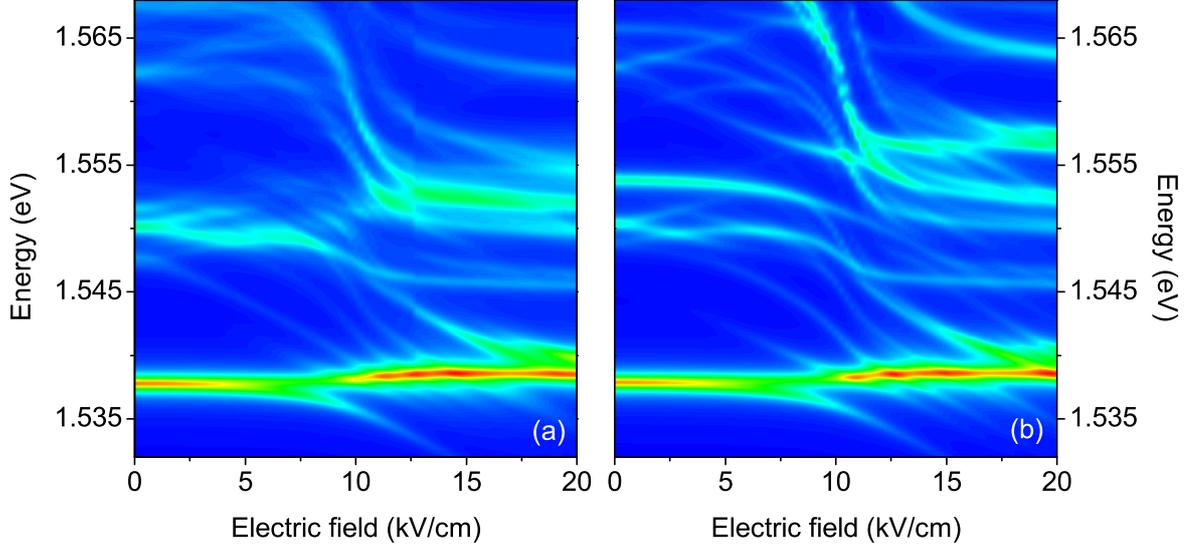
Figure 4.21: Absorption spectra in the presence of an electric field and the in-plane magnetic field $B_\parallel = 10$ T computed for 5×5 basis with (a) and without (b) the off-diagonal Luttinger $\hat{b}$ and $\hat{c}$ terms, $\Delta = 0.5$ meV.
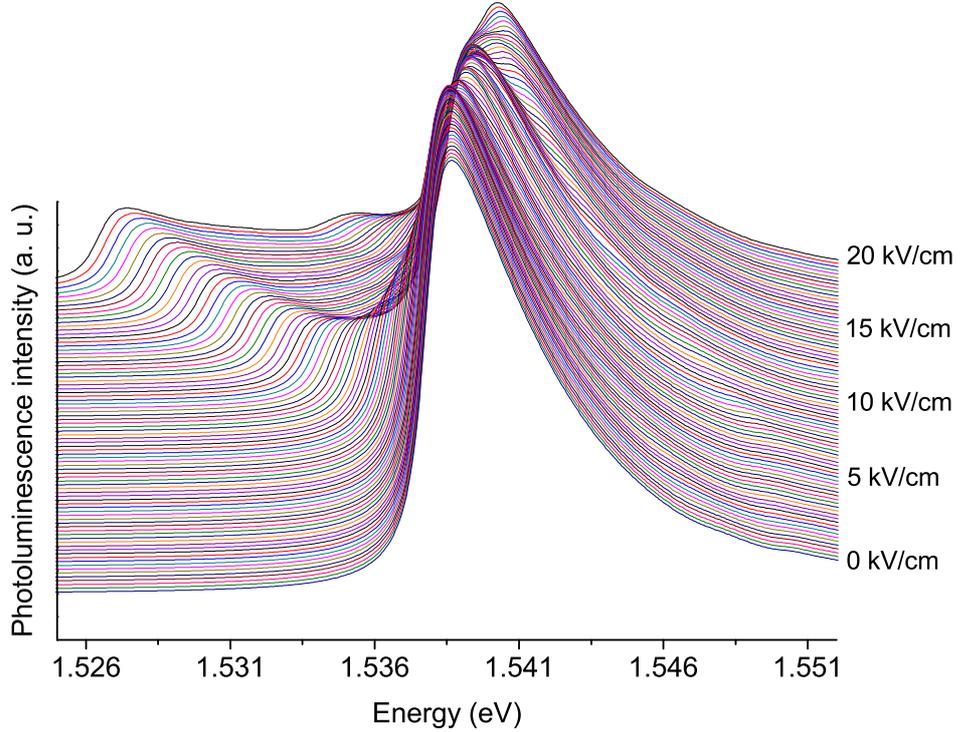
Figure 4.22: Photoluminescence spectra in the presence of an electric field and the in-plane magnetic field $B_\parallel = 10$ T computed for 5×5 basis, $T = 45$ K, $\Delta = 0.5$ meV.

contrast to Fig. 4.19, the intensity of direct transitions is much higher than the intensity of indirect ones.

We have presented the most important results of our work. Further discussion will be given in Chapter 5. At the whole end of this chapter, let us demonstrate the last category of results in our field of interest.

4.3 Probability density

In Sec. 3.3.8, we have derived a simple formula, Eq. (3.133), which can be used for computation of the probability density $|\Psi(x,y)|^2$, a quantity that describes the real-space charge density distribution of an exciton. We are about to demonstrate typical forms of $|\Psi(x,y)|^2$ in four interesting situations.

In Figs. 4.23a, b, the probability density of the ground excitonic level in the presence of the in-plane magnetic field for two values of K_y is shown. The ground level of an exciton with $K_y = 0$ is created from direct excitonic states. With increasing K_y, the contribution from direct states slowly decreases on behalf of that from indirect ones. For $K_y = 0.2$ nm^{-1}, the contributions from direct and indirect states are almost equal, the charge density distribution is wider and not so high. Such a trend proceeds until the dominant component of the ground level originates from indirect states and the corresponding probability density distribution is lower in height but wider in width than that of the direct exciton.

The full potential of our program, which is capable to perform the calculations in the presence of both a tilted magnetic field (i. e. $B_\perp \neq 0$, $B_\parallel \neq 0$) and an electric field in the growth direction, is demonstrated on the second pair of figures, Figs. 4.23c, d, where the difference in charge densities of the ground-level excitons in strong external fields is shown. Since the dispersion relations in such a case are not even, the energy of the exciton in Fig. 4.23c differs from the energy of the exciton in Fig. 4.23d. As the electric field of chosen orientation slants the dispersion lines from right to left, the state with $K_y = -0.2$ nm^{-1} is of lower energy and therefore more stable and with more localized probability density distribution than that with $K_y = 0.2$ nm^{-1}. The excitonic state in Fig. 4.23d is not as stable as in Fig. 4.23c, it is deformed by external fields, resulting in the shift of the charge density maximum away off the origin and different radii in perpendicular directions.
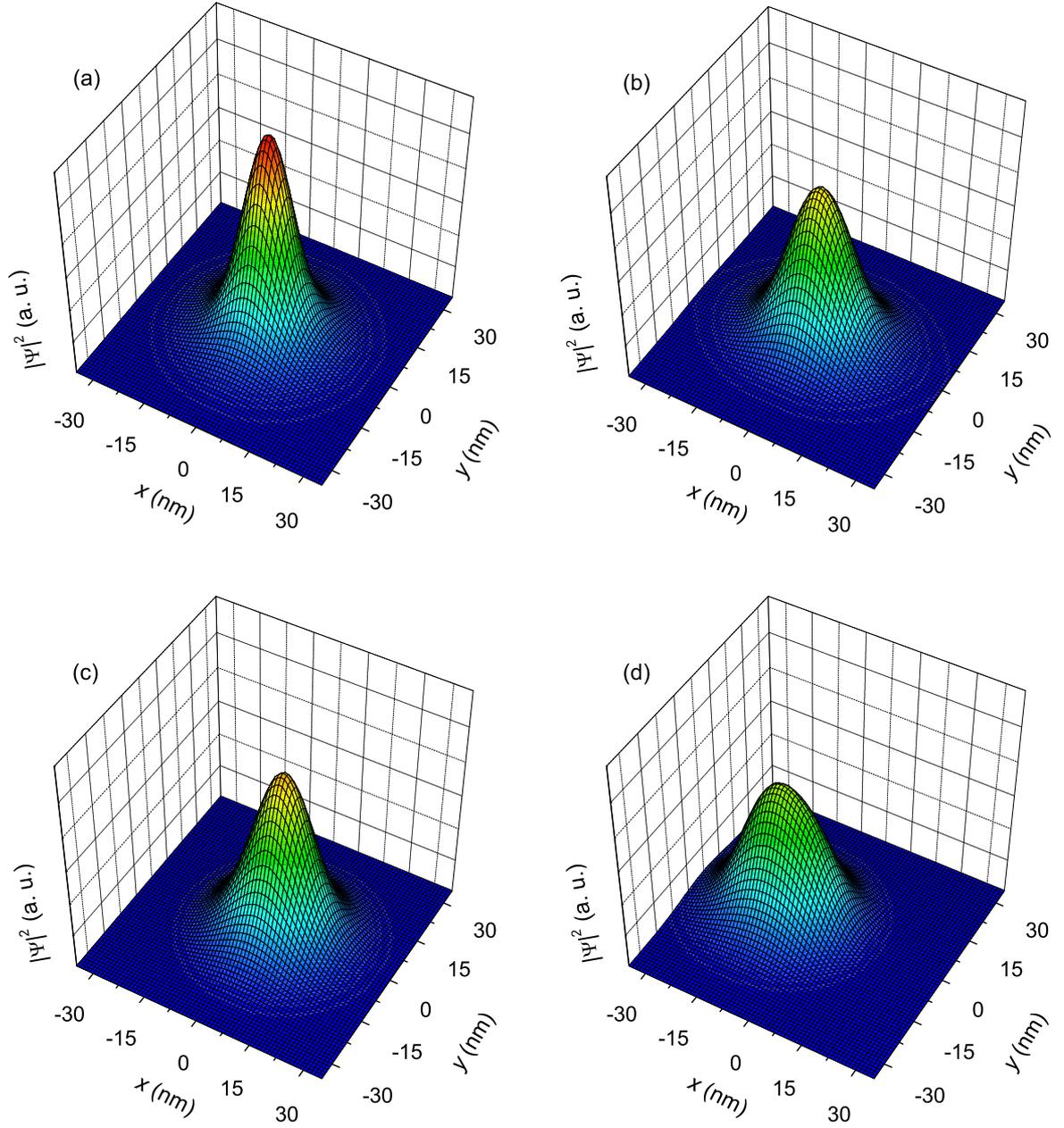
Figure 4.23: Charge density of the excitonic ground state for $B_\parallel = 10$ T and $K_y = 0$ (a) or $K_y = 0.2$ nm^{-1} (b), and for $\mathcal{E} = 20$ kV/cm, $B_\parallel = 5$ T, $B_\perp = 10$ T, and $K_y = -0.2$ nm^{-1} (c) or $K_y = 0.2$ nm^{-1} (d).

Chapter 5

Summary

In this chapter, we will summarize and further discuss important results achieved and presented in the previous chapters of this thesis.

We started our work with the Luttinger hamiltonian (2.30), introduced by Luttinger and Kohn in [19] and revised by Luttinger in [18]. This hamiltonian describes the "real" structure of the valence band of III-V semiconductors with $\mathcal{T}_d$ symmetry, since both light and heavy holes as well as the valence-subband mixing are taken into consideration. After the addition of the electronic hamiltonian (3.22) and confining DQW potentials for electrons and holes, we followed a common way of solving exciton-related problems. As the excitonic hamiltonian (3.21), written in the tight-binding basis (3.42), is a set of 24 coupled partial differential equations, its structure is very complex and one could do nothing but solve it numerically. Although a numerical solution is usually being expanded to the basis formed from the eigenfunctions of the diagonal part of the corresponding matrix hamiltonian, we were not able to find the analytic solution even of the diagonal part of Eq. (3.77) (since the particular equations were complicated). Therefore, we followed the procedure proposed in [12] and through the substitution of the Coulomb potential by the parabolic potential (3.113), we obtained the basis composed of the Hermite-Gauss functions (3.114) with one unknown parameter A. This parameter is related to the radius of an exciton. Similarly to [25], we used variational method to determine the optimal value of A. The variational procedure, as well as the whole program and associated utilities, was written in Fortran language. More details, which will not be of our interest here, are to be found in Sec. 3.3.9 and Appendix A.

Although the Hermite-Gauss functions are not the eigenfunctions of the diagonal part of the excitonic hamiltonian, we chose sufficiently large extension of the basis (including functions up to the 9th order in x, y) to be given as precise results as possible. The largest basis we used was composed of $10 \times 10 = 100$ functions. However, with the increasing basis extension, time taken for calculations rises as well. Time requirements of the computation are divided into two major parts: (1) the construction of the matrix hamiltonian, including the calculation of all matrix elements, and (2) the diagonalisation of the matrix obtained in the previous step. For smaller bases, both procedures are almost equally time-consuming (and performed promptly), but for larger bases, time requirements of the diagonalisation

exceed those of the construction. If N denotes the rank of the matrix hamiltonian, they are proportional to N^2 for the construction, but are of higher order for the diagonalisation. Therefore, before proceeding to the diagonalisation, we always tried to decompose the matrix to several blocks. If it was possible and the matrix was block-diagonal, the particular blocks were diagonalised separately to speed up the whole process.

The applicability of the chosen basis has already been discussed in Chapter 4. We saw that the results achieved for different bases were qualitatively the same, but the quantitative character altered. The stronger fields we are interested in, the larger basis is necessary to be used. The same holds if we are concerned in higher energies. Nevertheless, keeping these remarks in mind, it was proven that the basis composed of the Hermite-Gauss functions is well applicable both with and without the presence of external electric and magnetic fields.

Now we will focus our attention on the structure of the excitonic hamiltonian. We have mentioned before that to speed up all the calculations, we always searched for the block structure of the constructed matrix hamiltonian. In the absence of external fields, every energy level is twofold degenerate even for $K_y \neq 0$. This degeneracy is not lifted even if the off-diagonal Luttinger terms are assumed to be non-zero. However, if there are external fields applied on a studied DQW sample, the situations changes. The presence of either an electric or a magnetic field of any orientation lowers the symmetry, resulting in the splitting of energy levels as demonstrated in Figs. 4.3–4.4, 4.9, and many others. In some special cases, the matrix hamiltonian cannot be decomposed into several blocks and all its columns and rows are coupled together. But there are some other situations, in which such decomposition can be performed, although under certain conditions, the obtained blocks could be different, giving different eigenvalues. This appears for example for $K_y = 0$, $\mathcal{E} = 0$, but $B_\perp \neq 0$. For $B_\perp = 10$ T, the energy difference of every two successive eigenvalues is of order 0.1 meV and increases with increasing magnetic field. As the electronic hamiltonian has a simple form given by Eq. (3.31), this evidently originates from the hole part of the excitonic hamiltonian.

The effect of an external electric field in the growth direction has been demonstrated on our system, resulting in the Kramer's degeneracy splitting, see Fig. 4.3. Our results are in very good qualitative agreement with those achieved by Sanders and Bajaj in [6], although these authors performed their calculations for DQWs of different parameters. Though the field is applied along the z axis, it effects the dispersion relations in the perpendicular plane, xy. If one would be interested in the reason for such behaviour, after some investigation, everyone would find that not only the off-diagonal Luttinger $\hat{b}$ and $\hat{c}$ terms are responsible, but the existence of higher excited heavy-hole QW state is important as well. In the presence of an electric field, the non-zero $\hat{H}_{hh}^2$ term enables the coupling of the whole matrix hamiltonian and makes it impossible to decompose the matrix into several blocks. Strong valence-subband mixing then implies the degeneracy lifting.

It is well-known that the electric field separates indirect and direct excitonic levels. Whereas the energy of indirect ones decreases/increases linearly with the field magnitude, the position of direct levels does not change. We have observed this effect in Fig. 4.7, absorption spectra have proved it, too. With the help of Fig. 4.8, it was not hard to understand that for the chosen orientation of the electric field, the ground level was formed

from the indirect heavy-hole exciton with an electron in the left QW and a hole in the right QW. The next level corresponded to either direct heavy-hole exciton or indirect light-hole excitonic level, depending on the strength of applied field. The indirect heavy-hole level with the opposite localization of an electron and a hole was found to be higher in energy. It was also discovered that the electric field does not prefer any total angular momentum orientation: in all energy levels, states with $m_J = \pm\frac{3}{2}$ or $m_J = \pm\frac{1}{2}$ are represented equally. To get rid of such behaviour, the magnetic field has to be turned on.

We have calculated the binding energies of the ground-level excitons with $K_y = 0$ in a DQW both with and without an external electric field (see Sec. 4.1.1). Our results, giving 6.0 meV for the binding energy of the direct heavy-hole exciton in the absence of external fields and 2.2 meV for indirect heavy-hole exciton when an electric field is present, are confirmed by the corresponding excitonic radii provided by variational method: 14.1 nm in the first case and 23.0 nm in the second case. These results cannot be simply compared with those presented in [12], where the value of 12.2 nm for the direct heavy-hole exciton was achieved, since slightly different parameters (especially effective masses) were used there. Nevertheless, it is obvious that the less-bounded exciton is the one of the larger radius.

Now we proceed further and discuss some important remarks on optical spectra. We have demonstrated the effect of basis extension on absorption spectra computed in the absence of external fields. Once again, we have seen that the larger basis is taken, the more levels appear in spectra. The position of the three lowest-lying peaks and their identification gave the same results in all studied situations, no matter if only the ground levels or the full energy spectrum were used for calculations. As we have identified these peaks as being associated with direct heavy-hole excitons, indirect heavy-hole excitons, and direct light-hole excitons, respectively, our conclusions seem to be correct. In higher energy, there are many less-significant peaks corresponding to excited excitonic states. It has already been discussed that these peaks are localized above the absorption edge of the two-dimensional electron-hole gas. Though it is wrong, it is the natural result of variational method, which works well for the ground state, but gives worse results for excited levels. It is because the optimal "width" (radius) is found for the ground-state Gaussian function, but the damping of the wavefunction is too large to describe less-bounded excited states, since higher basis functions, given as a multiple of a polynomial and the ground-state basis function, converge too slowly.

Although the presence of excited excitons alters the character of theoretical absorption spectra calculated in different bases, it is not a substantial change because of two reasons: in actual experimental absorption spectra measured at low temperatures, (1) the ground-level peak is the strongest one, while the others vanish in the increasing signal from the background; (2) above the absorption edge, "sharp" excitonic peaks are localized in the continuum of states of the two-dimensional electron-hole gas, which complicates their identification. On the contrary, because only the lowest levels are visible, there is no such a problem in photoluminescence. Therefore, in the absence of external fields, the chosen method is well-suitable for description of the lowest excitonic levels, while for higher ones, its applicability decreases.

When studying a DQW subject to the perpendicular magnetic field, the Zeeman splitting is usually being considered. Van Kesteren *et al.* derived in [26] that such a contribution, linear in magnetic field, is given by

$$H_Z = \mu_B g_e \mathbf{S} \cdot \mathbf{B} - 2\mu_B \big(\kappa \mathbf{J} + q\mathbf{J}^3\big) \cdot \mathbf{B}, \tag{5.1}$$

where the first term corresponds to electrons and the second one is associated with holes, while $\mathbf{S}$ represents the spin of an electron, $\mathbf{J}$ marks the total angular momentum of a hole, μ_B is the Bohr magneton, g_e is the Landé g-factor and κ and q are the two more Luttinger parameters. The total Landé g-factor of an exciton, g_{ex}, is in accordance to [27] written as a sum of particular contributions, $g_{\mathrm{ex}} = g_e + g_h$, where g_h, the Landé g-factor of a hole, is connected to κ and q. Since we included the Zeeman splitting terms neither for electrons nor for holes but the splitting still takes place (see the text bellow), this is supposed to be an additional contribution to the g-factor. As $\kappa = q \equiv 0$, this contribution arises from the Luttinger terms (3.36)–(3.37) in the presence of an external magnetic field.

We have computed absorption and photoluminescence spectra for several important situations and depicted them "in cascade" to show changes when varying the strength of external fields. To demonstrate new findings of this work and to give a comparison to existing results, optical spectra both with and without the off-diagonal Luttinger $\hat{b}$ and $\hat{c}$ terms have been calculated. Let us discuss the particular situations one after another.

In the presence of the perpendicular magnetic field, the first important difference appeared. Whereas when the off-diagonal terms were neglected, there was only one ground level, energy of which was rising with increasing $B_\perp$, if $\hat{b}$ and $\hat{c}$ terms were considered, the ground level split for fields stronger that 5 T. It was discovered that this level corresponds to direct heavy-hole excitonic states and that the presence of the perpendicular magnetic field separates states with $m_J = \frac{3}{2}$ and $m_J = -\frac{3}{2}$ with an energy gap of approximately 3 meV for $B_\perp = 13$ T, leaving the $m_J = -\frac{3}{2}$ level energetically lower. If our results are correct, the ground level splitting would have to be observed with the help of circularly polarized light, since the selection rules for $m_J = \frac{3}{2}$ and $m_J = -\frac{3}{2}$ are different. However, we have discussed in the text above that any distinct behaviour of states with opposite sign of m_J, induced by the magnetic field, originates from the hole part of the excitonic hamiltonian only and that no Zeeman terms are considered in our work. This may cause the difference between theoretically predicted and experimentally measured spectra.

The similar behaviour accompanied us later. When an additional electric field in the growth direction was applied on a DQW structure, there was no doubt about the separation of direct and indirect excitons. But as the magnetic field was present, too, states with $m_J = \pm\frac{3}{2}$ or $m_J = \pm\frac{1}{2}$ were no longer twofold degenerate, but the degeneracy was lifted because of the same reason as mentioned before.

On the contrary, when studying optical spectra in the presence of the perpendicular magnetic field for various strengths of an external electric field, absorption spectra change its character as position of energy levels is determined by the electric field. Once again, indirect excitonic levels shift linearly while direct ones are not affected. Moreover, a nice demonstration of the anti-crossing effect is to be seen in Fig. 4.18. In contrast to the

in-plane magnetic field, the perpendicular field does separate energy levels by the hole total angular momentum projection, m_J.

We have calculated photoluminescence spectra as well. Since the intensity of higher levels is decreased by the Boltzmann exponential factor $\mathrm{e}^{-E/k_B T}$, not only the electron-hole overlap integral affects the strength of optical transitions. We have performed the computations for higher temperature $T = 45$ K, same as in [8], to provide sufficient population even for several higher states to have not only the ground level visible in spectra. As the energy of indirect excitons lowers with increasing electric field, the intensity of the corresponding peak increases on behalf of the intensity of direct excitonic peak, since the energy separation between them rises and thus the relative intensity is decreased exponentially. However, for stronger electric field, the increasing intensity of indirect excitonic peak is not usually experimentally observed as the exciton becomes dissociated by electron tunneling outside the DQW [8].

We have already discussed that variational method is generally well applicable to ground-level states, but with increasing energy, its applicability decreases. We have seen that in the absence of external fields, the character of optical spectra is mostly determined by ground and higher excited excitonic levels, whereas e. g. when the strong perpendicular magnetic field is applied, the transitions associated with excitonic levels originating from the Landau levels of electrons and holes are of the most importance. However, the transformation from a wavefunction describing well the states in the absence of external fields to that which is efficient for states in strong fields, remains unclear. It would be interesting to pay more attention on such a problem as a part of further theoretical research.

The last category of results we have presented in the previous chapter was associated with the visualisation of the probability density distribution. Analogously to [12], we have depicted the charge density of ground-level excitons for notable situations to illustrate and better understand the effects we are facing. From there on, we can easily imagine any process when direct and indirect excitons are merging into one another, since such a change is accompanied by shrinking or stretching of the charge density distribution. Furthermore, the effect of external fields on the excitonic radius was nicely illustrated. It was proven that the probability density of direct excitons is localized in a small area whereas that of indirect ones is spatially more spread. Moreover, the presence of both electric and magnetic fields for excitons with non-zero K_y breaks the axis symmetry, making radii in perpendicular directions different and shifting the maximum of the charge density distribution away off the origin.

We have discussed the most important results of this thesis. Since it is a theoretical work, the experimental proof of predicted effects is necessary. We know that the preparation of DQW samples satisfying all the strict requirements is not a simple process. Hence, keeping this in mind, we have written the main program and all other utilities in such a form that all presented calculations can be performed any time again with such a set of parameters, which would best characterize available samples.

Chapter 6

Conclusions

As the last chapter of our thesis, we will briefly conclude the most important results achieved when studying general properties of excitons in DQW structures.

We started from the well-known Luttinger hamiltonian of a hole in the valence band and after the addition of the electronic hamiltonian, confining DQW potentials for electrons and holes and the introduction of bounding Coulomb potential, the excitonic hamiltonian was derived. To find its eigenvalues and eigenvectors, we expressed the hamiltonian in the tight-binding basis, which enabled us to separate parallel and transverse motion (with respect to a DQW plane) and to derive the Schrödinger equation depending on the in-plane components only. After the centre-of-mass transformation, the form of which was discuss since we had to generalize it to include both light and heavy holes, the final set of 24 coupled partial differential equations was obtained.

To solve such a complicated problem, the numerical solution was preferred as we did not manage to find the analytical one. The expansion to the basis composed of the Hermite-Gauss functions was chosen and a Fortran code was written to construct and then diagonalise the matrix hamiltonian. As the basis functions contained one variable parameter (or two parameters in 2D variational computation), its value was determined by variational method to be given the lowest energy of the ground excitonic level. Comparisons between bases of different extensions and between the results of 1D and 2D variational calculations were given. Not only the main program, but many other utilities as well, were written in Fortran language to compute desired quantities from the output provided by the diagonalisation method.

Dispersion relations and the shift of energy levels in external fields were presented and described, confirming the validity of our model. However, the most important results proceeded from optical spectra calculations. Absorption and photoluminescence spectra were computed and depicted for several interesting situations both with and without external fields: the electric field in the growth direction and/or the in-plane and the perpendicular magnetic field. The achieved results were discussed in detail. Probability density distribution, showing the real-space charge density of an exciton, was illustrated as well.

Bibliography

[1] R. Dingle, W. Wiegmann, and C. H. Henry, Phys. Rev. Lett. **33** 827 (1974).

[2] Y. A. Goldberg, *Handbook Series on Semiconductor Parameters*, Vol. 2, ed. M. Levinshtein, S. Rumyantsev, and M. Shur (World Scientific, London, 1999).

[3] A. Baldereschi, N. C. Lipari, Phys. Rev. B **3** 439 (1971).

[4] M. Altarelli, N. O. Lipari, Phys. Rev. B **7** 3798 (1973).

[5] A. A. Gorbatsevich, I. V. Tokatly, Semicond. Sci. Technol. **13** 288 (1998).

[6] G. D. Sanders, K. K. Bajaj, Phys. Rev. B **35** 2308 (1987).

[7] M. M. Dignam and J. E. Sipe, Phys. Rev. B **43** 4084 (1991).

[8] J. Soubusta, R. Grill, P. Hlídek, M. Zvára, L. Smrčka, S. Maltzer, W. Geisselbrecht, and G. H. Döhler, Phys. Rev. B **60** 7740 (1999).

[9] S. K. Lyo, Phys. Rev. B **58** R10187 (1998).

[10] M. Orlita, M. Byszewski, G. H. Döhler, R. Grill, S. Malzer, J. Soubusta, and M. Zvára, Physica E **30** 1 (2005).

[11] M. Orlita, R. Grill, M. Zvára, G. H. Döhler, S. Malzer, M. Byszewski, and J. Soubusta, Phys. Rev. B **70** 075309 (2004).

[12] M. Grochol, *Luminescence Spectroscopy of Semiconductor Quantum Structures* (Diploma thesis, Faculty of Mathematics and Physics, Charles University, Prague, 2003).

[13] G. Bastard, *Wave Mechanics Applied to Semiconductor Heterostructures* (Monographies de physique, Paris, 1992).

[14] J. H. Davies, *The Physics of Low-dimensional Semiconductors* (Cambridge University Press, Cambridge, 1998).

[15] T. Westgaard, Q. X. Zhao, B. O. Fimland, K. Johannessen, and L. Johnsen, Phys. Rev. B **45** 1784 (1992).

[16] A. I. Ansel'm, *Úvod do teorie polovodičů* (Academia, Praha, 1967).

[17] E. O. Kane, J. Phys. Chem. Sol. **1** 249 (1957).

[18] J. M. Luttinger, Phys. Rev. **102** 1030 (1956).

[19] J. M. Luttinger, W. Kohn, Phys. Rev. **97** 869 (1955).

[20] R. C. Miller, D. A. Kleiman, W. T. Tsang, and A. C. Gossard, Phys. Rev. B **24** 1134 (1981).

[21] L. P. Gor'kov, I. E. Dzyaloshinskii, Sov. Phys. JEPT **26** 588 (1968).

[22] M. Orlita, *Study of GaAs/GaAlAs Quantum Wells* (Diploma thesis, Faculty of Mathematics and Physics, Charles University, Prague, 2002).

[23] W. H. Press, S. A. Teukolsky, W. T. Vetterling, and B. P. Flannery, *Numerical Recipes in Fortran 77: The Art of Scientific Computing*, Second Edition, Vol. 1 of Fortran Numerical Recipes (Cambridge University Press, London, 1997).

[24] L. D. Landau, E. M. Lifshitz, *Quantum Mechanics: Nonrelativistic Theory* (Pergamon Press, Oxford, 1977).

[25] J. Soubusta, *Study of Modulation-doped Quantum Wells and Superlattices in GaAs/GaAlAs Systems* (Diploma thesis, Faculty of Mathematics and Physics, Charles University, Prague, 1999).

[26] H. W. van Kesteren, E. C. Cosman, W. A. J. A. van der Poel, and C. T. Foxon, Phys. Rev. B **41** 5283 (1990).

[27] M. J. Snelling, E. Blackwood, C. J. McDonagh, R. T. Harley, and C. T. B. Foxon, Phys. Rev. B **45** 3922 (1991).

Appendix A

Main program and other utilities

We have spoken about the way data for construction of figures are acquired. Among all other programs, that one called DQW is of most importance. Let us give you some additional information about how it works and how to set up the program to compute what we are interested in.

A.1 Acquiring data for energy dependencies

Although a Fortran code is supplied, too, the compiled executable file `DQW.EXE` is to be found on the attached CD-ROM. The whole setup is performed through the input file `DQW.TXT`, which is located in the same directory. Each line of this file contains one adjustable parameter. The structure of the file is shown in Tab. A.1.

The first two lines, `basis_x, basis_y`, determine the basis extension. In the third line, the independent variable for calculation is chosen: e. g. if we want to compute dispersion relations, `variable` has to be set to 0. The setting of K_y and the strength of external fields comes next, followed by variables `step` and `numofsteps` used for step adjustment, allowing us to configure the difference between two successive values of the chosen independent variable, for which the computation is run, and the total number of computations. The next group of variables determines several parameters of the sample: the QW width (L), the distance between QWs (d), the relative permittivity of the sample (ϵ_r), and finally the effective masses for electrons (m_e) and holes (Luttinger γ_1, γ_2, and γ_3 parameters). It is followed by variables showing the energy gap, QW bound energies, and the tunneling matrix elements for both electrons and holes. Variable `variation` sets the type of variational method: set 1 for one-dimensional or 2 for two-dimensional computation. The following two groups of parameters enclose an area, where the variational method finds optimal values, and determine numerical precision. The last three lines can be used to enable/disable the off-diagonal Luttinger $\hat{b}$ or $\hat{c}$ terms by setting `bterms` or `cterms` to 1/0, and to export the matrix hamiltonian into an external file (`writehamiltn`). Before changing any value of `DQW.TXT`, please take care of the corresponding units.

Table A.1: Structure of the input file `DQW.TXT`.

basis_x =	$\vdots$	$\vdots$
basis_y =	$\gamma_2 =$	$v_a^{1D} =$
	$\gamma_3 =$	$v_b^{1D} =$
variable =		$v_c^{1D} =$
K_y (nm^{-1}) =	E_g (eV) =	$v_{\text{tol}}^{1D} =$
$\mathcal{E}$ (kV/cm) =	E_{e0} (eV) =	
$B_\parallel$ (T) =	E_{h00} (eV) =	$v_{x1}^{2D} =$
$B_\perp$ (T) =	E_{h10} (eV) =	$v_{y1}^{2D} =$
step =	E_{l0} (eV) =	$v_{x2}^{2D} =$
numofsteps =		$v_{y2}^{2D} =$
	t_e (eV) =	$v_{x3}^{2D} =$
L (nm) =	t_{h0} (eV) =	$v_{y3}^{2D} =$
d (nm) =	t_{h1} (eV) =	$v_{\text{tol}}^{2D} =$
$\epsilon_r =$	t_l (eV) =	
$m_e =$		bterms =
$\gamma_1 =$	variation =	cterms =
$\vdots$	$\vdots$	writehamiltn =

If `DQW.EXE` is executed, it reads the configuration from the input file and performs the desired computations. After all is done successfully, the directory `VYSLEDKY` is created (if it does not already exist) and the results are written in a subdirectory retaining information about the computation (K_y and external fields). Four files are created: in `PARAM.TXT`, values of variational parameters and the corresponding energy of the ground level are written, `ENERGIE.TXT` keeps the whole energy spectrum, and two more files, `VEKTOR_R.TXT` and `VEKTOR_I.TXT`, contain the expansion coefficients (eigenvector components) associated with all energy levels.

One more remark at the end: each component of any eigenvector is stored as a double-precision real number and thus takes 8 bytes of memory. When working with 10×10 basis, $24 \times 10 \times 10 = 2400$ energy levels are obtained. For each level, 2400 components representing the real part and 2400 components of the imaginary part of the corresponding eigenvector are provided, too. Globally, it stands $2 \times 2400 \times 2400 \times 8$ bytes ≈ 88 megabytes of data to be stored. Together with the information about energy levels and variational parameters, we have approximately 90 megabytes of data for one run of the program. Thus, hard-drive space requirements are quite high when performing many steps of larger-basis computation.

A.2   Computing optical spectra

From the results computed by the main program, dispersion relations and other energy dependencies can be constructed directly. However, very important information about the system is provided by optical spectra. Therefore, another helpful program, `SPEKTRA.EXE`, was written and is to be found on the attached CD-ROM, as well as the corresponding Fortran code. In contrast to previously discussed program, the setup of `SPEKTRA.EXE` is controlled from the keyboard.

This program uses all four files created by `DQW.EXE` to compute either absorption or photoluminescence spectra on the selected energy interval with an arbitrary step. The spectral-line broadening (the "width" of a peak) Δ is entered for both absorption and PL spectra calculations. Moreover, one additional parameter, the temperature T of the sample, is used for construction of PL spectra.

The output is written into the subdirectory `SPEKTRA`, which is created inside the directory containing the results of the main program, and whilst `AB_DELTA=[`Δ`]MEV.TXT` or `PL_DELTA=[`Δ`]MEV_T=[`T`]K.TXT` contain columns showing energy and the corresponding absorption or PL intensity, the file `PIKY.TXT` keeps the information about strength and type of transitions to simplify the identification of particular peaks.

A.3   Constructing probability density distribution

As well as the latter program, the utility `PSI.EXE` is used to process the acquired data. This program constructs the probability density distribution on the selected area, enclosed by coordinates x_1, x_2, y_1, and y_2. The setup of `PSI.EXE` is controlled through the external file `PSI.TXT`. The structure of this file is schematically depicted in Tab. A.2.

Table A.2: Structure of the input file `PSI.TXT`.

basis_x =	$\vdots$
basis_y =	x_1 (nm) =
	x_2 (nm) =
variable =	y_1 (nm) =
K_y (nm^{-1}) =	y_2 (nm) =
$\mathcal{E}$ (kV/cm) =	step_x (nm) =
$B_\parallel$ (T) =	step_y (nm) =
$B_\perp$ (T) =	
	level =
$\vdots$	record =

The first lines of `PSI.TXT` are identical with those in `DQW.TXT` and no further explanation is necessary. Variables `step_x` and `step_y` control the density of the square grid on which

the charge density is calculated. The meaning of the last two parameters is explained as follows: `level` determines the energy level, `record` sets from which record of the main program output files, the probability density is to be computed. The output is written into the new subdirectory, `HUSTOTA`, to a separate file for each level.

A.4   Other utilities

Except for already discussed programs, there are two more helpful utilities. The first one, `KOEF.EXE`, is used for the construction of expansion coefficients dependencies. With the help of this tool, Fig. 4.2 was calculated. The function of `KOEF.EXE` is customized through the external file `KOEF.TXT`, the structure of which is shown in Tab. A.3a. Since the meaning of all parameters remains the same as before, there is no need of any explanations.

The second utility, `HLADINA.EXE`, is not suited for the computation of any other quantity, but for easier identification of peaks and levels in optical spectra. The structure of its input file, `HLADINA.TXT`, is depicted in Tab. A.3b. Through the help of parameters loaded from `HLADINA.TXT` and few more entered via the keyboard, the character of desired level and the strongest contributions of the corresponding eigenvector expansion are printed on screen.

Table A.3: Structure of the input files `KOEF.TXT` (a) and `HLADINA.TXT` (b).

(a)
```
basis_x =
basis_y =

variable =
K_y (nm^-1) =
E (kV/cm) =
B_∥ (T) =
B_⊥ (T) =

record =
```

(b)
```
basis_x =
basis_y =

variable =
K_y (nm^-1) =
E (kV/cm) =
B_∥ (T) =
B_⊥ (T) =

level =
coeff =
```

Appendix B

Contents of the attached CD-ROM

As the CD-ROM containing the electronic version of this thesis, all program codes and executable applications, and some acquired data is attached, it is reasonable to make a mention of the directory tree on the disc:

MASTER'S THESIS: This directory contains the electronic version of the thesis, which is available as a Portable Document Format file and a Postscript file.

EXECUTABLE APPLICATIONS: In this directory, compiled Win32 applications described in Appendix A are placed. It has the following structure of subdirectories:

- MAIN PROGRAM: The most important part providing all results for further processing is stored here.

- OPTICAL SPECTRA: The program used for the computation of absorption and PL spectra on the selected energy interval.

- OTHER UTILITIES: Other useful tools discussed in Appendix A and their configuration files.

- PROBABILITY DENSITY: The utility for the construction of the charge density distribution and its configuration file.

OUTPUT DATA SAMPLES: To show the typical form in which the output of DQW.EXE is provided, some results computed for smaller basis and used in the thesis are to be found in this directory.

VISUAL FORTRAN PROJECTS: The directory where Microsoft Visual Fortran projects, including all files and complete Fortran codes, are located to enable further modifications.

As discussed in Appendix A, hard-drive space requirements are high for larger-basis computations. Hence, it is not possible to store data used for the construction of optical spectra on the attached CD-ROM.